DISSERTATION

THE SPLICEOSOME RECYCLING FACTOR, SART3, REGULATES H2B DEUBIQUITINATION BY USP15

Submitted by

Lindsey J. Long

Department of Biochemistry and Molecular Biology

In partial fulfillment of the requirements

For the Degree of Doctor of Philosophy

Colorado State University

Fort Collins, Colorado

Summer 2014

Doctoral Committee:

Advisor: Tingting Yao

Jennifer DeLuca
Karolin Luger
Jeffrey Wilusz

ABSTRACT

THE SPLICEOSOME RECYCLING FACTOR, SART3, REGULATES H2B DEUBIQUITINATION BY USP15

In eukaryotes plasticity of chromatin architecture is paramount to allow proper regulation of processes such as transcription regulation, DNA repair, and DNA replication. Modulation of chromatin dynamics is primarily achieved via signaling to chromatin modifiers and remodelers though a complex code of histone post-translational modifications (PTMs). These PTMs include methylation, acetylation, phosphorylation, and ubiquitination. In comparison to other histone PTMs, attachment of the 8.5 kDa ubiquitin (Ub) protein stands out due to its considerable size. The majority of histone monoubiquitination occurs on histones H2A and H2B (at lysine residues 119 and 120, respectively), and these modifications have roles in the regulation of many cellular processes including transcription, pre-mRNA processing, and DNA damage repair.

To uncover the mechanisms underlying various functions associated with ubiquitinated histones, we generated non-hydrolyzable Ub-histone mimics and assembled them into H2A/H2B dimers or nucleosomes. Quantitative mass spectrometry was employed to identify proteins that bound to unmodified or modified histone dimers and mononucleosomes. We also found that, within the context of a mononucleosome, Ub, when attached to H2B, partially obscures the H2A/H2B acidic patch.

Among the proteins that were identified, a deubiquitinating enzyme (DUB), Usp15, exhibited high affinity and specificity towards ubiquitinated histone dimers. Further characterization demonstrated that Usp15 is a bona fide histone DUB and preferentially

deubiquitinates Ub-containing histone octamers versus Ub-containing mononucleosomes. Usp15 associates with the U4/U6 spliceosome recycling factor, SART3, which we found also bound to histones. These interactions result in more efficient histone deubiquitination by Usp15. In cells, depletion of SART3 results in elevated ubH2B levels that we show is due to a decreased rate in H2B deubiquitination. These observations indicate SART3 may play a role in regulating ubH2B dynamics as a possible mechanism by which regulate alternative splicing and transcription.

Depletion of SART3 also alters transcriptional and alternative splicing patterns. By chromatin immunoprecipitation, we confirmed that SART3 localizes to at least a subset of genes whose transcription decreased upon SART3 depletion. Future studies will be designed to elucidate the mechanism by which Usp15, SART3, and ubH2B work together to regulate transcription and alternative splicing.

ACKNOWLEDGEMENTS

There are so many people who have influenced me and been involved in my journey the last few years. Most notably, I would like to thank my advisor, Dr. Tingting Yao. I joined Tingting's lab in a somewhat non-traditional manner. When I approached Tingting about joining her lab during my 3rd year of graduate school, she allowed me to join her lab despite the fact that she had never personally observed my lab skills. Because of my unusual circumstances, I was very nervous on my first day in the new lab. Much to my surprise, before my arrival, Tingting had already arranged a bench and desk space for me and reserved shelves and racks for me in all of the storage spaces. I will never forget this because these small gestures made me feel more welcome and at ease than Tingting will ever know…I felt like was wasn't in the lab on trial basis, but rather I was a permanent member of the lab.

Throughout the years, Tingting has invested an incredible amount of her personal time into training me. Not only did she personally train me in the lab concerning experimental procedures, but also she took the time to meet with me one-on-one at least once per week where we intensely discussed data and goals. Tingting also took an active role in my career development. I shared with Tingting that, in addition to research, I'd like to have a teaching component be a major part of my future career. Consequently, I was allowed to teach a lecture series in her LIFE201B course. Furthermore, Tingting encouraged me to apply to multiple IRACDA programs. These programs are unlike any other post-doctoral opportunity as they combine post-doctoral research with a teaching development component. Without Tingting, I would have never known about these programs. Furthermore, without her research training, excellent recommendation letters,

and teaching opportunities, I'm confident that I would never have been offered an opportunity to participate in the IRACDA program at the University of New Mexico.

I'd like to thank my committee members Dr. Jennifer DeLuca, Dr. Karolin Luger, and Dr. Jeff Wilusz. Not only did they take the time to critically think about my project, but they wrote me letters of recommendation, offered me teaching opportunities, and shared reagents and protocols with me. I'm extremely lucky to be surrounded by a group of such talented scientists who are so highly invested in my research and my future.

I'd also like to thank the members of the Yao and Cohen labs. Not only did they contribute to my development as a scientist, but also they are genuinely good people and excellent friends. I'd especially like to thank Ada Ndoja for our weekly runs where we release stress and talk about problems with our experiments; Nouf Omar for always being kind, asking about how my experiments are going, and for sharing my love of pop culture; Dr. Melonnie Furgason for being the HPLC guru, her extreme generosity with her time and reagents, and her love of Disney music; Aixin Song for all of her child-rearing advise and for showing me that it is possible to never say an unkind word; and Joe Thelen who is always calm, intelligent, funny, and truly a joy to work with.

I owe a huge thanks to my husband Dustin. Without contention, Dustin willing moved to Fort Collins and allowed me to start the long process of obtaining my post-graduate degree. During this time, he performed countless hours of volunteer work, started his own business, and received his Bachelor's degree. Now he has agreed to move our family to another state to allow me to further my career. He is the most selfless and hardest working person I know. And Drake is the cutest little human I know.

Finally, I'd like to thank my family. They've been so supportive during this entire process. They've forced me to de-stress by doing fun things like skiing, Doggy Olympics, grass volleyball tournaments, the Great Urban Race, running half-marathon races, and game nights. You are all so generous, caring, hilarious, and the most fun people on the face of this planet.

TABLE OF CONTENTS

CHAPTER 1: INTRODUCTION

In eukaryotes, the state of chromatin dictates all processes that require access to DNA, such as transcription, replication, and DNA repair. DNA accessibility is regulated, in part, by numerous post-translational modifications (PTMs) that occur on histones including: acetylation, methylation, phosphorylation, SUMOylation, and ubiquitination (Tan et al., 2011).

Ubiquitin (Ub) is a protein of 76 amino acids with a well-folded, highly stable structure. It is attached to other proteins through the formation of an isopeptide linkage between the C-terminal carboxylate of Ub and a lysine side chain of the substrate protein. Although all four core histones and linker histone H1 have been reported to undergo ubiquitination at various positions, the predominant forms of ubiquitinated histones in humans are H2A ubiquitinated at K119 and H2B ubiquitinated at K120 (ubH2A and ubH2B, respectively) (Kim et al., 2011; Osley, 2006). MonoUb attachment to histones H2A and H2B serves as signals in the regulation of gene expression, pre-mRNA splicing, and DNA repair processes. Dynamic conjugation and deconjugation of Ub is imperative as Ub histone-regulated processes must be tightly regulated. Deubiquitinating enzymes (DUBs) perform Ub deconjugation. My thesis will focus on the generation and application of ubiquitinated histone mimics, characterization of a histone DUB, Usp15, and its relationship with the spliceosome recycling factor, SART3, and transcription.

1.1 Ubiquitin conjugation

Ub conjugation is accomplished through a coordinated effort between a cascade of three enzymes: E1, E2, and E3 (Pickart and Eddins, 2004) (Figure 1.1). In an ATP-

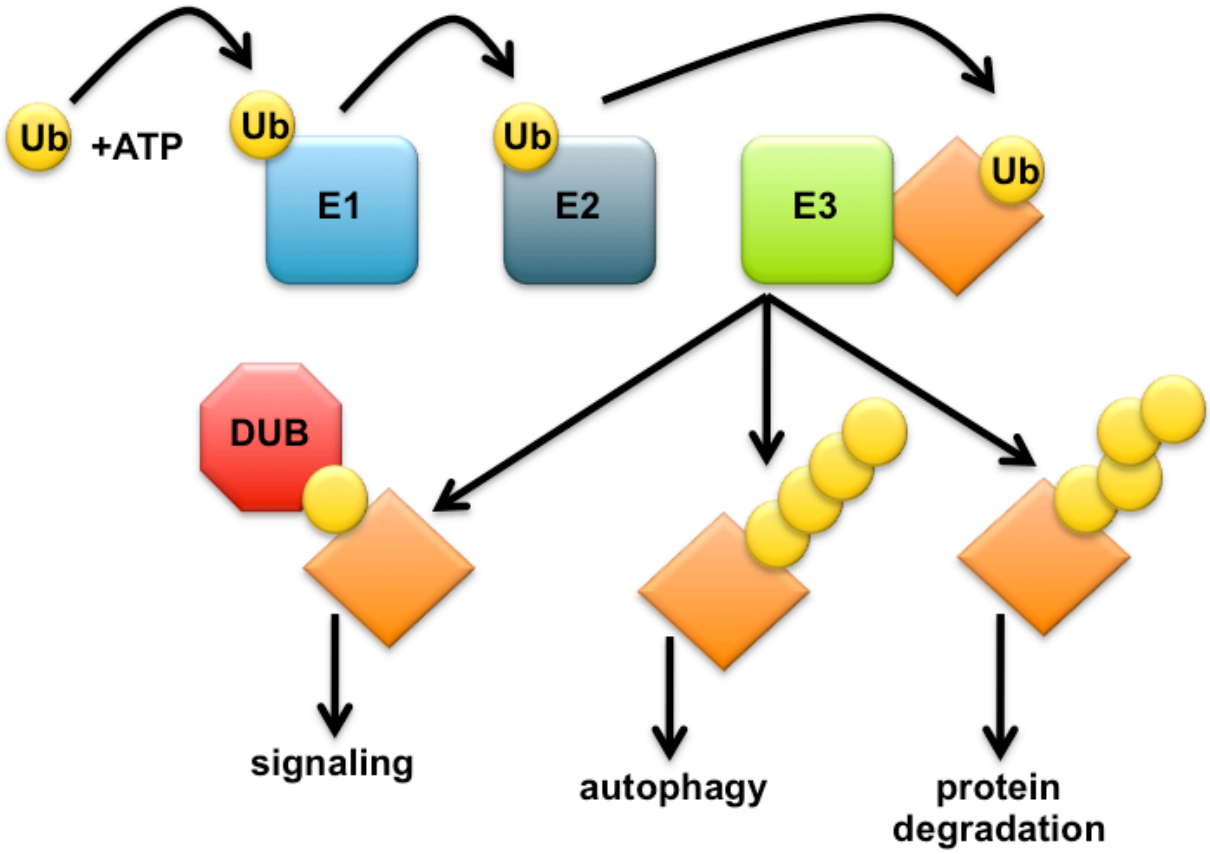

Figure 1.1. Scheme depicting ubiquitination conjugation cascade. Ub is activated in an ATP-dependent process and reacts with the active site cysteine residue on E1. Ub is then transferred to the active site cysteine on E2. The E2 and E3 enzymes cooperate to coordinate conjugation of Ub to a lysine residue on a substrate protein. Multiple rounds of ubiquitination can be used to build poly-Ub chains which are involved in multiple processes such as autophagy and protein degradation. Mono-ubiquitination of proteins often plays a role in signaling. Deubiquitinating enzymes (DUBs) reverse Ub conjugation by hydrolyzing the Ub-substrate linkage.

dependent process, Ub is activated and reacts with the active site cysteine residue on the Ub-activating enzyme (E1) to form an E1-Ub thiolester. Next, Ub is transferred from the E1 to the Ub conjugating enzyme (E2) active site cysteine. The transfer of Ub to a substrate is modulated through the activity of the Ub ligase (E3). The E3 is confers the ubiquitination substrate specificity and the mechanism of action differs between classes of E3s. Most E3 enzymes fall into the Really Important New Gene (RING) family. RING family ligases bind both the E2-Ub and the substrate to act as a bridging factor whereby Ub is transferred from the E2 to the substrate. The alternative mechanism of Ub ligation is carried out by the Homologous to E6AP Carboxy Terminus (HECT) family of E3 ligases. In this case, the HECT family E3 ligase also interacts with both the E2-Ub and the substrate; but rather than a direct transfer of Ub from the E2 to the substrate, the transference of Ub to the active site cysteine on the E3 is required prior to the final step of Ub conjugation to the substrate.

Ub is conjugated through the C-terminal carboxylate of Ub and the lysine side chain of the substrate protein, resulting in an isopeptide linkage. Because Ub itself encodes seven lysine residues (at positions 6, 11, 27, 29, 33, 48, and 63), in addition to lysine residues on other proteins, Ub may also serve as a target for Ub conjugation. In some cases, the target protein is first monoubiquitinated by the conjugation of a single Ub. Subsequently, Ub ligases can form chains of Ub by conjugating additional molecules onto the first (proximal) Ub, forming poly-Ub chains. Poly-Ub chains may be formed via linkages through a single lysine residue or by linkages through multiple different lysine residues within the same chain (branched or mixed chains), thus increasing the complexity of the Ub signal (Ye and Rape, 2009). The type of Ub chain that is formed is dictated by the E3, as certain Ub ligases specifically ligate the proximal Ub to the target protein or extend Ub chains through

particular linkage types. Notably, there is an additional class of enzymes, E4s, which function to extend poly-Ub chains (Hoppe, 2005).

The type of Ub linkage influences the fate of an ubiquitinated protein. Monoubiquitination of substrates is typically involved in cellular localization or protein-protein interactions while Lys-11 and Lys-48 linkages predominantly target proteins for proteosomal degradation. Adding to the complexity of signaling via ubiquitination, many Ub-like proteins (UBLs) have been identified such as Nedd8, Small Ub-like Modifier (SUMO), Hub1, Ufm1, Atg8, and ISG15 (van der Veen and Ploegh, 2012). These UBLs use conjugation machinery that is distinct from the Ub conjugation enzymes. Nedd8 is closest in homology to Ub (58% sequence identity) and often modifies Ub ligase components to enhance Ub conjugation. SUMOylated proteins are typically not targeted for degradation, but are involved in a variety of pathways including cell cycle and transcriptional regulation. In summary, multiple E2s and E3s, various Ub linkage types, and UBLs all contribute to the diversity of signaling achieved by the ubiquitination pathway.

1.2 Ubiquitin deconjugation

Ubiquitination is a reversible process carried out by a particular type of proteases: deubiquitinating enzymes (DUBs) (Ventii and Wilkinson, 2008). Ub deconjugation is critical in many processes. For example, substrates that are targeted for proteosomal degradation via poly-Ub chains are often deubiquitinated by proteasome-associated DUBs prior to degradation, thus allowing the Ub to be recycled and conjugated onto a new substrate. Additionally, proteins are often ubiquitinated during cellular processes such as transcription, cell cycle checkpoints, and autophagy; precise control of these processes

must be regulated by both ubiquitination and deubiquitination. DUBs have also been reported to deubiquitinate E3s that undergo auto-ubiquitination, thereby increasing the half-life of the Ub ligase by preventing Ub-mediated proteosomal degradation of the E3 (Eletr and Wilkinson, 2014).

Approximately 79 DUBs are encoded by the genome and are classified into five families: 1) Ub Specific Proteases (USP/UBP), 2) Ub C-terminal Hydrolases (UCH), 3) Ovarian Tumors (OTU), 4) Josephin domains (MJD), and 5) JAMM domain zinc-dependent metalloproteses. Notably, the USP/UBP family represents the largest group of DUBs as over 50 enzymes fall into this category. These DUBs are cysteine proteases characterized by the presence of both a highly conserved USP-fold and three catalytic residues contained within the Cys- and His-box motifs (Amerik and Hochstrasser, 2004). Mutation of any of these catalytic residues renders the DUB inactive.

The number of DUBs is small when compared to that of ubiquitinated proteins present in the cell. Therefore, regulation of DUBs must be achieved through multiple mechanisms to attain specificity. These points of regulation include subcellular localization, changes in expression, and PTMs. DUBs also achieve specificity by making direct contacts with both Ub and its substrate. For example, structural studies have shown Usp7 makes direct contacts with its substrate and Ub, indicating recognition of both Ub and the specific substrate are important for Ub hydrolysis (Hu et al., 2006). Additionally, *in vitro* studies showed Usp15 binds ubiquitinated histones with higher affinity than it binds Ub or histones alone (Long et al., 2014). Finally, many DUBs are associated with larger complexes through which regulation is mediated. In the case of Uch37, multiple mechanisms of regulation are employed to prevent promiscuous DUB activity. In one case, Uch37 is

recruited to the proteasome where auto-inhibition is relieved through an interaction with the proteosomal subunit protein, Rpn13 (Yao et al., 2006). In another mode of regulation, Uch37 is a component of the chromatin remodeling INO80 complex where its activity is repressed by the NFRKB subunit (Yao et al., 2008). Thus, DUBs may utilize multiple mode of regulation to enhance substrate specificity.

1.3 Histone post-translational modifications

In each human diploid cell, there are approximately 6 billion base pairs of DNA, which, if extended, would measure 2 meters in length. Paradoxically, this large amount of DNA needs to be compacted into the nucleus, which has an average diameter of 6 μm; therefore, a compaction of approximately 300,000-fold must occur to fit the DNA into the nucleus (Annunziato, 2013). This enigma is overcome through a mechanism of compaction whereby DNA is coiled around a set of histone proteins. This reaction is made favorable, in part, due to electrostatic interactions between negatively charged phosphate backbone of DNA and the positively charged histones. The compacted DNA is comprised of repeating units of nucleosome core particles (NCPs). NCPs are made-up of 146 base pairs of DNA wrapped around the core histone octamer, which contains of 2 copies each of histones H2A, H2B, H3, and H4 (Luger et al., 1997). Each nucleosome core particle is joined by ~20-90 base pairs of linker DNA, giving the appearance of "beads on a string" when analyzed by electron microscopy (Bei et al., 1983). Further compaction is accomplished via deposition of histone H1 onto the linker DNA, forming a thick 30-nanometer fiber (McBryant et al., 2010).

Within the cell, the machineries involved in processes such as DNA replication, DNA damage repair, and transcription require: 1) targeting to specific chromatin regions and/or 2) direct access to decondensed chromatin for functionality. Therefore, chromatin signaling, compaction, and decompaction must occur in a highly regulated manner to facilitate these processes. Much of this regulation comes in the form of histone PTMs. While histones contain a globular histone-fold domain, many of the PTMs occur within the more accessible, unstructured tail regions. These modifications include ubiquitination, acetylation, methylation, SUMOylation, phosphorylation, citrullation, and ADP-ribosylation (Arnaudo and Garcia, 2013). Preliminarily, a "histone code" was hypothesized whereby a particular combination of PTMs rigorously dictates the downstream affect (i.e. activation or repression of transcription) (Strahl and Allis, 2000). While it's true that specific patterns of histone PTMs participate in organizing particular regions of chromatin, emerging studies suggest the regulation of DNA processes by histone PTMs may involve more variables than was originally postulated.

Histone PTMs convey changes in chromatin through two major mechanisms. First, the modifications themselves can directly affect the stability of the nucleosome. For example, acetylation of lysine residues on histone tails can neutralize the positively-charged of the histone tail, effectively decreasing the affinity between the DNA and histone octamers (Hong et al., 1993). In another case, conjugation of a bulky Ub moiety to H2B (ubH2B) is antagonistic to chromatin compaction of nucleosomal arrays *in vitro* (Fierz et al., 2010). Furthermore, Fierz et al. showed that when nucleosomal arrays contained both acetylated H4 at Lys16 and ubiquitinated H2B (ubH2B), H4 acetylation predominantly exerted the adverse effect on internucleosomal interactions while the combination of

modifications worked synergistically to prevent oligomerization (intramolecular interactions) of nucleosomal arrays (Fierz et al., 2010). These data demonstrate how histone PTMs can work independently or synergistically to modulate the chromatin state through different mechanisms.

The second major method by which histone PTMs can affect downstream processes is through recruitment of effector proteins (Bottomley, 2004). Certain effector proteins "read" these PTMs using domains that interact with specific histone modifications. For example, bromodomain-containing proteins are recruited to chromatin through interactions with lysine-acetylated histone tails (Dhalluin et al., 1999; Kanno et al., 2004). In another case, many chromodomain-containing proteins are recruited to particular chromatin regions through binding of methylated histones (Jacobs and Khorasanizadeh, 2002; Nielsen et al., 2002). These effector proteins have a wide array of functions by which chromatin-mediated processes are executed including perpetuation of additional histone PTMs and recruitment of additional factors such as histone chaperones or DNA damage repair machinery. Notably, this is a relatively simplistic overview about the mechanism of histone PTMs modulation of chromatin dynamics as many additional factors are involved in regulating these dynamic processes.

1.4 Histone ubiquitination

Among the various types of histone PTMs, histone ubiquitination is particularly striking, as the modification size (~8.5 kDa) is substantially large when compared with other PTMs such as acetylation or methylation (Figure 1.2). In mammalian cells, all four core histones are modified by the attachment of a single Ub (monoUb) at particular

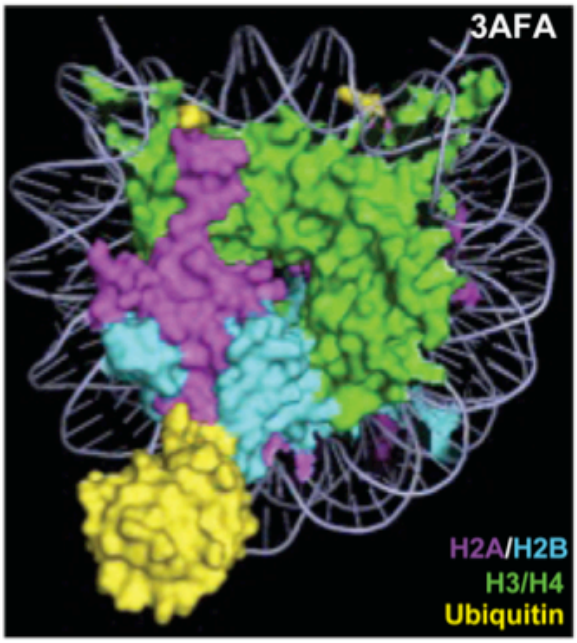

Figure 1.2. Ub modeled onto H2B within the nucleosomal structure. The crystal structure of Ub is modeled onto the site of H2B monoubiquitination within the nucleosome core particle structure (Luger et al., 1997). Ub is a remarkably large PTM when compared to other histone PTMs such as acetylation or methylation.

residues, and these modifications play roles in several specific processes (Table 1.1). In addition, linker histone H1 was also demonstrated to be ubiquitinated in *Drosophila* embryos, resulting in transactivation of a subset of genes (Pham and Sauer, 2000).

Histone H2A was the first ubiquitinated protein to be identified (Goldknopf et al., 1975) and was later realized to be one of the most abundant ubiquitinated proteins in the nucleus. While monoubiquitinated H2A (ubH2A) has not been described in *S. cerevisiae*, approximately 5-15% of total H2A in metazoans is monoubiquitinated at Lys119 (Hatch et al., 1983; Wu et al., 1981; Wunsch et al., 1987). Although only one E2 (UbcH5) has been identified to play a role in H2A monoubiquitination, multiple E3 enzymes coordinate Ub conjugation to H2A (Chen et al., 2002). These include RING1A/RING1B/BMI1, 2A-HUB, and BRCA1/BARD1, all of which fall into the RING family of Ub ligases (Cao et al., 2005; Chen et al., 2002; Gearhart et al., 2006; Zhou et al., 2008; Zhu et al., 2011). Recently reports have identified Lys13 and Lys15 as additional sites of H2A monoubiquitination although this modification seems to be less abundant than ubiquitination at Lys119 (Gatti et al., 2012; Mattiroli et al., 2012).

Monoubiquitination of H2B (ubH2B) at Lys120 (Lys123 in yeast) is fairly abundant and has broad functional roles within the cell. Approximately 1-2% of total H2B is ubiquitinated (Wu et al., 1981), and this is primarily mediated through the RING family Ub ligase heterodimer RNF20/RNF40 (orthologous to Bre1 in yeast). This E3 ligase cooperates with the E2, RAD6A/B (Rad6 in yeast), to modify H2B (Kao et al., 2004; Kim et al., 2005; Robzyk et al., 2000). Additional sites of H2B monoubiquitination include Lys34 and Lys125, although these are much less abundant than modification at K120 (Table 1.1) (Minsky and Oren, 2004; Wu et al., 2011).

Table 1.1. Histone monoubiquitination at different sites are associated with different functions.

Histone (human)	MonoUb Sites	Associated Functions	References
H2A	13, 15	DNA damage response	Mattrioli et al., 2012; Gatti et al., 2012
H2A	119	Transcription silencing and DNA damage response. Corresponding positions in H2A.X, H2A.Z, and MacroH2A1.2 have been reported to undergo similar ubiquitination.	Reviewed in Weake and Workman, 2008 and Wright et al., 2012
H2B	34	Transcription activation	Wu et al., 2011
H2B	120	Transcription initiation, elongation, pre-mRNA splicing, mRNA export	Reviewed in Weake and Workman, 2008 and Wright et al., 2012
H2B	125	Transcription repression	Minsky and Oren, 2004
H3	23	Maintenance of DNA methylation during DNA replication	Nishiyama et al., 2013
H4	31	Transcription activation	Kim et al., 2013
H4	91	DNA damage response	Yan et al., 2009

1.5 Histone deubiquitination

Many H2A and H2B DUBs have been identified. Whereas some DUBs deubiquitinate both H2A and H2B, others specifically deubiquitinate either H2A or H2B (Table 1.2). Characterizing enzymatic properties of histone DUBs has proven difficult as a obtaining a purified, ubiquitinated substrate is problematic. Using recombinantly expressed and purified E1, E2 (RAD6A/B), and E3 (RNF20/RNF40) along with Ub and H2B in an *in vitro* ubiquitination assay to obtain ubiquitinated histones are problematic for two reasons. First, the yield of ubiquitinated product is extremely low (less than 5%). Second, the E3 ligase exhibits promiscuity as reaction products contain the Ub modification at sites other

Table 1.2. Histone deubiquitinating enzymes have different substrate specificities. Substrate specificities for histone DUBs are discussed in section 1.5 and references are listed therein.

DUB	Organism	Substrate	Nucleosomal substrate	Free histone substrate
Usp16 (Ubp-M)	Human	H2A	+	-
Usp21	Human	H2A	+	-
2A-DUB	Human	H2A	+	n.d.
BAP1	Human/*Drosophila*	H2A	+	n.d.
Ubp8	Yeast	H2B	+	-
Ubp10	Yeast	H2B	n.d.	n.d.
Usp7 (HAUSP)	Human	H2B	n.d.	+
Usp44	Human	H2B	n.d.	n.d.
Usp49	Human	H2B	+	-
Usp3	Human	H2A & H2B	n.d.	n.d.
Usp4/Usp15	Human	H2A & H2B	?	?
Usp12/Usp46	*Xenopus*	H2A & H2B	+	-
Usp22	Human	H2A & H2B	+	+

than Lys120 (Kim and Roeder, 2011). Another strategy used to obtain ubiquitinated histones is by purification from tissue culture cells (Joo et al., 2007; Lee et al., 2005). This Ub-histone substrate is less than ideal as purified histones are heterogeneous due to a variety of naturally occurring PTMs. These additional PTMs could affect the efficiency or specificity of deubiquitination, thus convoluting *in vitro* deubiquitination assay results. In fact, we know that the H2A-specific DUB, 2A-DUB, more effectively deubiquitinates ubH2A-containing chromatin that also contain high levels of H3 and H4 acetylation when compared to chromatin with unperturbed acetylation levels (Zhu et al., 2007). The Brik group has combined protein ligation and peptide synthesis to generate a native ubH2B at H2BK120, H2BK34, and H2AK119 (T.Y. and A.B., unpublished results) (Long et al., 2014; Siman et al., 2013). In addition to the highly specialized and technically challenging method employed, the yield of ubiquitinated histone is extremely low. These obstacles make it

especially challenging to systematically identify and study histone DUBs. In addition to analyzing DUB substrate specificity *in vitro*, DUB activity is often assayed using *in vivo* techniques. Typically, the histone DUB is either depleted or overexpressed and changes in ubH2A and ubH2B levels are assayed by western blotting for ubH2A or ubH2B.

H2A-specific DUBs include Usp16, Usp21, 2A-DUB, and BAP1 (Joo et al., 2007; Nakagawa et al., 2008; Scheuermann et al., 2010; Shanbhag et al., 2010; Zhu et al., 2007). In each case, perturbation of the cellular levels of each DUB resulted in changes in ubH2A levels, and not ubH2B levels. With the exception of BAP1, free histone or nucleosomal substrates isolated form cellular extracts were used to assay deubiquitinating activity *in vitro*. (Scheuermann et al. used the E1, E2, E3 conjugating system to ubiquitinate H2A, which was then used in a nucleosomal substrate context to analyze Bap1-mediated histone deubiquitination.) In the case of Usp16 and Usp21, both DUBs deubiquitinated a ubH2A-containing nucleosomal substrate but could not hydrolyze Ub from free histones (Joo et al., 2007; Nakagawa et al., 2008). These data indicate one mode of histone DUB regulation may involve recognition of the ubiquitinated histones within a certain context (i.e. nucleosomal vs. free histones).

In yeast, both Ubp8 and Ubp10 have been characterized as H2B-specific DUBs (Daniel et al., 2004; Emre et al., 2005; Henry et al., 2003). Ubp8 is part of the Spt-Ada-Gcn5-Acetyltransferase (SAGA) complex, an important transcriptional co-activator. Within the SAGA complex, Ubp8 and three additional proteins (Sgf11, Sus1, and Sgf73) make-up a smaller functional unit called the DUB module ($SAGA^{DUB}$) (Kohler et al., 2010). *In vitro* and *in vivo* studies have shown Ubp8 can only deubiquitinate H2B within the context of the DUB module. (Daniel et al., 2004; Henry et al., 2003; Lee et al., 2005). While Ubp10 also

deubiquitinates H2B *in vitro* and *in vivo*, data suggest Ubp8 and Ubp10 act on different subsets of ubH2B in the cell. This was demonstrated by the fact that a Δubp8Δubp10 yeast strain results in a more dramatic increase in ubH2B when compared to deletion of either Ubp8 or Ubp10 alone (Emre et al., 2005). Furthermore, Ubp8 and Ubp10 localize to distinct DNA loci, supporting the hypothesis that multiple histone DUBs exist to fine tune the regulation of histone deubiquitination through mechanisms such as localization and substrate specificity.

Other H2B-specific DUBs include Usp7 (HAUSP), Usp44, and Usp49 (Fuchs et al., 2012; van der Knaap et al., 2005; Zhang et al., 2013). Proper temporal regulation of H2B deubiquitination by Usp7 and Usp44 are required for proper development. Specifically, in *Drosophila,* Usp7 is critical in silencing homeotic genes (van der Knaap et al., 2005) while in human and mouse embryonic stem cells (ESCs), diminished Usp44 levels correspond with an increase in ubH2B levels. Perturbation of ubH2B homeostasis results in ESC differentiation defects (Fuchs et al., 2012). On the other hand, Usp49 perturbation has incremental effects upon gene expression but has been identified as playing a major role in the regulation of differential splicing (Zhang et al., 2013).

In addition to H2A and H2B-specific histone DUBs, multiple DUBs have been characterized that deubiquitinate both H2A and H2B including Usp3, Usp12/Usp46, and Usp22 (Joo et al., 2011; Nicassio et al., 2007). Deubiquitination of histones by Usp3 is required for progression through S phase and genome stability (Nicassio et al., 2007). Usp12/Usp46 regulate ubH2B levels at specific promoters during *Xenopus* development (Joo et al., 2011). Like its yeast ortholog Ubp8, Usp22 is a component of the $SAGA^{DUB}$ in

humans and has been shown to play a role in transcription activation, cell cycle progression, and mRNA export (Kohler et al., 2008; Zhang et al., 2008; Zhao et al., 2008).

1.6 Usp15

Usp15 is one of the most recent members of the histone DUB family (Long et al., 2014). It is classified as a USP/UBP DUB and contains an N-terminal Domain present in Ub Specific Proteases (DUSP) domain, two Ub-Like (UBL) domains, and three residues that function as the catalytic triad. Usp15 is part of a subfamily comprised of Usp4 (61% sequence identity) and Usp11 (32% sequence identity), which are characterized by the presence of both a DUSP domain and UBL domains (collectively called DU). Additionally, Usp15 contains a Zn finger necessary for deconjugating poly-Ub chains (Hetfeld et al., 2005).

Although the structure of full-length Usp15 has not yet been solved, NMR and crystal structures of particular domains has revealed specific intra- and inter-molecular interactions. The N-terminal DU domain of Usp15 and Usp4 interact in tandem and the UBL domain is unlikely to play a role in regulation through an auto-inhibition mechanism (Harper et al., 2011). In agreement with Harper et al. (2011), a recent study showed that neither the N-terminal or C-terminal UBL domains had an auto-inhibitory effect on Usp11 (Harper et al., 2014).

Unlike Usp15, Usp4 has a deep hydrophobic pocket within the DUSP domain that could contribute to differences in substrate specificity between Usp4 and Usp15 (Harper et al., 2011). Despite this difference, there is a large overlap of Usp4/Usp15 interacting proteins (Sowa et al., 2009). Usp4 shuttles between the nucleus and cytoplasm using NES

and NLS signals recognized by importin α/β (Soboleva et al., 2005). Although NLS and NES sequences have not been explicitly characterized, immunofluorescence staining shows Usp15 localizes to both the nucleus and cytoplasm (Long et al., 2014). In accordance, both cytoplasmic- and nuclear-localized substrates have been identified for Usp15.

Like many other DUBs, Usp15 can function alone or as part of a larger complex. Usp15 is part of the large COP9 signalosome (CSN) complex. The CSN is comprised of 8 subunits and is significantly similar to the 26S proteasome lid in both sequence and structure (Hetfeld et al., 2005). The large CSN participates in a wide array of processes, including deneddylation of the cullin family of Ub ligases. Within the context of the CSN complex, Usp15 deubiquitinates and stabilizes the cullin Ub ligase, Rbx1 (Emre et al., 2005). Usp15 also stabilizes other E3 Ub ligases, including Keap1 and RNF40 (Long et al., 2014; Villeneuve et al., 2013).

Other substrates of Usp15 include factors involved in the immune response such as Tripartite Motif protein 25 (TRIM25) and cell growth like TGF-β type I receptor (TβRI) (Eichhorn et al., 2012a; Pauli et al., 2014). Usp15 is also involved in the regulation of transcription through deubiquitination and stabilization of transcription factors such as RE1 Silencing Transcription factor (REST) and SMAD proteins (Faronato et al., 2013; Inui et al., 2011).

Recently, Usp15 was described as a histone DUB (Long et al., 2014). Unlike Usp22, Usp15 preferentially deubiquitinates ubH2B-containing histone octamer rather than ubH2B-containing mononucleosomes. These results could have further implications in defining substrate specificity between the multiple histone DUBs present in the cell.

1.7 The role of ubH2A in transcription and DNA damage repair

As previously mentioned, ubH2A is not present in yeast but exists in metazoans. Primarily, ubH2A is vital for transcriptional repression and DNA damage repair. Strikingly, ubH2A is localized to transcriptionally silent regions of chromatin, such as the telomeres and the inactivated X chromosome (Fang et al., 2004). Correspondingly, H2A Ub ligases are associated with repressive complexes such as the Polycomb Repressive Complex 1 (PRC1), which is targeted to regions of chromatin bearing H3K27me3 (a modification antagonistic to transcription initiation) (Cao et al., 2005; Wang et al., 2004). UbH2A-mediated transcriptional repression is refereed through multiple mechanisms. First, ubH2A facilitates the compaction of chromatin through the recruitment of the linker histone H1 (Zhu et al., 2007). Within the context of a nucleosome, the C-terminal tail of H2A, where monoUb attaches, is predicted to juxtapose the globular domain of H1, perhaps facilitating deposition of H1 through direct interactions (Luger et al., 1997). Indeed, *in vitro* studies showed ubH2A-containing nucleosomes enhanced binding of H1 to linker DNA when compared to nucleosomes containing unmodified H2A (Jason et al., 2005).

A second method by which ubH2A represses transcription is through the inhibition of Facilitates Chromatin Transcription (FACT) recruitment (Zhou et al., 2008). FACT is an H2A/H2B histone chaperone comprised of two subunits: Spt16 and SSRP1 (Winkler et al., 2011). FACT plays a critical role in chromatin reorganization in processes such as transcription, DNA damage repair, and DNA replication where chromatin remodeling is paramount. Because FACT recruitment is essential for transcription elongation through a chromatin template, it's not surprising that ubH2A-mediated inhibition of FACT recruitment results in transcriptional repression (Orphanides et al., 1999).

UbH2A is required for signaling in the nucleotide excision repair (NER) pathway, although the role of ubH2A at sites of DNA damage is somewhat controversial. One theory suggests that ubH2A signals to recruit DNA damage repair machinery during nucleotide excision repair (NER) (Bergink et al., 2006). Another theory stems from studies demonstrating that ubH2A is recruited to sites of DNA damage by the histone chaperone, CAF-1, and the modified ubH2A persists for a substantial amount of time after UV irradiation, suggesting ubH2A marks sites of prior DNA damage repair (Zhu et al., 2009). Additionally, the histone variants H2A.X and H2A.Z are monoubiquitinated at the residue equivalent to Lys119 in H2A, and this modification is also associated with transcriptional silencing and DNA damage repair.

1.8 The role of ubH2B in transcription

Unlike ubH2A, ubH2B is typically associated with activation of transcription. The mechanism of ubH2B-regulated transcription is highly debated as ubH2B has also been described to have a role in transcriptional repression. Presented below is a description of some of the most critical studies used to decipher the mechanism of ubH2B-regulated transcription.

Nucleosome stability vs. nucleosome instability—Many approaches have been used to answer the question of whether ubH2B promotes nucleosome stability or nucleosome instability. Because ubH2B promotes transcription elongation and the core histones are removed during transcription to facilitate RNAPII processivity, some hypothesized conjugation of a bulky Ub moiety may contribute to nucleosome instability (Schwabish and Struhl, 2004; Weake and Workman, 2008). *In vitro* studies showed ubH2B had only

moderate effects on mononucleosome stability when compared to mononucleosomes containing unmodified H2B (Fierz et al., 2012b). In a more complex *in vitro* system, nucleosomal arrays showed ubH2B prevented inter- and intra-nucleosomal interactions while conjugation of a Ub-like protein, Hub1, to H2B had no effect on chromatin compaction (Fierz et al., 2010). These data suggest the mechanism of Ub-mediated chromatin decompaction cannot simply be attributed to the bulkiness of Ub.

Alternatively, another study analyzed the role of ubH2B on nucleosome stability *in vivo* and concluded that ubH2B stabilized nucleosomes (Chandrasekharan et al., 2009). In agreement with Fierz et al., Ub did not affect transcription by acting as a "wedge" to destabilize chromatin because conjugation of another Ub-like protein, SUMO, did not affect chromatin stability. Chandrasekharan and colleagues found ubH2B was increased in both ORFs of actively transcribed genes and promoters of transcriptionally repressed genes. It was suggested that ubH2B plays a role in elongation of active genes by acting as a "platform" to bind elongation factors and regulates transcription initiation by stabilizing nucleosomes at promoters. Currently, the predominantly accepted model is ubH2B acts as a platform to recruit specific ubH2B-interacting proteins (Shema-Yaacoby et al., 2013).

Transcription activation: elongation—Several lines of evidence point to ubH2B as a point of regulation for transcription elongation. Initially, Rad6 and Bre1 (RAD6A/B and RNF20/RNF40 in humans) were identified as localizing to promoters of actively transcribed genes (Henry et al., 2003; Wood et al., 2003a). Further evidence for a positive role for ubH2B in elongation was that the H2B ubiquitination machinery travels along with RNAPII upon transcription activation, and this is accompanied by an increase in ubH2B in ORFs (Xiao et al., 2005). Abolishment of Ser5 phosphorylation of the RNAPII C-terminal

domain (CTD), a mark seen in early elongation, abrogates H2B ubiquitination. The role for ubH2B in transcription elongation was further emphasized as perturbation of ubH2B levels during ESC differentiation most notably affected transcript levels of relatively long genes where effective elongation processivity is particularly critical (Fuchs et al., 2012).

Processive elongation via ubH2B is mediated by several different factors. *In vitro* and *in vivo*, recruitment of the H2B ubiquitination machinery to promoters is not sufficient to obtain ubH2B (Pavri et al., 2006; Wood et al., 2003b; Xiao et al., 2005). Rather, elongation factors such FACT and the Polymerase Associated Factor (PAF) complex are additionally required for H2B ubiquitination. Additionally, *in vitro* transcription assays using purified factors showed ubH2B, FACT, and the PAF complex are absolutely required for the elongation phase of transcription (Pavri et al., 2006). Mechanistically, ubH2B likely recruits the histone chaperones FACT and SWI/SNF, which then promote transcription elongation via chromatin remodeling (Pavri et al., 2006; Shema-Yaacoby et al., 2013). In addition to nucleosome disassembly, ubH2B and FACT are required for nucleosome reassembly in the wake of elongating RNAPII (Fleming et al., 2008; Pavri et al., 2006). *In vivo*, ubH2B is required for nucleosome reassembly in ORFs (Chandrasekharan et al., 2009). Abolishment of either FACT or ubH2B results in transcription initiation from cryptic starts sites and an increased RNAPII elongation rate, and this is attributed to poor reassembly of nucleosomes (Fleming et al., 2008; Kaplan et al., 2003). Reciprocally, transcription elongation stimulates H2B ubiquitination in that phosphorylation of the RNAPII CTD Ser5 by Cdk9 (Bur1/Bur2 in yeast) promotes H2B ubiquitination (Laribee et al., 2005; Shchebet et al., 2012; Wood et al., 2005). Furthermore, H2B ubiquitination and

Cdk9 seem to work in a positive feedback loop as ubH2B enhances Cdk9 recruitment and Cdk9 promotes H2B ubiquitination (Sanso et al., 2012).

Transcription activation: methylation-dependent vs. -independent elongation: Another mechanism by which ubH2B promotes transcriptional elongation is through recruitment of histone methyltransferases. Histone H3 methylation at specific sites are associated with active transcription (H3K4me and H3K79me) while methylation at other sites are associated with repressed transcription (H3K9me and H3K27me). Initially, it was described that ubH2B mediated elongation by promoting H3K79 trimethylation (H3K79me3) by the methyltransferase, Dot1 (DOT1L in mammals) (Ng et al., 2002). Others showed ubH2B is required for H3K4me3 and H3K79me3 by the Set1 and Dot1 methyltransferases, respectively (Wood et al., 2003b). Histone methylation by these complexes is mediated through both direct interactions between ubH2B and the methyltransferase and by ubH2B-mediated stimulation of methyltransferase activity (Lee et al., 2007).

In contrast, there are reported instances where ubH2B stimulates elongation independent of histone methylation. Specifically, ubH2B depletion displayed defects in RNAPII elongation, independent of H3 methylation status. Reciprocally, H3 methlylation in the absence of ubH2B isn't sufficient to promote proper transcriptional elongation (Shukla and Bhaumik, 2007). Together, these data suggest ubH2B may promote elongation via histone methylation on a subset of genes while, in other cases, ubH2B uses alternative methods to promote transcription activation.

Transcription repression: Although ubH2B promotes transcriptional elongation via multiple mechanisms, instances of ubH2B-mediated transcriptional repression have also

been reported. Depletion of one subunit of the H2B E3 ligase, RNF20, causes a global decrease in ubH2B. Microarray expression analysis of RNF20-depleted cells showed that while the majority of transcripts were unaffected by RNF20 depletion, a subset of genes was repressed (Shema et al., 2008). Interestingly, despite the decrease in transcript levels, RNAPII levels within the coding regions was high, suggesting a defect in elongation. Correspondingly, a subset of genes was activated upon RNF20 knockdown (ubH2B was antagonistic to transcription), indicating dual roles for ubH2B in transcription.

In another study, Shema *et al.* showed ubH2B inhibits recruitment of TFIIS, a factor primarily responsible for promoting elongation from stalled RNAPII complexes (Shema et al., 2011). Just as the H2B ubiquitination machinery associates with elongating RNAPII, USP22 (Ubp8 in yeast), a component of $SAGA^{DUB}$, is a histone DUB that also travels along with RNAPII during elongation. In fact, *in vivo* studies have shown that, in addition to H2B ubiquitination, deubiquitination of H2B is also required for proper elongation (Emre et al., 2005). Specifically, Ubp8 is required for recruitment of the RNAPII Ser2 kinase, Ctk1 (CTDK1 in metazoans), which is a mark associated with transcription initiation (Wyce et al., 2007). Together, these data suggest that, in addition to promoting elongation, ubH2B may induce RNAPII pausing and serve as a "checkpoint" before initiation of progressive elongation. Together, these data suggest that dynamic ubiquitination and deubiquitination of H2B is required for productive elongation.

1.9 The role of ubH2B in DNA damage repair and DNA replication

Although ubH2A has been most strongly associated with DNA damage repair, ubH2B also plays a role in this pathway. Upon induction of DNA double strand breaks

(DSBs), RNF20/RNF40 ubiquitinates H2B and this monoubiquitination is required for repair through both the nonhomologous end joining (NHEJ) and homologous recombination repair (HRR) pathways (Moyal et al., 2011; Nakamura et al., 2011).

A role for ubH2B has also been described during DNA replication. UbH2B and RNF20/RNF40 are localized to origins of replication. While ubH2B is not required for initiation of replication, it is required for replication processivity and subsequent S-phase progression. As previously mentioned, ubH2B cooperates with FACT to reassemble nucleosomes in the wake of elongating RNAPII. Similarly, ubH2B is required for FACT recruitment and deposition of nucleosomes on newly synthesized DNA (Trujillo and Osley, 2012).

1.10 The role of ubH2B in mRNA splicing, processing, and export

One of the earlier reports of ubH2B's involvement in mRNA processing came when Narita *et al.* found that knockdown of CDK9 or RNF20/RNF40 resulted in an increase in polyadenylated histone mRNAs (Narita et al., 2007). Additional studies identified enrichment of RNF20/RNF40 and ubH2B at the 3' end cleavage site of the *HIST1H2BD* gene and depletion of CDK9 impaired recruitment of splicing factors to this site (Pirngruber et al., 2009b). Others showed inhibition of H2B ubiquitination resulted in an accumulation of polyadenylated mRNAs in the nucleus and this was caused by defects in mRNA processing and export (Vitaliano-Prunier et al., 2012). Roles for H2B deubiquitination in mRNA export have also been suggested as Sgf73 (Ataxin7 in mammals), a component of $SAGA^{DUB}$ is involved in recruitment of mRNA export machinery (Kohler et al., 2008).

Schor *et al.* demonstrated chromatin structure plays a role in regulating binding of splicing factors. This group showed perturbation of chromatin structure through various methods (such as histone hyperacetylation, chromatin decompaction, and inhibition of transcription) inhibited proper recruitment of splicing factors to nascent RNA (Schor et al., 2012). A role of ubH2B in pre-mRNA splicing in yeast was highlighted upon the discovery that combining a strain where H2B could not be ubiquitinated (*htb-K123R*) with deletion of components of the U2 snRNP resulted in lethality (Shieh et al., 2011). Further studies showed ubH2B (but not H3K4me3 or H3K79me3) recruits early splicing factors such as U1 and U2 snRNPs onto nascent RNA (Herissant et al., 2014). ChIP-seq analysis showed ubH2B levels are increased at intron/exon boundaries of highly expressed genes and high levels of ubH2B is correlated with exon skipping (Jung et al., 2012). Relatedly, knockdown of Usp49 resulted in an increase in ubH2B and, correspondingly, an increase in alternative splicing. This was accompanied by a reduction in splicing factors binding to nascent RNA and chromatin and a concomitant decrease in splicing efficiency (Zhang et al., 2013). Possible mechanisms for ubH2B-medated regulation of pre-mRNA splicing are discussed in Chapter 5.

1.11 Pre-mRNA splicing

In higher eukaryotes, a large number of transcribed genes contain exons and introns. To ultimately obtain a functional protein, introns from nascent RNAs must be removed. Additionally, inclusion or exclusion of exons in alternative splicing increases the number of protein isoforms, escalating the degree of complexity encoded within the genome.

A complex network of proteins and catalytic RNAs, called snRNPs, modulate splicing (Wahl et al., 2009). As the nascent RNA emerges from the elongating RNAPII, it is bound by Serine-Arginine (SR) proteins. SR proteins typically contain a RS (Arg-Ser repeat) domain and multiple RNA-recognition motifs (RRMs), which mediate interactions between RNA and SR proteins. In general, the splicing machinery forms four distinct complexes to execute removal of introns or alternative exons: complexes E, A, B, and C (Figure 1.3) (Chen and Manley, 2009). Intron/exon regions typically encode four RNA sequence elements that are recognized by the splicing machinery: 5' splice site, branch point sequence (BPS), polypyrimidine tract (PPT), and the 3' splice site. Initially, the U1 snRNP binds the 5' splice site while the splicing factor 1 (SF1) recognizes the branch point. The U2AF snRNP interacts with both the PPT and 3' splice site to complete the formation of Complex E. Progression into Complex A is mediated by displacement of SF1 followed by the U2 snRNP binding to the BPS. Next, the U4/U6.U5 tri-snRNP is recruited to the emerging splicesosome to form Complex B. Upon catalytic activation, the spliceosome undergoes rearrangements where the interaction between U6 and U4 is destabilized and while U2 and U6 undergo base pairing. The U2, U5, and U6 snRNPs form the catalytic splicing unit (Complex C). Following catalysis, U2, U5, and U6 are released from the spliced RNA. The lariat intron is degraded by nucleases while the pre-mRNA is destined for further processing and export.

The work presented herein will focus on the identification of unmodified and ubiquitinated histone binding proteins. Additionally, the functional relationship between SART3 and Usp15 with regards to histone deubiquitination is explored. These studies

provide further insight into the mechanisms by which histone ubiquitination and deubiquitination governs chromatin-regulated processes in the cell.

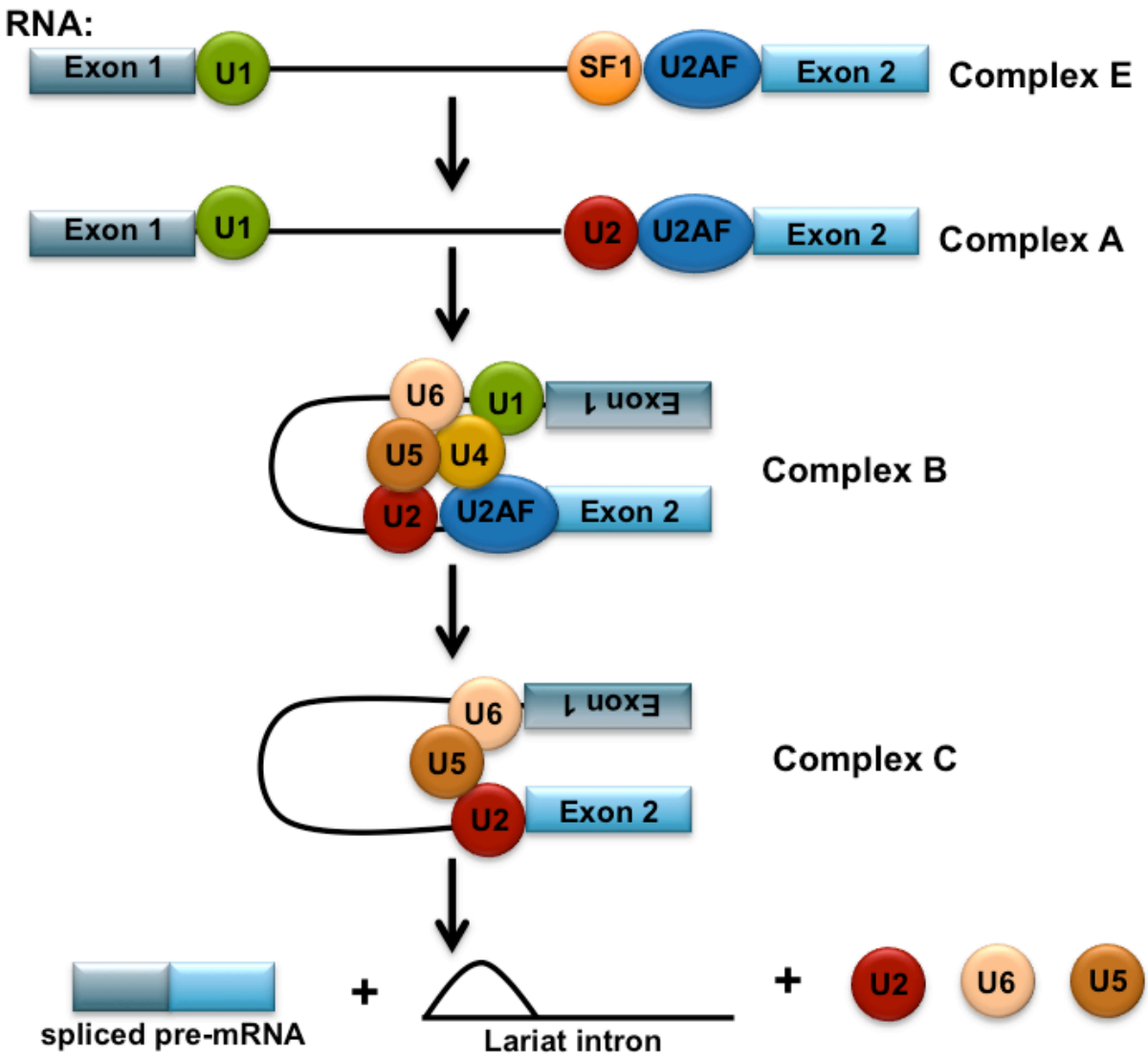

Figure 1.3. Schematic of splicing mechanism. The splicing snRNP complexes U1, SF1, and U2AF bind regulatory sequences on the unspliced pre-mRNA to form Complex E. In Complex A, SF1 is displaced and U2 binds the branch point sequence. Complex B is formed by the recruitment of the tri-snRNP (comprised of U4/U6.U5) to the assembling spliceosome. The spliceosome undergoes rearrangement, resulting in the formation of the catalytic splicing unit in Complex C. Finally, the two exons are spliced together and the lariat intron and U2, U5, U6 are released. The spliced pre-mRNA is destined for further processing while the lariat intron is rapidly degraded.

CHAPTER 2: GENERATION OF NONHYDROLYZABLE UBIQUITIN-HISTONE MIMICS

[1]Histone proteins undergo various types of post-translational modifications (PTMs) to regulate dynamic processes in the cell, including transcription and DNA damage repair. One type of histone PTM is the attachment of a small protein, ubiquitin (Ub). In eukaryotic organisms, a single Ub is attached to specific lysine residues of histones H2A and H2B in a modification that, unlike many other forms of ubiquitination in the cell, does not signal degradation. Instead, both attachment and removal of a single Ub (monoUb) to histones has been shown to affect gene transcription, pre-mRNA splicing, and DNA damage repair, but the mechanistic details by which histone ubiquitination governs these processes is not well understood. In an effort to identify "readers" of Ub-histones, we developed a straightforward crosslinking strategy to generate nonhydrolyzable Ub-histone mimics. These mimics were assembled into Ub-histone-containing dimers or nucleosomes. We demonstrate that they can be used in pulldown assays to identify proteins that differentiate unmodified and ubiquitinated histones. Additionally, Ub-histone mimics were used to examine inter- and intra-molecular interactions of Ub-histone-containing H2A/H2B dimers and nucleosomes.

2.1 Introduction

Histones undergo a variety of post-translational modifications, including phosphorylation, acetylation, methylation, citrullation, and ubiquitination (Kouzarides,

[1] This chapter is related to Long, L., Furgason, M., and Yao, T. (2014) Generation of nonhydrolyzable ubiquitin-histone mimics. Methods. (Submitted for review in April 2014). Figure 2.1 is included in the submitted manuscript. Furgason, M. developed the Ub-histone cross-linking method. I carried out all the experiments described in the rest of the chapter.

2007; Patel and Wang, 2013). Addition and removal of these modifications is crucial for the proper regulation of many cellular processes including DNA damage repair, DNA replication, and transcription. Although many of these modifications have been correlated with specific events in the cell, in many cases, the mechanisms by which these modifications are modulated remain elusive. One approach used to untangle these detailed mechanisms is to identify proteins that preferentially bind either the modified histone or the unmodified histone, in effect, identifying modulators of histone modification-driven events. Typically, biotinylated synthetic histone peptides that have been methylated, acetylated, or phosphorylated at specific residues are incubated with nuclear extract and bound proteins are identified using LC-MS/MS.

In metazoans, both histone H2A and H2B are monoubiquitinated at specific lysine residues (K119 and K120, respectively) (Osley, 2006). Whereas H2A ubiquitination is associated with transcriptional repression and silencing, H2B ubiquitination is associated with actively transcribed regions and has multiple roles in initiation, elongation and mRNA processing (reviewed in (Weake and Workman, 2008; Wright et al., 2012)). Both H2A and H2B ubiquitination have also been implicated in DNA double strand break (DSB) repair (Pinder et al., 2013). Additionally, H2B ubiquitination has been reported to enhance nucleosome assembly during DNA replication in yeast (Trujillo and Osley, 2012). Despite accumulating evidence of the functional significance of histone ubiquitination, surprisingly little is known about how the modification elicits specific functions. This is in part due to difficulty in obtaining chemically-defined Ub-histone conjugates for *in vitro* studies.

The identification of ubH2A and ubH2B effectors through pull-down studies has proven problematic as obtaining large amounts highly purified monoubiquitinated

histones is difficult. First, purification of ubiquitinated histones from cell extracts results in isolation of a heterogenous population of histones, which in addition to monoubiquitinated H2A and H2B, contain a variety of naturally occurring PTMs. Secondly, preparing ubiquitinated histones using the E1, E2, and E3 system *in vitro* results in a low yield of ubiquitinated histones, making biochemical studies with these substrates difficult (Kim et al., 2009; Kim and Roeder, 2011). This is further complicated by the fact that the product formed by ubiquitination with the native enzymes results in the additional conjugation of Ub at sites other than H2BK120 (Kim and Roeder, 2011). Hydrolyzable forms of ubH2A and ubH2B have been synthesized using both protein ligation and peptide synthesis, but these methods are cumbersome and technically challenging (Fierz et al., 2012b; Haj-Yahya et al., 2012; Kumar et al., 2011; Long et al., 2014; McGinty et al., 2008). To overcome these obstacles, we have developed a strategy to synthesize a nonhydrolyzable ubiquitinated histone mimic that we can purify in large amounts to homogeneity and is impervious to deubiquitination in the presence of cellular extracts. Here we describe in detail the method of producing these ub-histone mimics and offer examples of using these mimics to understand how the Ub modification modulates chromatin structure and function.

2.2 Experimental Procedures

2.2.1 Generation of ubiquitinated histone mimics

Expression and purification of recombinant proteins—A 6xHis tag was inserted at the N-terminus of Ub to facilitate purification of Ub-histone crosslinked products. To express His6-Ub(G76C), BL21(DE3) *E. coli* bearing the expression plasmid were grown to log phase and expression was induced with 0.4 mM IPTG at 37 °C for 3 h. Cell lysis (Protocol 9) and

batch purification under native conditions using Ni-NTA agarose (Protocol 12) were performed according to the manufacturer's protocol (QIAGEN, 2003). The only modification was that all buffers were supplemented with 5 mM β-mercaptoethanol (βME). Eluates were then dialyzed against 10 mM Tris, pH 8.0, 50 mM NaCl, 0.2 mM EDTA, 10 mM βME at 4 °C overnight. To remove minor impurities, dialyzed eluates were passed through Q Sepharose Fast Flow resin (GE Healthcare). His6-Ub(G76C) remained in the flow-through, which was dialyzed exhaustively against 1 mM HOAc before lyophilization. The use of 1 mM HOAc in the final step prior to lyophilization helps to prevent oxidation of cysteine thiols. Typically, 200 mg of purified proteins were obtained from 4-liter cultures.

Site-directed mutagenesis was used to introduce the K119C mutation in human H2A. Mutant histones were expressed and purified according to Dyer et al. (Dyer et al., 2004) with the modification that they were dialyzed in 1 mM HOAc before lyophilization.

Crosslinking—Lyophilized His6-Ub(G76C) or H2A(K119C) was resuspended in 10 mM HOAc, 7 M urea at ~10 mg/mL, as the crosslinking reaction is more efficient when the reactants are at high concentrations. As a quality control step, Ellman's reagent (5,5'-dithio-bis-(2-nitrobenzoic acid), also known as DTNB) was used to determine the percentage of cysteines in the reduced state for each batch of purified protein. Briefly, an aliquot of dissolved His6-Ub(G76C) or H2A(K119C) is diluted in stock buffer (100 mM NaPi, pH 7.5, 1 mM EDTA) to a final concentration of 25 mM. 1 mL of the diluted protein is then mixed with 0.5 mL of 0.4 mM DTNB at room temperature for 30 min. A yellow color will develop and absorbance at 412 nm is measured to determine the sulfhydryl concentration using an extinction coefficient of 14150 $M^{-1}cm^{-1}$. Subsequently, sulfhydryl concentrations are used in place of protein concentrations to reflect true concentrations of the reactants.

Pilot-scale crosslinking reactions were performed with varying Ub:histone ratios to determine the optimal condition with each protein preparation (Figure 2.1B). We found that a Ub:histone molar ratio of 1:2 usually gave the highest yield. A typical crosslinking reaction is performed as follows:

(1) Mix dissolved His6-Ub(G76C) and H2A(K119C) at 1:2 molar ratio (i.e., in terms of reduced-cysteine concentrations) in 50 mM sodium tetraborate, pH 8.5, 6 M urea.

(2) Add 1 M TCEP (tris(2-carboxyethyl)phosphine) stock (adjusted to neutral pH) to reach 5 mM final concentration and incubate at room temperature for 30 min.

(3) Freshly prepare 0.1 M 1,3-dichloroacetone in *N,N'*-dimethylformamide. Add an amount of crosslinker equal to one-half of the total sulfhydryl groups in the reaction. After incubation on ice for 30 min, the reaction is stopped with the addition of 5 mM βME.

The resulting products contain a mixture of unreacted Ub and H2A, Ub*Ub, ub*H2A and H2A*H2A; these are separated in the subsequent purification steps.

Purification of the Ub-histone mimic—Unreacted histones are removed by nickel affinity purification. The crosslinking reaction was diluted 1:10 in denaturing binding buffer (50 mM NaPi, pH 8, 300 mM NaCl, 6 M urea, 10 mM imidazole, 5 mM βME) and incubated with Ni-NTA agarose at 4 °C for 1 h. After extensive washes with the binding buffer, bound proteins were eluted with the binding buffer supplemented with 250 mM imidazole (Figure 2.1C). Eluates will contain Ub, Ub*Ub and ub*H2A. The presence of Ub and Ub*Ub will not interfere with subsequent refolding of histone dimers or octamers. The mixture can be dialyzed into water and lyophilized for long-term storage. Alternatively, it can be directly used in the subsequent refolding steps without change of buffer.

Reconstitution of histone dimers or octamers containing Ub-histone mimics—Reconstitution of histone dimers or octamers was done as described by Dyer *et al.* (Dyer et al., 2004). Lyophilized proteins were resuspended in unfolding buffer (6 M guanidinium hydrochloride, 20 mM Tris, pH 7.5, 5 mM DTT) and allowed to unfold for at least 30 min prior to determining protein concentration by measuring the absorbance at 276 nm. As the eluates from the nickel affinity purification contain a mixture of Ub-containing species, the concentration of ub*H2A was estimated by SDS-PAGE and Coomassie staining. For dimer reconstitution, ub*H2A and H2B were mixed at equal molar ratio. Slight excess of H2B can be used to ensure all ub*H2A is incorporated into the dimer. For octamer reconstitution, ub*H2A, H2B, H3 and H4 were mixed at equal molar ratio. Total protein concentration should be ~ 2 mg/mL. These mixtures were then dialyzed into refolding buffer (10 mM Tris, pH 7.5, 2 M NaCl, 1 mM EDTA, 5 mM βME).

After refolding, histone dimers or octamers were purified by gel filtration on a Superdex 75 or Superdex 200 column, respectively (Dyer et al., 2004). Typically, excess histones will elute as aggregates in the void volume, whereas the much smaller Ub and Ub*Ub will elute later (Figure 2.1D). Purified dimers or octamers are concentrated to ~ 3.5 mg/mL with Amicon Ultra Centrifugal filters. Octamers were supplemented with glycerol to 20% v/v and stored at -80 °C in small aliquots.

2.2.2 Assembly of mononucleosomes

Purification of 147 bp DNA—The 147 bp fragment containing the 601 nucleosome positioning sequence was purified as previously described (Dyer et al., 2004).

Amplification and purification of biotinylated 183 bp DNA—The biotinylated 183 bp DNA fragment containing the 147 bp 601 positioning sequence was amplified by PCR (Forward primer: 5'-GCTGTTCAATACATGCACAGGATGTATATATC-3', Reverse primer: 5'-Biotin-TACACGTACTAGAAGCTTCCCTGGAGAATCCCGGTGC-3'). 1 ng of pGEM 601 was used as the DNA template in a PCR mixture containing 450 nM of each forward and reverse primers, 200 μM dNTPs, 5 uL DMSO, 1x Dream Taq buffer, and 0.5 μL Dream Taq in a final volume of 100 μL. The amplification cycle was as follows:

1) 4 minutes at 94 °C
2) 30 seconds at 94 °C
3) 30 seconds at 61 °C
4) 40 seconds at 72 °C
    - Repeat steps 2-4 for 40 cycles
5) 10 minutes at 72 °C
6) Hold at 10 °C

PCR products were purified on a Mono Q column using a 0.46-0.82 M linear gradient of NaCl over 20 column volumes in a buffer of 20 mM Tris, pH 7.5, and 0.1 mM EDTA. The desired biotinylated 183 bp (B-183mer) eluted from the column at approximately 71% B (0.74 M NaCl) (Figure 2.5B). Elution fractions were pooled and 2.5 times of 100% EtOH (v/v) was added to the elutions and incubated at -20 °C for at least 1 hour. The solution was then transferred to 1.7 mL eppie tubes. Glycogen was added at 20 μg/mL prior to centrifugation at 14,000 xg at 4 °C for 30 minutes. DNA pellets were washed twice with 70% EtOH, air dried, and resuspended in TE buffer (10 mM Tris, pH 8.0, 0.1 mM EDTA). We obtained a yield of approximately 285 μg of B-183mer from 50 PCR reactions.

Assembly of mononucleosomes containing unmodified histones and Ub-histone mimics—Histone octamers containing ub*H2A (at K119) or ub*H2B (at K120) were assembled into mononucleosomes by salt dilution (McGinty et al., 2008). Dilution buffers were supplemented with 0.1 mg/mL BSA. For nucleosomes assembled using the B-183mer DNA fragment, reactions were diluted in dilution buffer #1 (10 mM Tris, pH 7.6, 1 mM EDTA) only until the final NaCl concentration was 250 mM (final volume of 80 µL per reconstitution). DNA and histone octamers were mixed at an initial concentration of 1.5 µM. (For assembly of nucleosomes with the 147 bp DNA, an initial concentration of 1.15 uM of DNA and octamer was used.) Mononucleosomes were assembled at DNA:octamer ratios of 1:1, 1:1.2, 1:1.4, and 1:1.6 to determine the ideal DNA:octamer ratio. Nucleosomes were separated on a 6% TBE gel and visualized by EtBr staining.

Immobilization of B-183mer nucleosomes to magnetic strepavitdin beads—124.5 µg of Dynabeads (Dynabeads® MyOne™ Streptavidin T1, Invitrogen) were washed once with 50 µL of 1x B&W buffer (5 mM Tris, pH 7.5, 0.5 mM EDTA, 1 M NaCl) and twice with 50 µL of nucleosome reconstitution buffer containing 250 mM NaCl (10 mM Tris, pH 7.6, 1 mM EDTA). Assuming 90% of DNA in a single reconstitution reaction formed nucleosomes, 1.63 µg of nucleosomal DNA was added to the beads (70 µL of an 80 uL nucleosome reconstitution reaction) and was incubated at 25 °C for 30 minutes in a Thermomixer at 1200 rpm. The unbound fraction was removed and the bound fraction was washed twice with 70 µL of reconstitution buffer containing 250 mM NaCl. (Dynabeads were immobilized by a brief centrifugation and a 30 second incubation on magnetic eppendorf tube stands.) To analyze the fraction of DNA bound to beads, 5 uL of 0.1% SDS, 10 mM EDTA was added to 5 µL of the input, bound, and unbound fractions. Samples were boiled for 5 minutes,

separated on a 2% agarose gel, and visualized by EtBr staining. Typically, approximately 70-85% of biotinylated nucleosomes were seen in the bound fraction (Figure 2.5D).

2.2.3 Generation of isotope-labeled nuclear extracts

SILAC media—SILAC media with light isotope- or heavy isotope-containing lysine and arginine were made as previously described (Ong and Mann, 2006). Briefly, DMEM containing 10% of dialyzed FBS, 100 units/mL pen/strep (Life Technologies), 100 mg/L lysine, and 84 mg/L arginine was filter sterilized using 22 μm filter (Millipore SCGPS05RE). DMEM was kept at 4 °C for long-term storage.

Trial incorporation of heavy isotope-labeled amino acids—HeLa cells were plated in two 6 cm dishes in either light isotope- or heavy isotope-containing media (abbreviated light and heavy). Cells were allowed to undergo approximately 8 generations before harvesting in 1xPBS, 1% NP-40, 2 mM EDTA, 0.1% SDS, and PIC (protease inhibitor cocktail: 1 mM PMSF, 1 mg/mL pepstatin, 1 mg/mL leupeptin, 1 mg/mL aprotinin) and lysing on ice for 30 minutes. Lysates were centrifuged at 14,000 x*g* at 4 °C for 10 minutes and protein concentration was measure using BCA protein assay kit. 20 μg of light isotope- and heavy isotope-labeled lysates were separated on a 12.5% SDS-PAGE gel and stained with Coomassie. To maintain a keratin-free environment, glass plates were soaked in a 0.5% SDS solution before pouring the SDS-PAGE gels. Five bands present in both the light and heavy lysates were excised and processed according to the CSU Proteomics Facility trypsin in-gel digestion protocol. Samples were analyzed by MALDI-TOF to determine the percent of heavy isotope incorporation. Identifying corresponding peptides in the light and heavy extracts and verifying the absence of an unlabeled peptide in the heavy spectra

determined percent incorporation of the heavy amino acids. Over 50 peptides were analyzed to determine that 100% of the analyzed peptides incorporated the heavy isotope-labeled amino acids.

Large-scale incorporation of heavy isotopes—HeLa cells were plated in two 6 cm dishes, gradually expanded into 42 x 15 cm dishes, and grown to confluency. Nuclear extract was purified as previously described (Abmayr et al., 2006). Approximately 10 mL of nuclear extract was obtained at either 5.00 mg/mL (light isotope-labeled extract) or 3.37 mg/mL (heavy isotope-labeled extract).

2.2.4 Pulldown assays with Ub-histone mimics

Histone dimer pulldown—Flag-tagged histone dimers were prepared as described above. These include: Flag-H2A/H2B, H2A/Flag-H2B, ub*H2A/Flag-H2B, and Flag-H2A/ub*H2B. Typically, 20 µg histone dimers or 7 µg Flag-Ub (BostonBiochem) in refolding buffer was diluted to 150 µl to adjust salt concentration to 300 mM NaCl and then incubated with 20 µl anti-Flag M2 affinity gel (Sigma A2220) at 4 °C for at least 2 h. Unbound proteins were removed and the agarose beads were washed twice with high-salt binding buffer (10 mM Hepes, pH 7.9, 470 mM NaCl, 10 mM KCl, 1.5 mM $MgCl_2$, 0.2% Triton X-100, 10% glycerol).

HeLa nuclear extract was prepared from HeLa S3 cells as previously described (Abmayr et al., 2006). It was then diluted to 2.5 mg/mL with high-salt binding buffer. Additional NaCl was added to reach the final concentration of 470 mM. To remove contaminating proteases, DNA, and RNA, nuclear extract was routinely supplemented with 0.5 mM PMSF, 1 µg/mL pepstatin, 1 µg/mL leupeptin, 20 µg/mL DNase I and 20 µg/mL

RNase A, and then incubated at room temperature for 30 min and centrifuged at 18,000 x *g* for 30 min at 4 °C to remove precipitates.

Typically, 500 μg nuclear extract was added to each pulldown reaction; tubes were incubated for 3 h at 4 °C with rotation. Unbound proteins were removed and the agarose beads were washed 3-times with 200 μL high-salt binding buffer. Bound proteins were eluted by incubation with 3xFlag peptide (Sigma) at 0.2 mg/mL in binding buffer at 4 °C for 30 min. The elution step was repeated and eluates were pooled. Fractions of the eluates (5-10%) were analyzed by SDS-PAGE and silver staining. The rest of the eluates were subject to LC-MS/MS to identify the bound proteins.

SILAC Nucleosome Affinity Purification (SNAP)—Nucleosome pulldown experiments were performed using the conditions in Bartke *et al.* as a guideline (Bartke et al., 2010). Initial pulldown experiments were performed using 1/12 the amount of nucleosome material used by Bartke *et al.* so reactions were scaled down accordingly. Nucleosomes were bound to Dynabeads as described above. Each reaction was incubated with 41.7 μg of light isotope- or heavy isotope-labeled extract in a final volume of 85 μL in SNAP binding buffer (20 mM Hepes, pH 7.9, 150 mM NaCl, 0.2 mM EDTA, 20% glycerol, 0.1% NP-40, 1 mM DTT, and PIC) while rocking at 4 °C for 4 hours. Reactions included unmodified nucleosomes (wt) + light extract (wt-L), wt + heavy extract (wt-H), ub*H2A-L, ub*H2A-H, ub*H2B-L, and ub*H2B-H. Note that wt nucleosome-containing reactions were duplicated because they will be compared with both ub*H2A and ub*H2B-containing reactions downstream. After incubation with the extracts, beads were washed 3 times for 5 minutes each at 4 °C in 85 μL binding buffer. Samples were eluted by the addition of 20 μL of 0.1% SDS, 10 mM EDTA at 37 °C for 5 minutes. 12% of the elution was separated by SDS-PAGE

on a 4-18% gradient gel. Proteins were stained using SYPRO Ruby and imaged on the Typhoon imager.

Densitometry measurements with Image Quant software were used to quantitate 3 bands that are presumably DNA-binding proteins in the elutions. We used the quantity of these proteins to normalize between pulldown reactions assuming that these proteins (most likely PARP1, Ku70 and Ku80) bind to different nucleosomes with equal affinity. Marker intensities were also used in normalization to account for differences in staining efficiency between gels. Based on these quantitations, equal amounts of eluted proteins from different pulldowns were mixed in a 1:1 ratio in a final volume of <50 μL prior to analysis by trypsin digest and quantitative LC-MS/MS. (Note: Initially the concentration of the light extract was underestimated. Pull-downs using heavy extract were repeated to generate a higher yield of bound proteins.)

Nucleosome pulldown using unlabeled nuclear extract—Pulldowns using unlabeled nuclear extract were performed as described in the SNAP protocol. Bound fractions were separated by SDS-PAGE and visualized by either silver staining or western blotting.

2.2.5 Nucleosome gel shift assays

Unmodified and ub*H2A- or ub*H2B-containing nucleosomes were assembled as previously described using the 147 bp 601 nucleosome positioning sequence. Nucleosomes were concentrated to approximately 150 nM with Amicon Ultra 0.5 mL (50K cutoff) concentrators. Nucleosome concentrations were determined by running various dilutions of a known concentration of DNA alongside the reconstituted nucleosomes on a 6% TBE gel. DNA and nucleosomes were visualized by EtBr staining and imaged on the Typhoon

imager. Densitometry measurements using Image Quant was used to generate a standard curve according to the DNA dilutions, and nucleosome concentrations were calculated based on this standard curve.

Gel shift assays were performed at a final NaCl concentration of 300 mM in reaction buffer (10 mM Tris, pH 7.6, 1 mM EDTA, 0.05% NP-40, 10% glycerol, 0.1 mg/mL BSA, 1 mM DTT). All reactions contained 452 pmol of nucleosomes and GST-LANA 1-23 was titrated from 251 nM to 20 μM. GST was used as a negative control at a concentration of 20 μM. Final reaction volumes of 3 μL were incubated on ice for 2 hours; then 1 μL of 20% sucrose was added to each reaction prior to separation on a 6% TBE gel and imaging as previously described. To calculate the apparent Kd (Kd_{app}), the percentage of GST-LANA peptide-bound nucleosomes were calculated according to densitometry measurements and the data were analyzed using a Hill coefficient nonlinear regression fit where $y=Bmax * (X^n/(X^n+Kd^n))$.

2.2.6 Differential scanning calorimetry

Unmodified and ub*histone dimers were extensively dialyzed into 10 mM sodium phosphate, pH 7.6, 1 mM EDTA, pH 8.0, 300 mM NaCl. All buffers and protein-containing samples were degassed prior to analysis by differential scanning calorimetry (DSC). To ensure the dialysis buffer was stable during the DSC heating and cooling cycles, a heating and cooling program from 0 °C to 90 °C was performed and compared to a water reference sample. Next, 3 buffer-to-buffer cycles were run to obtain a baseline curve. Histone dimers were diluted to a range from 0.2 to 0.4 mg/mL in dialysis buffer and scans from 37 °C to 75 °C were performed. Duplicate samples were analyzed for both unmodified and

ubiquitinated histone dimers. The buffer baseline curve was subtracted from each scan and thermodynamic properties were extrapolated from the resulting curves.

2.3 Results

2.3.1 Characterization of histone dimer thermodynamic properties

Because ubH2A and ubH2B have functionally different roles, we proposed that identification of ubiquitinated histone "readers" or "effectors" would give some insight as to how H2A and H2B monoubiquitination mechanistically signals in particular cellular pathways. To identify histone-binding proteins, we used unmodified or ubiquitinated histones in pulldown assays. Obtaining large amounts of Ub-histone is necessary for this type of biochemical study, which is somewhat problematic as generating ubH2B using the ubiquitination cascade enzymes (E1, E2, E3) results in a very low yield of ubiquitinated product. Furthermore, ubiquitination at sites other than Lys120 was observed when using this system to obtain ubH2B (Kim and Roeder, 2011). Ubiquitinated histones can be isolated from cellular extracts, but the isolated histones, in addition to monoUb, contain a heterogeneous mixture of other PTMs. To circumvent these difficulties, we generated nonhydrolyzable Ub-histone mimics using a strategy derived from a method previously employed to generate di-Ub (Yin et al., 2000a) and ubiquitinated PCNA (Carlile et al., 2009) analogs. This method takes advantage of a highly reactive bifunctional thiol crosslinker, 1,3-dichloroacetone. Since neither Ub nor H2A contain naturally occurring cysteine residues, we can implement site-specific crosslinking by introducing cysteine at the C-terminus of Ub (G76C) and the native ubiquitination site of human H2A (K119C) or H2B(K120C). Compared to a native Ub-protein isopeptide linkage, the crosslinked product

contains an additional carboxylate group and is one C-C bond longer (Figure 2.1A). The crosslinked ub*H2A and ub*H2B mimics (* denotes the crosslink) were further assembled into H2A/H2B dimers (Figure 2.1D).

One way that Ub modification can affect chromatin function is to perturb its structure. To investigate whether Ub attached to either H2A or H2B affects the stability of H2A/H2B dimer, we analyzed the thermodynamic properties of H2A/H2B, ub*H2A/H2B, and H2A/ub*H2B using differential scanning calorimetry (DSC). DSC can be used to measure enthalpic properties of proteins and protein complexes by measuring the amount of heat required to denature the protein. Typically, protein structures that are stabilized by an increased number of intramolecular interactions exhibit a higher T_m than those that form fewer or weaker inter- and intra-molecular interactions. Under this assumption, we proposed that H2A/ub*H2B would exhibit different thermodynamic properties than either H2A/H2B or ub*H2A/H2B due to possible differences in intramolecular interactions between Ub and the histones within the same histone dimer molecule or intermolecular interactions between histone dimer molecules. Histone dimers were dialyzed together in buffer containing 300 mM NaCl. Initial scans analyzing unmodified histone dimers showed the unfolding and refolding was not reversible as the peaks observed in the heating and cooling phases of the scan did not overlap (data not shown). Analysis showed there were no major differences in the T_m or enthalpic properties of unmodified and ubiquitinated histone dimers (Table 2.1 and Table 2.2). These results suggest that Ub attached to either H2A or H2B minimally contributes to inter- and intra- molecular interactions. Notably, the T_m for Ub is above 90 °C and, therefore, does not contribute to the overall T_m of the ubiquitinated histone dimers in this analysis.

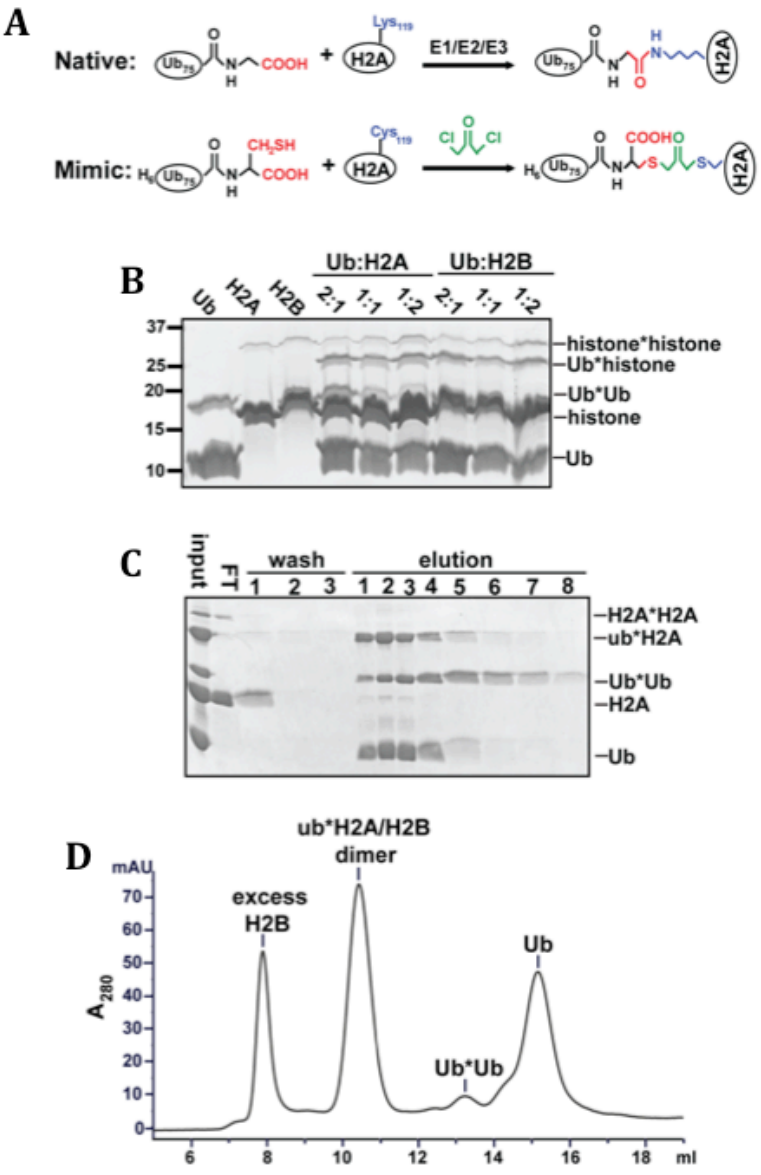

Figure 2.1. Synthesis and purification of ubiquitinated histone mimics. (A) Schematic comparing native ubH2A and the crosslinked mimic. In the mimic, Gly76 of Ub and Lys-119 of H2A were mutated to cysteines. Crosslinking with 1,3-dicholoroacetone produces a dithioether linkage that is one C-C longer than an isopeptide linkage, contains an additional carboxylate, and is resistant to cleavage by DUBs. **(B)** Pilot-scale crosslinking reactions were done by varying the ratio of Ub and histones. Products were separated by SDS-PAGE and visualized by Coomassie blue staining. **(C)** Crosslinked products were purified using Ni-NTA agarose. Eluates (containing Ub, Ub*Ub, and Ub*histones) were separated by SDS-PAGE and visualized by Coomassie blue staining. FT: flow-through. **(D)** HPLC chromatogram of purification of ub*H2A/H2B dimers. Histone dimers were injected on a Superdex 75 column. Absorbance at 280 nm was monitored over time and eluates were visualized by SDS-PAGE and Coomassie blue staining. ub*H2A/H2B eluted at ~10.4 ml. H2B, Ub*Ub, and Ub eluted at approximately 7.9, 13.2, and 15.1 ml, respectively.

Table 2.1. Enthalpic properties of histone dimers as determined by DSC analysis.

Histone dimer	T_m (°C)	ΔG (kJ/mol)	ΔH (kJ/mol)	ΔS (kJ/mol*K)
H2A/H2B	55.88 ± 0.71	29.65 ± 0.91	325.19 ± 19.58	0.99 ± 0.06
ub*H2A/H2B	55.05 ± 0.13	26.88 ± 2.12	313.78 ± 45.44	0.96 ± 0.15
H2A/ub*H2B	55.45 ± 0.10	26.22 ± 0.54	297.48 ± 1.86	0.91 ± 0.00

Table 2.2. Calculated differences in histone dimer enthalpic properties. Enthalpic properties for unmodified and ubiquitinated histone dimers were averaged together. The percent standard deviation was calculated to numerically determine the degree of difference in enthalpic characteristics in all sample types. The low percent standard deviation values indicate unmodified and ubiquitinated histone dimers share similar inter- and intra-molecular interaction characteristics.

	T_m (°C)	ΔG (kJ/mol)	ΔH (kJ/mol)	ΔS (kJ/mol*K)
Average	55.46	27.58	312.15	0.95
Standard deviation	0.49	1.95	25.41	0.08
Percent deviation	0.89	7.05	8.14	8.36

2.3.2 H2B Ubiquitination weakens LANA interaction with the nucleosome

Although DSC analysis suggested there were no major changes in the thermodynamic properties of unmodified and ubiquitinated histone dimers, it was still possible that: 1) the DSC measurements were not sensitive enough to detect minor changes in histone dimer stability and 2) ub*H2B sterically occludes the acidic patch without forming additional inter- or intra-molecular interactions and, therefore, was not detectible by DSC analysis.

Between these sites of Ub attachment is a patch of acidic residues localized on the H2A/H2B dimer (Figure 2.2B). These residues stand out for 2 reasons: first, the residues in the histone dimer are predominantly basic so the acidic patch provides an alternatively charged region and secondly, multiple proteins interact with histones via this acidic patch (Luger et al., 1997; Wyrick et al., 2012). We modeled the attachment of Ub to either H2A or H2B (at K119 and K120, respectively) and used HADDOCK to assess the ability of Ub to

access the H2A/H2B acidic patch. Modeling suggested that Ub, when attached to H2B could sterically hinder access to the acidic patch. On the other hand, Ub attached to H2A is unlikely to sterically occlude the acidic patch due to the increased distance between the site of Ub attachment and the acidic patch. The Kaposi's sarcoma-associated herpes virus (KSHV) encodes a viral protein KSHV latency-associated nuclear antigen (LANA). As viral genomes don't contain centromeres, the segregation of viral DNA is mediated in a LANA-dependent mechanism whereby LANA specifically interacts with the acidic patch within the NCP to tether the viral genome to mitotic centromeres (Barbera et al., 2006) (Figure 2.2C). The N-terminal residues of LANA (LANA 1-23) mediate the interaction with the NCP acidic patch. To measure the effect of Ub on the acidic patch accessibility in the NCP, we measured the affinity between unmodified and ub*H2A- or ub*H2B-contianing mononucleosomes and the LANA peptide. Mononucleosomes were assembled on a 147 bp fragment of DNA encoding the 601 nucleosome positioning sequence. LANA 1-23 was tagged with GST and purified as previously described (Barbera et al., 2006). Increasing amounts of GST-LANA 1-23 were incubated with mononucleosomes. Complexes were separated on a 6% TBE gel and visualized by EtBr staining. Binding of GST-LANA 1-23 to nucleosomes was observed by an upward shift in nucleosome migration (Figure 2.3A). The percent of shifted nucleosome was quantitated, plotted, and analyzed using a nonlinear regression fit to obtain an apparent dissociation constant (Kd_{app}) where the Hill coefficient is approximately 2.2 (Figure 2.3B). We observed a small, but reproducible increase in the Kd_{app} for ub*H2B-containing nucleosomes (Figure 2.3C). These data indicate that Ub when attached to H2B partially obscures the binding site for acidic patch-binding proteins such as LANA.

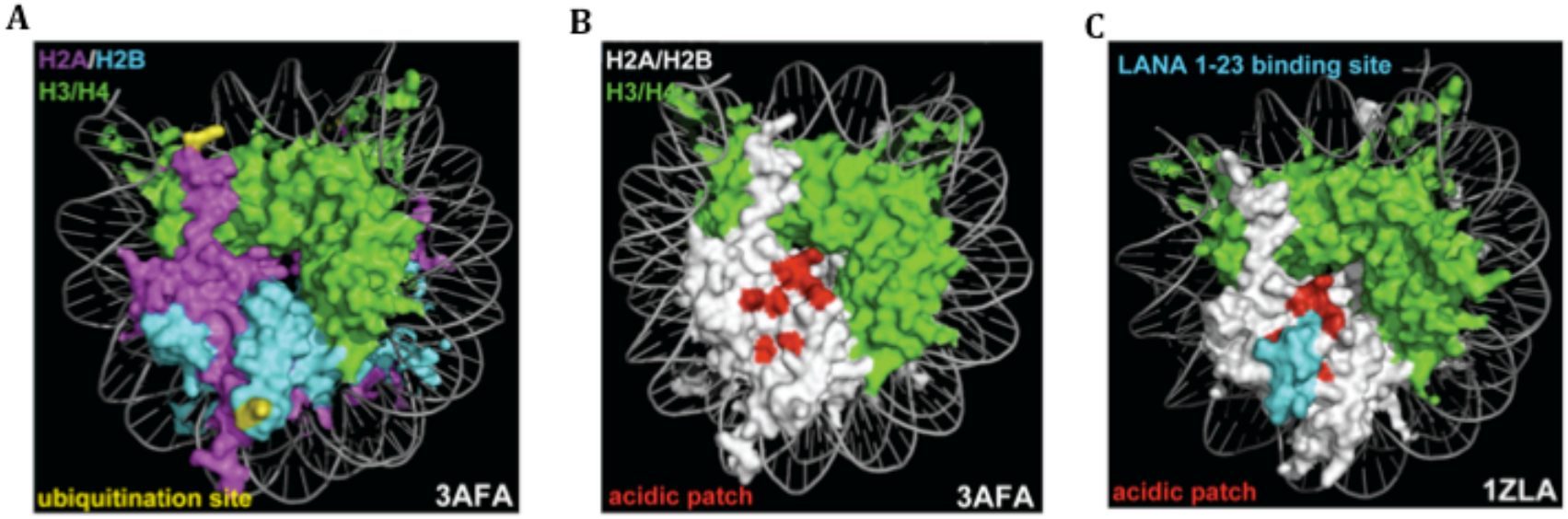

Figure 2.2. Schematic of ubiquitination sites, acidic patch, and LANA binding site within the NCP. (A) Structure of NCP where H2A is colored in magenta, H2B is cyan, and H3/H4 are green. Sites of H2A and H2B monoubiquitination are highlighted in yellow (at K119 and K120, respectively). Protein Data Bank (PDB) accession number is 3AFA (Luger, et al. 1997). **(B)** Structure of NCP where H2A/H2B are colored in white and H3/H4 are green. Residues comprising the H2A/H2B acidic patch are highlighted in red (Luger, et a., 1997). **(C)** The H2A/H2B acidic patch within the NCP is highlighted in red and the residues involved in LANA 1-23 binding are highlighted in cyan. H2A/H2B and H3/H4 are colored as described in (B). PDB accession number is 1ZLA (Barbera, et al, 2006).

2.3.3 SILAC Nucleosome Affinity Purification (SNAP)

Some histone-binding proteins preferentially bind histones within the context of an H2A/H2B dimer, H3/H4 tetramer, or when assembled into a NCP. This is partially evidenced by the substrate specificity observed for many histone DUBs (Table 1.2). Therefore, we proposed the binding patterns of ubiquitinated histone dimers versus ub*H2A- or ub*H2B-containing nucleosomes are different and identification of these interacting proteins would give further insight into the mechanisms by which ub*H2A and ub*H2B are regulated and signal in the cell.

In a previous study, effectors of H3 methylation at various lysine residues were identified by reconstituting modified histones into biotinylated mononucleosomes and used mass spectrometry to identify bound proteins (Bartke et al., 2010). In particular, this study used a Stable Isotope Labeling of Amino acids in Cell culture (SILAC) approach for quantitative mass spectrometry rather than semi-quantitative approaches such as spectral counting. We sought to utilize a similar approach to identify "readers" of unmodified and ub*H2A- or ub*H2B-containing nucleosomes. Similar as the previous study, we reconstituted mononucleosomes with a biotinylated 183 bp DNA fragment (Figure. 2.4A). This fragment is consisted of 16 bp of DNA upstream and 20 bp downstream of a 147 bp 601 nucleosome positioning sequence. The 183 bp fragment was prepared by amplification with a biotinylated reverse primer and further purified on a MonoQ sepharose column (Figure 2.4B). Unmodified, ub*H2A, or ub*H2B histones were assembled into histone octamers and used to reconstitute mononucleosomes (Figure 2.4C). In comparison with unmodified nucleosomes, Ub*histone-containing nucleosomes migrate slower on a native polyacrylamide gel due to the presence of two Ub moieties in each nucleosome. For use in

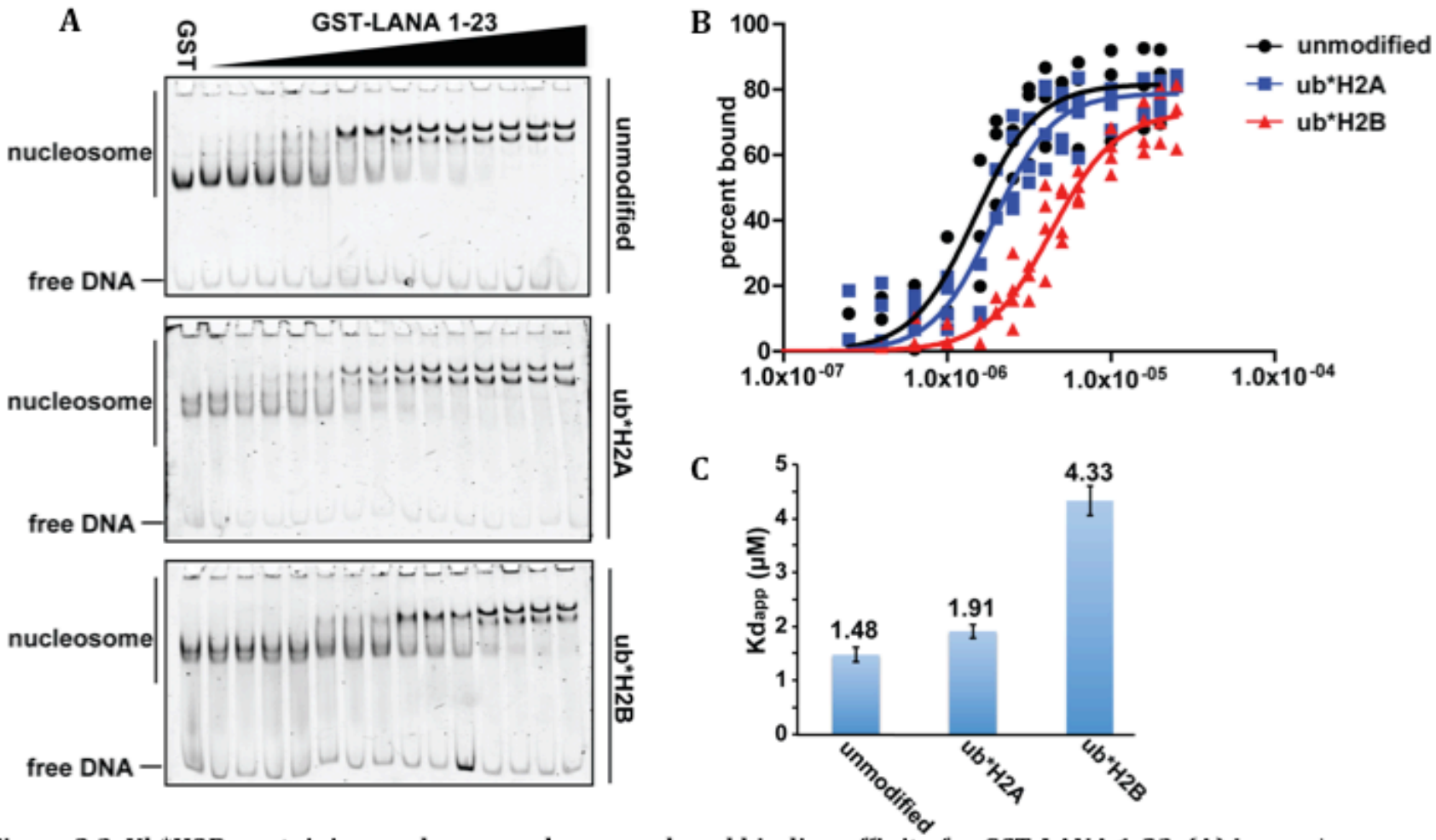

Figure 2.3. Ub*H2B-containing nucleosomes have a reduced binding affinity for GST-LANA 1-23. (A) Increasing amounts of GST-LANA 1-23 was incubated with unmodified and ub*H2A- or ub*H2B-containing nucleosomes. Complexes were separated on a 6% TBE gel, stained with EtBr, and visualized on the Typhoon imager. Representative gels are shown. **(B)** The intensity of the shifted band was quantified as the percent GST-LANA-bound nucleosome from 4 independent experiments and was fit using a Hill coefficient non-linear regression model to calculate apparent Kd (Kd_{app}) where y=Bmax * ($X^n/(X^n+Kd^n)$) and n is approximately 2.2. **(C)** Kd_{app} values calculated in (B) are plotted for comparison. Error bars represent standard error.

pulldown assays, biotinylated nucleosomes were immobilized onto magnetic streptavidin Dynabeads (Figure 2.4D).

SILAC is a popular method for obtaining reliable quantitative mass spectrometry data in pulldown assays where cell extract is supplied as the source of prey proteins. In this method, cells are cultured in media containing either light isotope-labeled $^{12}C_6$ L-Lysine and $^{12}C_6$ $^{14}N_4$ L-Arginine or heavy isotope-labeled $^{13}C_6$ L-Lysine and $^{13}C_6$ $^{15}N_4$ L-Arginine. Upon full incorporation of heavy or light amino acids, nuclear extract is prepared from these cells. The light extract is then incubated with unmodified nucleosomes while the heavy extract is incubated with modified nucleosomes. Bound fractions from unmodified and modified nucleosomes are mixed in equal ratios, trypsin digested, and analyzed by LC-MS/MS. Peptides from proteins bound by modified nucleosomes can be identified by a mass shift of +6 Da (Lysine) or +10 Da (Arginine) as trypsin cleaves after lysine and arginine residues. In a "reverse" experiment, unmodified nucleosomes are incubated with the heavy extract while modified nucleosomes are incubated with the light extract. For each identified protein, the heavy/light (H/L) ratios from both the forward and reverse experiments are plotted. Proteins that prefer binding the modified nucleosomes can be distinguished from those that prefer binding the unmodified nucleosomes (Figure 2.5). The major advantage of using this method is that elution samples from both unmodified and modified nucleosomes are mixed prior to analysis by LC-MS/MS. This eliminates erroneous quantitation due to differences in processing such as variation in digestion or sample complexity.

For generation of light isotope- and heavy isotope-labeled nuclear extracts, cells were grown in the presence of either light or heavy lysine and arginine (Figure 2.6A). To

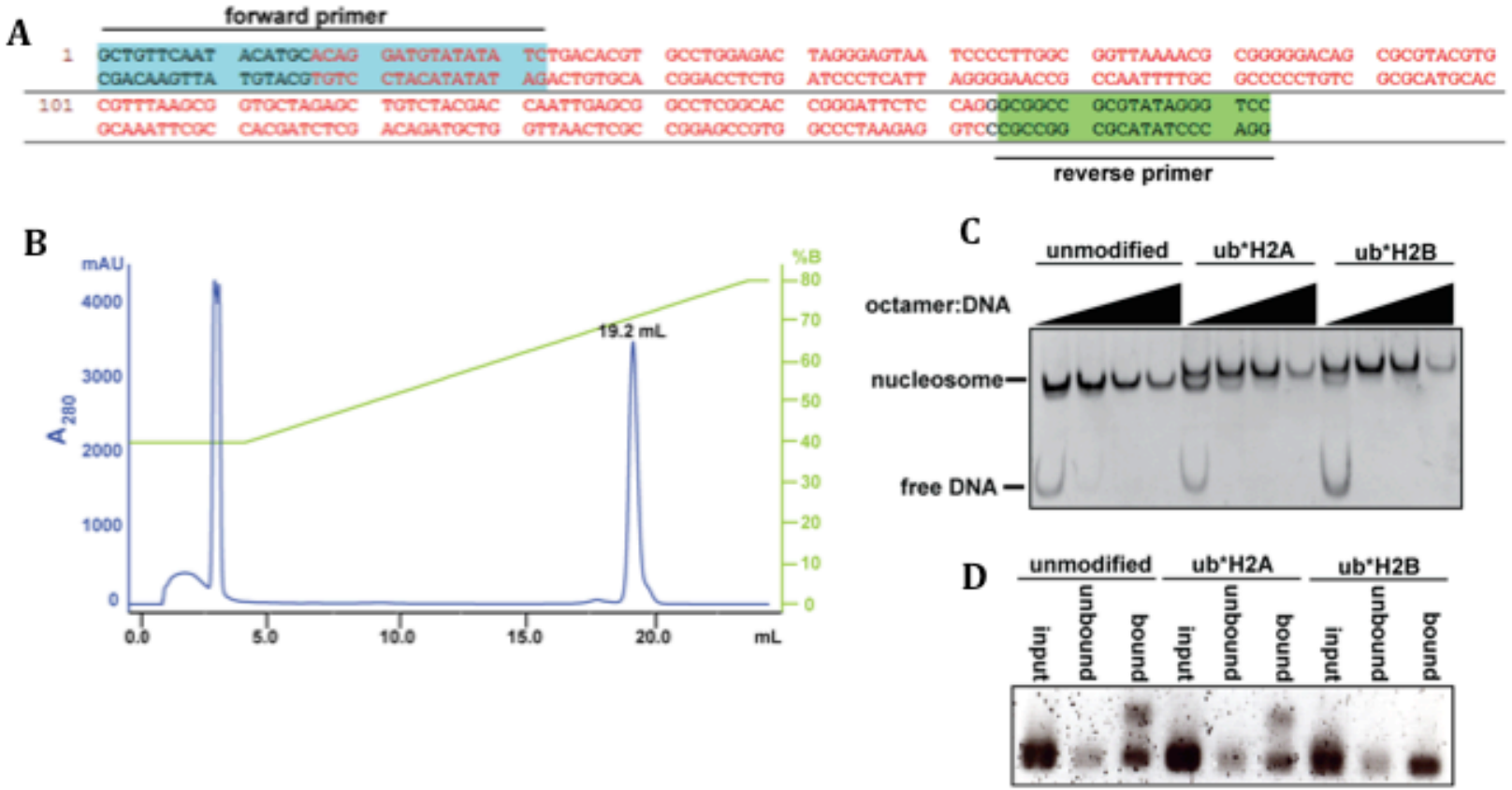

Figure 2.4. Reconstitution and immobilization of biotinylated nucleosomes (A) Schematic of the 183 bp DNA sequence used in nucleosome reconstitution for SNAP experiments. The 601 nucleosome positioning sequence is centrally positioned (colored in red) and flanked by a 5' extension of 16 bp and a 3' extension of 20 bp. Forward and reverse primers used for amplification are highlighted in cyan and green, respectively. The reverse primer is biotinylated. **(B)** Purification of the biotinylated 183 bp DNA fragment in (A). PCR products were loaded onto a MonoQ sepharose column and purified over a 40%-80% linear gradient of Buffer B (contains 1 M NaCl) vs. Buffer A (contains 100 mM NaCl) over 20 column volumes. The biotinylated 183mer eluted around 0.74 M NaCl (19.2 mL) **(C)** Purified histone octamers containing unmodified histones, ub*H2A or ub*H2B mimics, were assembled into mononucleosomes with 183 bp sequence in (A). Assembly was done by salt dilution and the octamer:DNA ratio was titrated in order to achieve the optimal condition. **(D)** Nucleosomes from (C) were immobilized on Dynabeads. Binding efficiency was evaluated by visualizing both the bead-bound and unbound fractions on a 2% agarose gel and EtBr staining.

ensure full incorporation of the heavy isotope-labeled amino acids, cultured cells were grown for ~8 cell divisions, lysed, and proteins were separated by SDS-PAGE and visualized by coomassie staining. Five bands from both the light isotope- and heavy isotope-labeled cell extracts were excised and subjected to in-gel trypsin digestion (Figure 2.6B). Digested peptides were subject to MALDI-TOF analysis (Figure 2.6C, top panel). Incorporation of the heavy isotope-containing amino acids was observed by a shift of either 6 or 10 Da (Figure 2.6C, bottom panels). Full incorporation of supplemented amino acids was achieved as analysis of over 50 peptides showed spectra detected in the light sample were all shifted by 6 or 10 kDa in the heavy spectra. Upon confirmation of heavy isotope-labeled amino acid incorporation, cells were expanded for a large-scale preparation of nuclear extract.

For SNAP experiments, unmodified, ub*H2A, and ub*H2B-containing mononucleosomes were assembled with the biotinylated 183 bp fragment and immobilized to Dynabeads. Nucleosomes were incubated with light or heavy nuclear extract. Bound proteins were eluted and visualized by SDS-PAGE and silver staining (Figure 2.7). We noticed pulldowns using light extract as a source of prey proteins had an increased number of bound proteins. Because silver staining of the 1% input for light and heavy extracts was also unequal, reevaluation of the total protein concentration by BCA of the light nuclear extract showed the concentration was previously underestimated. Although internal standards can be used for normalization of SILAC mass spectrometry data, data analysis is simpler and more reliable if similar amounts of light and heavy pulldown elution samples are mixed before LC-MS/MS analysis. To account for differences in the amount of bound proteins, 3 bands corresponding to DNA-binding proteins were quantitated and

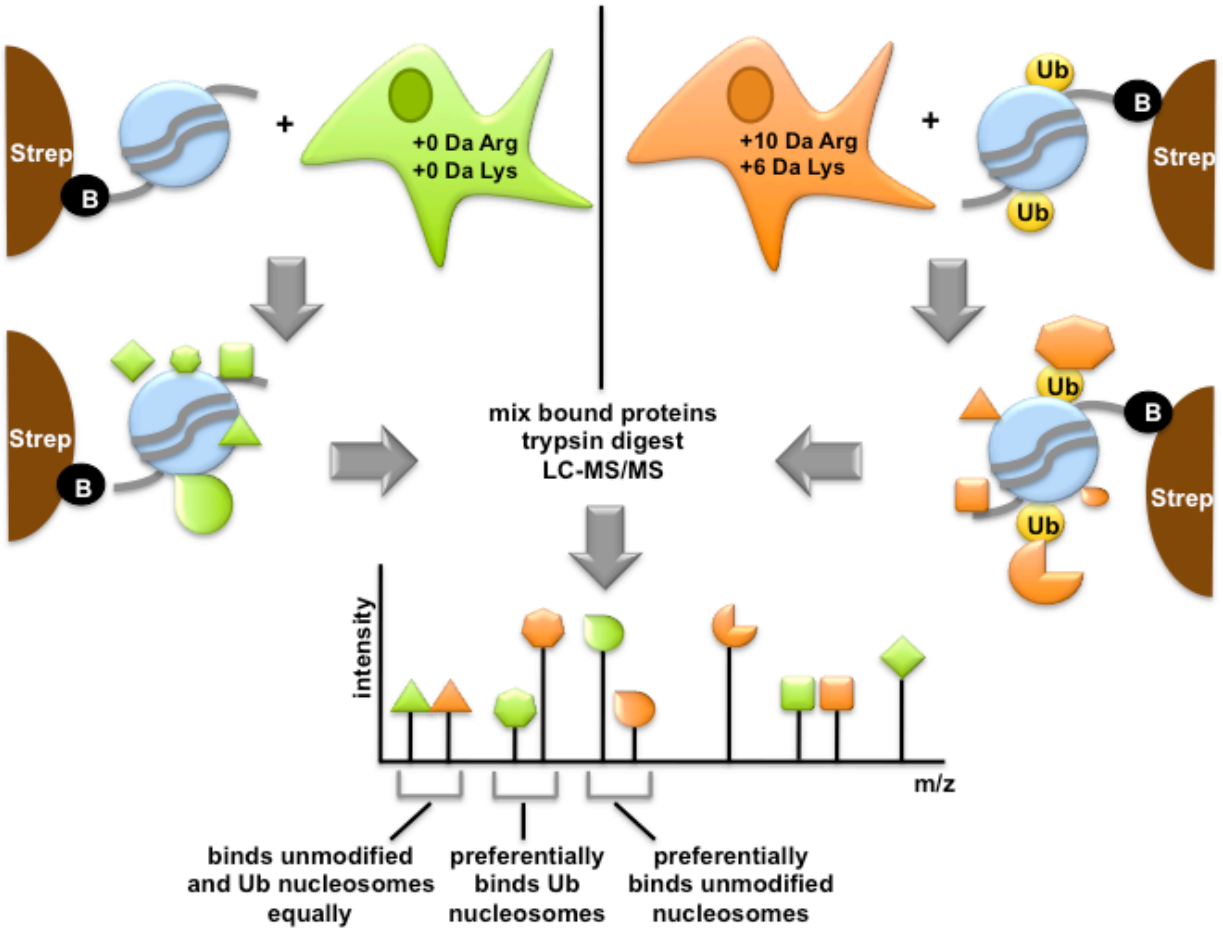

Figure 2.5. Schematic of SNAP methodology. Biotinylated unmodified and ubiquitinated histone-containing nucleosomes are immobilized on streptavidin beads and incubated with either light isotope- or heavy isotope-labeled extract (depicted as a green and orange cells, respectively). Bound proteins are trypsin digested and identified by LC-MS/MS. Peptides that incorporated heavy isotope-labeled peptides can be identified by a m/z shift of 6 or 10 Da. These spectra can be used to determine preferential binding of bound proteins for unmodified or ubiquitinated histone-containing nucleosomes.

used as a reference for normalization of total bound proteins. Based upon this normalization, equal amounts of light and heavy elution fractions were mixed and sent for LC-MS/MS analysis. Unfortunately the results from the mass spectra results were difficult to interpret and, in many cases, reliable quantitation was not possible due to poor coverage. Optimization of future SNAP experiments is discussed in Section 2.4.

2.3.4 FACT preferentially binds ub*H2B-containing mononucleosomes

A number of proteins have been functionally linked to ubH2B *in vivo*. In particular, FACT plays a major role in H2B ubiquitination and ubH2B-related processes such as transcription elongation and reassembly of nucleosomes during transcription and DNA replication (see Section 1.8). We found that FACT preferentially bound H2A/ub*H2B and, because of its role in nucleosome disassembly and reassembly, were curious to see if FACT also bound ub*H2B-containing nucleosomes. Mononucleosome pulldown experiments were performed as described above with the modification that unlabeled nuclear extract was used as the source of prey proteins (Figure 2.8A). Bound proteins were separated by SDS-PAGE and detected by either silver staining or western blotting. Results showed that FACT preferentially bound ub*H2B-containing nucleosomes (Figure 2.8B). We also blotted for a histone DUB, Usp15, which bound ubiquitinated histone dimers in our previous pulldown studies and found that Usp15 did not bind unmodified or Ub-containing mononucleosomes. Debuiquitination assays showed Usp15 preferentially deubiquitinates free histones rather than mononucleosomes, providing further evidence that the histone dimer or nucleosomal context of ubiquitinated histones is a point of regulation of histone-binding proteins (Long et al., 2014). Identifying proteins that preferentially bind

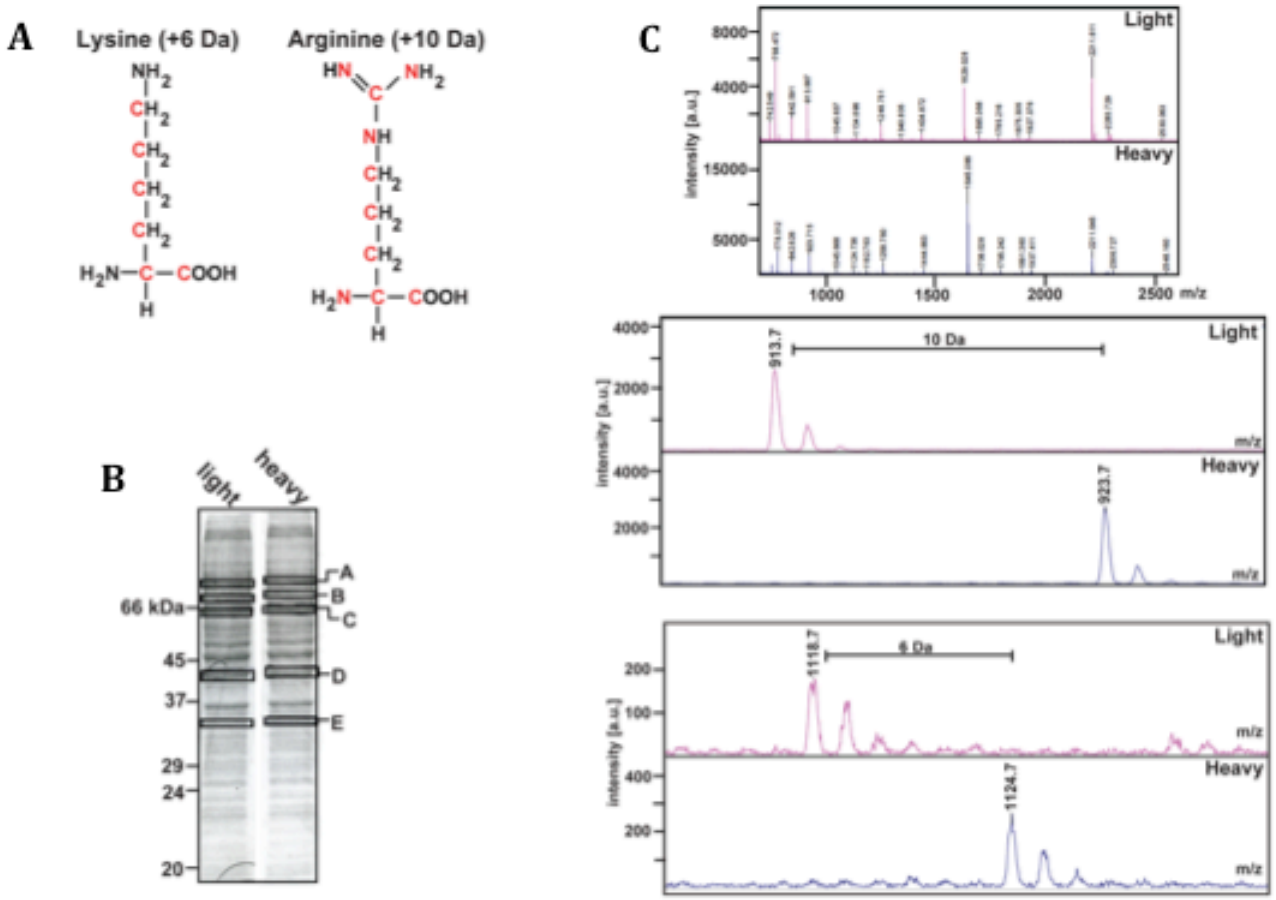

Figure 2.6. Evaluation of incorporation of light isotope- and heavy isotope-labeled amino acids in cell culture (A) Chemical structure of lysine and arginine. Molecules highlighted in red are substituted with either ^{13}C or ^{15}N in place of ^{12}C or ^{14}N in the heavy isotope media for a molecular weight shift of 6 and 10 Da. **(B)** 20 ug of light isotope- or heavy isotope-labeled nuclear extract were separated on a 12.5% SDS-PAGE and stained using coomassie brilliant blue. The five indicated bands were excised and prepared for analysis by mass spectrometry by in-gel trypsin digestion. **(C)** MALDI-TOF analysis of a gel band excised from (B). The top panel compares the total observed peptides from the "light" and "heavy" bands from a m/z from 0 to ~2500. The second panel is a zoomed-in view of 2 peptides from the top panel. Full incorporation of a heavy arginine residue is observed by the complete 10 Da shift in the "heavy" sample compared to the light sample. The third panel demonstrates full incorporation of a heavy lysine residue in the "heavy" sample as is observed by a 6 Da shift.

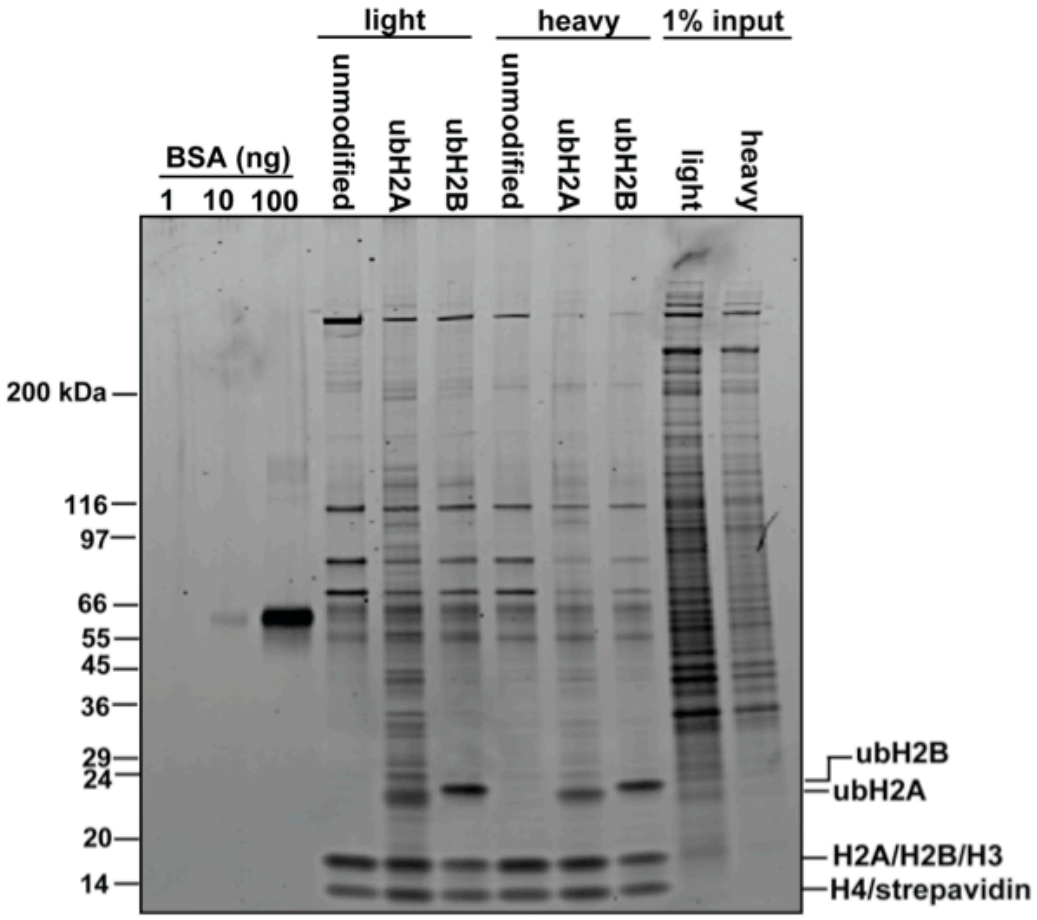

Figure 2.7. Visualization of SNAP elution fractions. 12% of SNAP pulldown elution fractions using either light isotope- or heavy isotope-labeled nuclear extracts were separated by a 4-18% SDS-PAGE gradient gel and visualized by silver staining. A 1% input of light and heavy extract used in the pulldown assays was loaded as a reference. 1, 10, and 100 ng of BSA were loaded at a protein concentration reference.

ubiquitinated histone dimers versus Ub-histone containing nucleosomes could provide further mechanistic insight into the signaling mechanisms by which monoubiquitinated histones function in various cellular processes.

2.4 Discussion

*Advantages of nonhydrolyzable Ub*histone mimics*—We developed a method to generate large amounts of highly stable, nonhydrolyzable Ub*histone mimics. Pull-down assays using these mimics identified effectors of ubiquitinated histone dimers by proteomics. Select proteins with distinct binding profiles were chosen for further validation by western blotting using specific antibodies.

Traditionally, identification of histone modification-binding proteins is performed using modified (acetylated or methylated) histone peptides as baits in pull-down assays. Employing our method of Ub*histone generation, we were able to use the full-length modified histone as bait in our pull-down assays. Utilizing the entire histone protein rather than a histone peptide is advantageous in multiple ways. First, some Ub-interacting proteins recognize their substrates through direct interactions with both Ub and the substrate protein (Bienko et al., 2005). Because multiple surfaces are often required for protein-protein interactions, using an entire modified histone rather than modified histone peptides in pull-down assays may result in the identification of more physiologically relevant modification readers.

Another advantage of using full-length ubiquitinated histones is these proteins can be assembled into a variety of complexes including nucleosomes and H2A/H2B dimers (Figure 2.1D and 2.4C). Using these different complexes in pull-down assays could refine

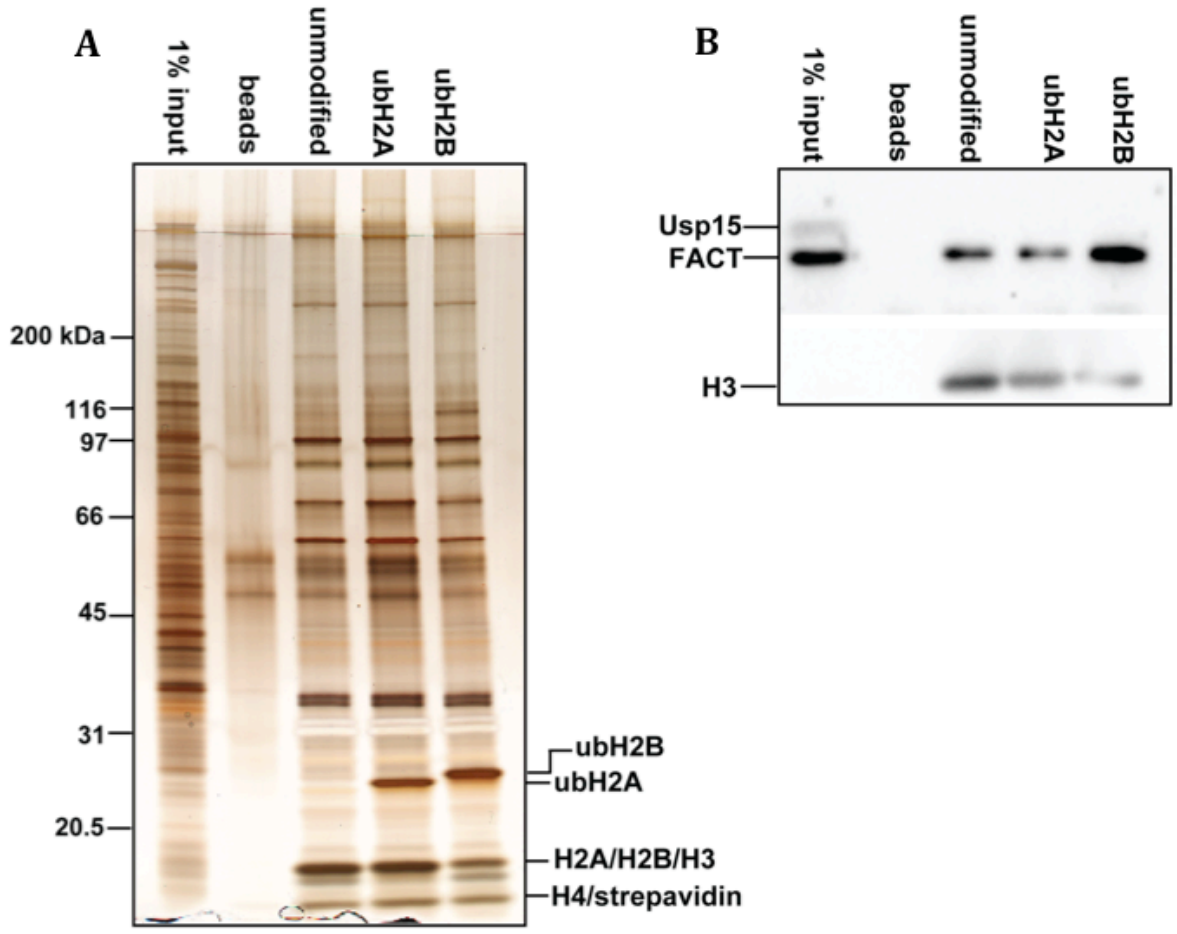

Figure 2.8. FACT preferentially binds ub*H2B-containing mononucleosomes. (A) Pulldowns using biotinylated mononucleosomes were immobilized on magnetic streptavidin-coated beads (Dynabeads). HeLa S3 nuclear extract was used as a source of prey proteins. 15% of elutions were separated on a 4-18% SDS-PAGE and visualized by silver staining. **(B)** 50% of the nucleosome pulldown elutions were separated by 12.5% SDS-PAGE and Usp15, FACT (anti-SSRP1), and H3 were visualized by immunoblotting.

our knowledge of Ub-histone effectors by defining the structural context in which specific interactors bind ubiquitinated histones. Particularly, multiple cases have been reported where histone DUB activity preferentially deubiquitinates free histones or nucleosomal histones (Table 1.2). As our Ub*histone mimics are nonhydrolyzable, these substrates can be used within different structural contexts to obtain binding affinities with histone DUBs.

Recently, a pulldown study was carried out with nucleosome arrays assembled with chemically synthesized ubH2B, which contains the native isopeptide linkage (Shema-Yaacoby et al., 2013). In comparison with these semi-chemical synthesis strategies, our crosslinking-based method is much simpler. Additionally, our Ub*histone mimics are not susceptible to cleavage by DUBs present in the nuclear extract, thus enhancing the probability of identifying effector proteins. Notably, the recently published pulldown assay using nucleosomal arrays containing the native ubH2B isopeptide linkage did not identify any DUBs. Additionally, in contrast to our pulldown using histone dimers, many of the proteins identified in the nucleosomal pulldown identified multiple components of the transcriptional elongation machinery including components of the NELF, DSIF, and SWI/SNF complexes.

Many sites of mono-ubiquitination have been identified on H2A, H2B, H3, and H4 in mammalian cells (Table 1.1). Compared to the extensive studies analyzing monoubiquitination of H2A (Lys119) and H2B (Lys120), little is known about the effectors of histone ubiquitination at other lysine residues. Therefore, generation of a variety of monoubiquitinated histones could prove a useful tool for identifying effectors at these other sites of ubiquitination. In addition to ubiquitination, the conjugation of an ubiquitin-like protein, small Ub-related modifier (SUMO), onto histones has been described in

multiple eukaryotes (Nathan et al., 2006; Shiio and Eisenman, 2003). Like Ub, SUMO does not contain any naturally occurring cysteine residues. In principle, this technique of generating Ub*histones could also be applied to the generation of nonhydrolyzable SUMO*histone mimics. Generation of a variety of ubiquitinated or SUMOylated histones could prove to be useful tools to identify downstream effectors and to provide new mechanistic insights into the functions of these modifications.

*Instability of H2A/ub*H2B*—In the histone dimer pulldown assays, Flag-H2A/ub*H2B was consistently unstable as ub*H2B dissociated from Flag-H2A upon incubation with nuclear extract (M.F. and T.Y., unpublished results). We investigated the possibility that Ub, when attached to H2B, interacts with H2A/H2B surface and perturb the stability of the dimer.,DSC analysis unveiled no major changes in the stability of unmodified and Ub-containing histone dimers. From these data, we propose that H2A/ub*H2B is not inherently less stable, but dissociate more easily in the presence of the nuclear extract. One possiblity is,that H2A/ub*H2B are destabilized by particular protein(s) in the nuclear extract. Alternatively, the unmodified and ub*H2A-containing histone dimers are simply stabilized by proteins in the nuclear extract that are excluded from binding to ub*H2B-containing histone dimers.

In support of the latter possibility,, binding assays using the GST-LANA 1-23 peptide showed that, in the nucleosomal context, ub*H2B at least partially obscured the H2A/H2B acidic patch. It is unclear whether ub*H2B also blocks binding proteins whose interactions are mediated by the acidic patch within the context of the histone dimer. In the gel shift assays we noticed that, at high concentrations of GST-LANA 1-23, the shifted band migrated as two distinct bands. Due to the presence of the GST tag, it's likely that GST-LANA 1-23

exists as a dimer. Because each nucleosome contains two LANA peptide-binding sites, it's possible that the slower migrating band represents the binding of two GST-LANA peptides while the faster migrating complex has bound only one GST-LANA peptide. Alternatively, it's conceivable that one GST-LANA 1-23 dimer may bind acidic patch residues within the same nucleosome or each monomer within the dimer may bind two different nucleosomes, which may result in a change in migration pattern.

The GST-LANA 1-23 binding data were best described using a Hill coefficient model with an n value of approximately 2, suggesting a certain degree of cooperative binding. The dimerization property of GST could also be a contributing factor to this cooperative binding as the binding of one GST-LANA peptide could enhance the affinity for binding of the corresponding GST-LANA peptide to the same nucleosome or a nucleosome near where the first binding event occurred. Further studies using monomeric GST-LANA 1-23 or MBP-LANA 1-23 could provide insight as to the degree of influence of the GST tag possesses with respect to LANA peptide-nucleosome binding models.

SNAP optimization—Obtaining reliable, quantitative mass spectrometry data was unsuccessful in the pilot SNAP experiment and this is most likely a result of two major factors. First, many of the proteins that bound the mononucleosomes were DNA-binding proteins. These interactions were presumably enhanced by the DNA overhangs present on either side of the positioning sequence (Figure 2.4A). Due to the sheer abundance of these DNA-binding proteins, detection of nucleosome-specific interactors by the mass spectrometer was more difficult.

Secondly, the previous study by which we modeled our SNAP experiment used more nucleosomes and more isotope-labeled nuclear extract per pulldown condition. Using

nucleosomal arrays, the nucleosome:free DNA ratio would increase, thereby increasing the abundance of nucleosome-interacting proteins and decreasing the abundance of DNA-binding proteins. Consequently, identification of nucleosome-binding proteins by the mass spectrometer would be enhanced. Coupling an increase in nucleosome concentration with an increase in SILAC extract for each pulldown would result in a greater quantity of eluted proteins to be analyzed by mass spectrometry. Increasing the concentration of analyzed sample is necessary for two reasons: this would enhance the identification of low abundance nucleosome-interacting proteins and would increase the spectral counts of identified proteins, thereby improving the quantitation data. We plan to repeat the SNAP experiments using unmodified and Ub-containing nucleosomal arrays to gather more reliable SILAC quantitation data in the future.

CHAPTER 3: THE U4/U6 RECYCLING FACTOR SART3 HAS HISTONE CHAPERONE ACTIVITY AND ASSOCIATES WITH USP15 TO REGULATE H2B DEUBIQUITINATION

[2]Post-translational modifications (PTMs) of histone proteins produce dynamic signals that regulate the structure and function of chromatin. Monoubiquitination of H2B in the histone tail (at K123 in yeast or K120 in humans) is a conserved modification that has been implicated in the regulation of transcription, replication, and DNA repair processes. In a search for direct effectors of ubH2B, we identified a deubiquitinating enzyme, Usp15, through affinity purification with a nonhydrolyzable ubH2B mimic. In the nucleus, Usp15 indirectly associates with the ubH2B E3 ligase, RNF20/RNF40, and directly associates with a component of the splicing machinery, SART3 (also known as TIP110 or p110). These physical interactions place Usp15 in the vicinity of actively-transcribed DNA. Importantly we found that SART3 has previously unrecognized histone chaperone activities. SART3, but not the well-characterized histone chaperone Nap1, enhances Usp15 binding to ubH2B and facilitates deubiquitination of ubH2B in free histones but not in nucleosomes. These results suggest that SART3 recruits ubH2B, which may be evicted from DNA during transcription, for deubiquitination by Usp15. In light of the function played by SART3 in U4/U6 di-snRNP formation, our discovery points to a direct link between eviction-coupled erasure of the Ub mark from ubH2B and co-transcriptional pre-mRNA splicing.

---

[2] This chapter is related to Long, L. et al. (2014) J Biol Chem *289*, 8916-8930. Published figures include 3.1, 3.2A, 3.2C, 3.4, 3.5, 3.6A, 3.6B, 3.7A, 3.8B, 3.8C, 3.10A, 3.11A-D, 3.11F, 3.12, 3.13, 3.14, 3.15, 3.16D, and 3.17. I heavily contributed to experimental conception, data collection, and analysis including all *in vivo* experiments, *in vitro* deubiquitinating assays, and supercoiling assays. Joe Thelen carried out the experiments in figures 3.3B, 3.11D, 3.13A, and 3.14A-B under my supervision.

3.1 Introduction

In eukaryotes, the state of chromatin affects all processes that require access to DNA, such as transcription, replication and DNA repair. DNA accessibility is regulated in part by numerous post-translational modifications (PTMs) on histones; these include acetylation, methylation, phosphorylation, ADP-ribosylation, ubiquitination, and sumoylation. The reversibility of these covalent modifications and their combinatorial occurrence contribute to their function as highly diverse and dynamic signals (Kouzarides, 2007; Patel and Wang, 2013). In comparison to most other PTMs, ubiquitination stands out because of its considerable size. Ubiquitin (Ub) is a protein of 76 amino acids with a well-folded and highly stable structure. It is attached to other proteins through the formation of an isopeptide linkage between the C-terminal carboxylate of Ub and a lysine sidechain of the substrate protein. In addition, Ub can be attached to other Ub molecules to form poly-Ub chains (Pickart and Eddins, 2004). Although all four core histones and linker histone H1 have been reported to undergo ubiquitination at various positions, the predominant ubiquitinated histones in humans are H2A ubiquitinated at K119 and H2B ubiquitinated at K120 (hereafter referred to as ubH2A and ubH2B) (Osley, 2006). Monoubiquitination of histones H2A or H2B does not lead to their degradation, but instead serves as a non-proteolytic signal that regulates gene expression and DNA repair processes. Interestingly, the same modification on different histones is associated with opposite effects: whereas ubH2A is associated with gene silencing, ubH2B is implicated primarily in active transcription (Weake and Workman, 2008).

UbH2B is conserved from yeast to man (Osley, 2006). In humans, it is catalyzed by the RNF20/RNF40 heterodimeric E3 ligase, which interacts with the PAF complex and

rides with the RNA polymerase II (RNAPII) in transcription elongation (Kim et al., 2005; Kim and Roeder, 2009; Xiao et al., 2005). Consistently, genome-wide localization studies suggest that ubH2B is largely associated with actively-transcribed genes (Jung et al., 2012; Minsky et al., 2008; Shieh et al., 2011). However, how ubH2B regulates transcription elongation has been enigmatic. Multiple observations that link ubH2B to various steps of the elongation process include: 1) ubH2B stimulates H3K4 di- and tri-methylation as well as H3K79 di- and tri-methylation (Lee et al., 2007; Sun and Allis, 2002); 2) ubH2B inhibits compaction of nucleosomal arrays *in vitro* (Fierz et al., 2010); 3) ubH2B co-operates with the histone chaperone FACT and remodeling enzyme Chd1 to reassemble nucleosomes in the wake of elongating RNAPII (Fleming et al., 2008; Lee et al., 2012; Pavri et al., 2006); 4) ubH2B inhibits recruitment of elongation factors, such as Ctk1 in yeast (Wyce et al., 2007) and TFIIS in humans (Shema et al., 2011), to impede elongation. Inhibitory functions of ubH2B in promoter regions have also been reported (Batta et al., 2011; Turner et al., 2002). That ubH2B can affect transcription both positively and negatively underscores the importance of ubH2B dynamics.

Several deubiquitinating enzymes (DUBs) have been reported that target ubH2B (Weake and Workman, 2008). The best-characterized histone DUB, the Spt-Ada-Gcn5-acetyltransferase (SAGA) complex, is conserved throughout eukaryotes and has important roles in transcription and mRNA export (Henry et al., 2003; Rodriguez-Navarro, 2009). Recent reports that ubH2B is enriched at the intron-exon boundaries in yeast, flies and humans suggest a novel link between ubH2B and co-transcriptional pre-mRNA splicing (Jung et al., 2012; Shieh et al., 2011). In yeast, deletion of the ubH2B ligase has mild splicing defects but exhibits synthetic sickness with components of the U1, U2 and U5 snRNP

(Moehle et al., 2012; Shieh et al., 2011). Whether and how ubH2B regulates splicing directly or indirectly is unclear.

We have developed a method to synthesize nonhydrolyzable mimics of ubH2A and ubH2B in large quantities. Using these proteins in pulldown assays from nuclear extracts, we identified a DUB, Usp15, that binds to ubiquitinated histones with high affinity. We also found that Usp15 associates indirectly with the ubH2B ligase RNF20/RNF40 and directly with a component of the splicing machinery, SART3. Our characterization of the Usp15/SART3/ubH2B interactions points to a direct link between H2B deubiquitination and co-transcriptional pre-mRNA splicing.

3.2 Experimental Procedures

3.2.1 Plasmids and antibodies

The coding sequences of Usp15[8], Usp15^{NTD}(1-222), Usp15^{CTD}(256-952), Usp4[9] and SART3[10], were cloned into the pcDNA5 FRT/TO vector (Life Technologies) downstream of a tandem Flag-Flag-HA epitope tag. Site-directed mutagenesis was used to generate all point mutations. The following plasmids were used for bacterial expression: pMal-C2 Usp15, pGEX4T-2 Usp15-His6, pGEX4T-2 Usp4-His6, pET21a Flag-HA-H2A, pET21a Flag-HA-H2B, pET21a H2A(K119C), pET21a H2B(K120C), and pET3a His6-Ub(G76C). For expression in Sf21 insect cells, the coding sequences of Usp15, SART3, RNF20, and RNF40 were cloned into pBacPAK6 vectors with N-terminal His6-Flag or His6-Myc sequences and recombinant viruses were generated following the manufacturer's instructions (Clontech).

Antibodies were purchased for detection of tubulin (DM1A) (Sigma T9026), Usp15 (abcam ab56900), Usp4 (Bethyl A300-830A), RNF20 (Abcam ab32629), RNF40 (Abcam

ab26082), SART3 (Abcam ab36137), Nap1L1 (Abcam ab21630), ubH2A (Cell Signaling 82405), ubH2B (MediMabs MM-0029P), H2B (Millipore 07-371), H3 (Abcam ab1791), H3K4me3 (Abcam ab8580), H3K79me2 (Abcam ab3594), H3K36me3 (Abcam ab9050), RNAPII CTD S2P (Abcam ab5095), RNAPII CTD S5P (Abcam ab5131), RNAPII CTD (Covance MMS-126R), Myc (9E10) (Millipore 05-419), Flag (Sigma F7425), and Flag (Pierce MA1-91878).

3.2.2 Cell culture, transfections and treatments

DMEM supplemented with 10% fetal bovine serum (FBS), 2 mM GlutaMAX, 100 units/mL pen/strep (Life Technologies) was used to culture HeLa, HEK293 and their derivatives. DMEM/F-12 (1:1) supplemented with 2.5 mM L-Glutamine, 10% FBS, 15 mM Hepes-KOH, pH 7.5, and antibiotics as described above was used to culture hTERT-RPE-1 cells. Stable cell lines were generated with pcDNA5 FRT/TO constructs using the parental Flp-In T-REx cell lines (Life Technologies) as described by Yao et al. (Yao et al., 2006). Doxycycline at 1 μg/mL was routinely used to induce target gene expression. Sf21 cells were cultured at 27 °C in Sf900-II SFM medium according to ATCC guidelines.

DNA and siRNA were transfected with Lipofectamine 2000 or Lipofectamine RNAiMax (Life Technologies), respectively, according to manufacturer's instructions. Depletion of RNAi target was assayed 72 hours post-transfection by reverse transcription (iScript, BioRad) and real-time PCR (SYBR Green Supermix, Bio-Rad), or by immunoblotting. siRNA sequences used are: Usp4 (5'CGAAGAAUGGAGAGGAACAUU3'), RNF20 (5'GAAGGCAGCUGUUGAAGAU3'), SART3 #1 (5'GGAGACAGGAAAUGCCUUA3'), and

SART3 #2 (5'GAUGUGGUGUCCUGAGAUA3'). siGenome pools against Usp15 and Usp11 were purchased from Dharmacon.

For cycloheximide chase experiments, cells were treated with 100 μg/mL cycloheximide 72 hours after siRNA transfection. At indicated times, cells were harvested in SDS-lysis buffer (50 mM Tris, pH 8.1, 10 mM EDTA, 1% SDS) and target protein levels were analyzed by SDS-PAGE and quantitative immunoblotting. The same procedure was employed for experiments with the E1 inhibitor, except that cells were treated with 10 μM E1 inhibitor. Quantitative immunoblots used fluorescent secondary antibodies and were analyzed with a Li-COR Odyssey scanner and Image Studio Software.

3.2.3 Recombinant proteins

For recombinant proteins expressed in bacteria, BL21(DE3) *E. coli* bearing the expression plasmid were grown to log phase and expression was induced with 0.4 mM IPTG at 37 °C for 3 hours. The only exception was MBP-Usp15, whose expression was induced at 19 °C for 16 hours before harvesting.

GST-Usp15-His6 purification: cell pellets were resuspended in PBS containing 1% Tween-20 and PIC (protease inhibitor cocktail: 1 mM PMSF, 50 mM TLCK, 1 mg/mL Pepstatin, 1 mg/mL Leupeptin) and lysed by sonication. Affinity purification with glutathione-agarose (GE Healthcare) was performed according to manufacturer's instructions. The eluate was further purified with Ni-NTA agarose (Qiagen) following manufacturer's instructions. Final elutions containing >90% full-length Usp15 were dialyzed into PBS, 5 mM bME (b-mercaptoethanol), 10% glycerol and stored at -80 °C in aliquots.

MBP and MBP-Usp15 purification: cell pellets were lysed in 50 mM Tris, pH 7.6, 300 mM NaCl, 1 mM EDTA, 10 mM $MgCl_2$, 0.01 mg/mL DNase I, 5 mM bME; affinity purification with amylose resin (New England Biolabs) were done according to manufacturer's instructions. Eluates containing purified proteins were dialyzed against 20 mM Tris, pH 7.6, 50 mM NaCl, 5 mM bME, 10% glycerol. MBP-Usp15 was further purified on a Mono Q column using a 0.05-0.8 M linear gradient of NaCl.

His6-Ub(G76C) was purified using Ni-NTA agarose according to manufacturer's protocol except that 5 mM bME was added in all buffers. Eluates were dialyzed against 10 mM Tris, pH 8.0, 50 mM NaCl, 0.2 mM EDTA, 10 mM bME, and then passed through Q Sepharose Fast Flow resin (GE Healthcare). His6-Ub(G76C) remained in the flow-through, which was dialyzed into 1 mM HOAc prior to lyophilization.

Recombinant histones were expressed and purified according to Dyer et al. (Dyer et al., 2004). Those that contained the cysteine substitution were dialyzed into 1 mM HOAc in the final step prior to lyophilization. His6-Usp2cc and His6-Nap1 were purified as described (Baker et al., 2005; McBryant et al., 2003).

His6-Flag-SART3 was expressed in Sf21 insect cells using the BacPAK baculovirus expression system (Clontech). 72 hours post- infection with recombinant virus, cells were harvested and recombinant SART3 was enriched with Ni-NTA agarose. Eluates from the Ni-NTA column were dialyzed against 20 mM Tris, pH 7.6, 50 mM NaCl, 5 mM bME, followed by further purification on a Mono Q 5/50 GL column (GE Healthcare) by HPLC. A linear gradient of 0.05–0.8 M NaCl in 20 mM Tris, pH 7.6, 5 mM bME, 10% glycerol was applied and SART3 was eluted at 450 mM NaCl. To eliminate contaminating DUB activities that co-purified with SART3, peak fractions from the Mono Q column were diluted to lower the salt

to 200 mM, incubated with 1.7 μM Ub-vinyl sulfone (Ub-VS; BostonBiochem) for 2 hours at 37 °C, and then passed through a Superdex 200 column to remove excess Ub-VS. The Ub-VS-treated SART3 did not affect Ub-AMC hydrolysis by Usp15 (data not shown).

3.2.4 Histone dimer, octamer and mononucleosome reconstitution

147 bp DNA containing 601 positioning sequence were prepared according to Dyer et al. (Dyer et al., 2004). Purified recombinant human H2A, H2B (or semi-synthetic ubH2B), H3.3 and H4 were assembled into octamers and further purified on a Superdex 200 column. H2A/H2B dimers were assembled similarly and further purified on a Superdex 75 column. Canonical mononucleosomes were reconstituted by salt dialysis (Dyer et al., 2004) and ubH2B-containing nucleosomes were prepared by salt dilution according to McGinty et al. (McGinty et al., 2008). Acid-extracted histones were prepared as described by Rogakou et al. except that acid-soluble proteins were dialyzed against water to allow refolding of histones (Rogakou et al., 2000). To prepare native nucleosomal substrates, HEK293 cells were lysed in hypotonic buffer (20 mM Tris, pH 8.0, 10 mM KCl, 1 mM $MgCl_2$, 0.3% NP-40, 30 mM N-ethylenemaleimide and PIC) on ice for 10 minutes and centrifuged to collect nuclei. Nuclei were resuspended at $1x10^8$ cells/mL in hypotonic buffer supplemented with 420 mM NaCl. Nuclei were again pelleted and washed twice in MNase (micrococcal nuclease) digestion buffer (50 mM Tris, pH 8, 10 mM $CaCl_2$, 2 mM $MgCl_2$). Digestion was performed with 80 U/mL MNase at 25 °C for 30 minutes and then the soluble fraction was collected and digested again with 20 U/mL MNase to achieve homogeneous mononucleosome products.

3.2.5 Semi-synthesis of native ubH2B

The coding sequence of H2B(1-116) was cloned into pTXB1 vector (New England Biolabs) between NdeI and SapI sites. The resulting plasmid was transformed into ER2566 cells (New England Biolabs) and expression of H2B(1-116)-intein fusion was induced with 0.5 mM IPTG at 25 °C for 6 h. Cells were harvested and lysed in lysis buffer (50 mM Tris, pH 7.6, 200 mM NaCl, 1 mM EDTA, supplemented with 10 mM MgCl2, 20 ug/mL DNase I and PIC). Cleared lysates were incubated with chitin beads at 4 °C overnight, followed by extensive wash of the beads with lysis buffer. To generate H2B(1-116)-a-thioester, beads were incubated with lysis buffer containing 50 mM mercaptoethansulfonate at 4 °C overnight, followed by elution with SAU buffer (20 mM NaOAc, pH 5.2, 7M urea). Eluates were further purified on a Mono S column by HPLC. Fractions containing >90% H2B(1-116) were pooled and presence of the thioester was confirmed by MALDI-TOF mass spectrometry. Subsequent synthesis follows the scheme as reported previously (Haj-Yahya et al., 2012).

3.2.6 Supercoiling assay

Supercoiling assays were performed as described previously (Dechassa et al., 2011) except that pGEM3Z plasmid DNA was used instead of pBR322 and the final products were separated by electrophoresis in a 1.2% agarose gel and visualized by ethidium bromide staining.

3.2.7 Immunofluoresence

Cells were cultured on coverslips and fixed with 2.5% paraformaldehyde at 37 °C for 10 minutes. After washing with PBS, cells were permeabilized in wash buffer (PBS, 0.1% Triton X-100) at 25 °C for 20 minutes. This was followed by blocking in PBS, 5% BSA, 0.1% Triton X-100, 2 mM MgCl2 for 10 minutes, and incubations with primary and secondary antibodies with washes in between. Cells were then stained with DAPI (1ug/mL) for 5 minutes before coverslips were mounted to glass slides with ProLong Gold antifade reagent (Life Technologies). For staining using ubH2B antibody (Cell Signaling), cells were fixed and permeabilized as described above. Next, chromatin was unwound by treating with 2 M HCl in PBS for 10 minutes at 37 °C. The remainder of the staining protocol was as described above except PBS was used for all wash steps.

3.2.8 Generation of crosslinked ub*histone mimics

Crosslinking reactions adopted the procedure described by Yin et al. (Yin et al., 2000b). Lyophilized His6-Ub(G76C), H2A(K119C), or H2B(K120C) was resuspended in 10 mM HOAc, 7 M urea at 10 mg/mL. Histone and Ub were at a 2:1 molar ratio in 6 M urea, 50 mM sodium borate, pH 8.5, 5 mM TCEP (tris(2-carboxyethyl)phosphine). The crosslinker, 1,3-dichloroacetone, was added at a molar concentration equal to half of the sum of all free cysteines in the reaction. After incubation on ice for 30 min, the reaction was stopped with 5 mM βME. To remove unreacted histones, the mixture was diluted 1:10 in denaturing binding buffer (50 mM NaPi, pH 8, 300 mM NaCl, 6 M urea, 10 mM imidazole, 5 mM βME) and incubated with Ni-NTA agarose. After washing with the same buffer, the bound fraction, which contained Ub, Ub*Ub and Ub*histones, was eluted with the binding buffer

plus 250 mM imidazole. Eluate was used to reconstitute either histone dimers or octamers directly. Ub and Ub*Ub were removed during the subsequent gel filtration step.

To generate ub*GSH (Ub crosslinked to glutathione), a 1:5 molar ratio of His6-Ub(G76C) to glutathione was used to perform the crosslinking as described above, except that urea was omitted from the reaction. The reaction mixture was loaded on a Mono S 5/50 column in 50 mM ammonium acetate, pH 5.5, 5 mM βME and proteins were eluted with a linear gradient of 0–1 M NaCl in the same buffer. Peak fractions containing ub*GSH were pooled and purified further with the same column. The ub*GSH product was confirmed by MALDI-TOF mass spectrometry (data not shown).

3.2.9 Deubiquitination assays

For deubiquitination of Ub-AMC (BostonBiochem), reactions were performed in assay buffer (50 mM Hepes, pH 7.5, 0.5 mM EDTA, 0.5 mg/mL BSA, 200 mM NaCl, 5 mM DTT) with 2 nM enzyme unless otherwise indicated; 0.05% Brij-35 was added to reactions containing SART3. In competition assays, competitor proteins were added to an enzyme-containing master mix and reactions were initiated by addition of the substrate. Ub-AMC hydrolysis was monitored continuously for 1 h at 30 °C on a fluorescence plate reader (BioTek Synergy 4, λex = 340 nm and λem = 440 nm); initial velocities of fluorescence increases were converted to concentration of AMC released per min by reference to an AMC standard. Data were fitted with the Michaelis-Menten equation and, for competition assays, with a one-site binding model using PRISM (Graphpad Software).

Qualitative deubiquitinating assays using native or semi-synthetic ubH2B substrates were done at 37 °C for indicated times in reaction buffer (10 mM Hepes, pH 7.5, 200 mM NaCl, 0.05% Brij-35, 25 μM ZnSO4, 5 mM DTT, 0.5 mg/mL BSA).

3.3 Results

3.3.1 Usp15 and Usp4 bind to monoubiquitinated histone H2A or H2B *in vitro*

Although ubiquitination of histone H2A or H2B has been associated with a variety of biological consequences in the cell, few direct effectors of ubiquitinated histones have been identified. We aimed to identify proteins that bind preferentially to either unmodified, ubH2A-containing, or ubH2B-containing histone dimers. To avoid heterogeneous post-translational modifications that naturally occur on histones prepared from cells, we adopted a strategy that was previously employed to synthesize nonhydrolyzable di-Ub analogues (Yin et al., 2000b) and mono- and poly-ubiquitinated PCNA (Carlile et al., 2009) from recombinant proteins. Because there are no native cysteines in Ub, H2A, or H2B, we used site-directed mutagenesis to incorporate a cysteine at the C-terminus of Ub (UbG76C) and the primary ubiquitination site on H2A or H2B (H2AK119C and H2BK120C, respectively). Each mutant protein was expressed in *E. coli* and purified to homogeneity. Ub was then crosslinked to each histone with a bifunctional thiol crosslinker, dichloroacetone (Figure 3.1A). The resulting crosslink is one C-C bond longer than an isopeptide linkage and bears an additional carboxylate group, but has the advantage that it is highly stable and not susceptible to deubiquitinating activities. Purified ub*H2A or ub*H2B (* denotes the crosslink), was assembled with Flag-tagged H2B or H2A into histone dimers (Figure 3.1B) and used in pull-down assays to isolate interacting proteins from HeLa cell nuclear extract.

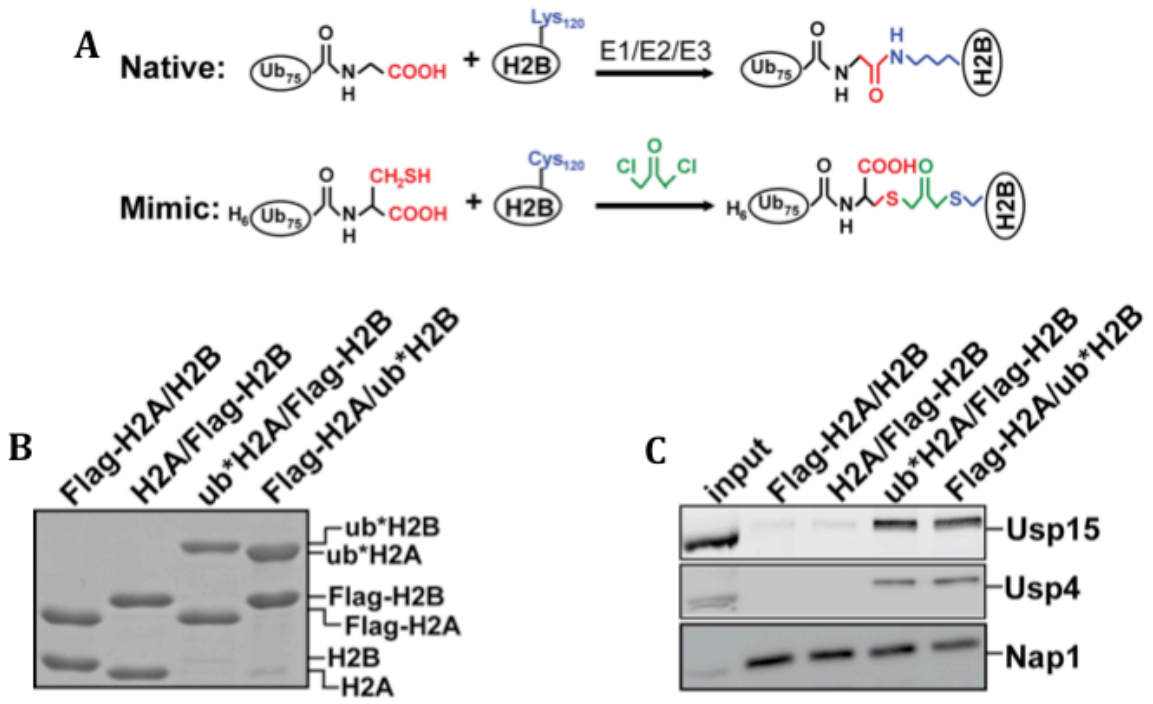

Figure 3.1. Usp4 and Usp15 bind to monoubiquitinated histone H2A or H2B *in vitro*. (A) Schematic comparing native ubH2B and the crosslinked mimic. In the mimic, Gly76 of Ub and Lys120 of H2B were mutated to cysteines; crosslinking with dicholoroacetone produces a dithioether linkage that is resistant to cleavage by DUBs. **(B)** A Coomassie-stained gel of purified Flag-tagged H2A/H2B dimers that are either unmodified or contain a ubiquitinated histone mimic (i.e., ub*H2A or ub*H2B). **(C)** Usp15 and Usp4 bind to ubiquitinated H2A/H2B dimers. The Flag-tagged H2A/H2B dimers shown in (B) or Flag-Ub were immobilized on anti-Flag agarose and incubated with HeLa nuclear extract adjusted to 470 mM NaCl. Bound proteins were analyzed by SDS-PAGE and immunoblotting.

Proteins bound to unmodified or ubiquitinated dimers under stringent conditions (470 mM NaCl) were identified by mass spectrometry. Among the few proteins that preferentially bound to ub*H2A or ub*H2B-containing histone dimers, we identified Usp15. Immunoblotting analysis confirmed that Usp15 bound only to ubiquitinated histone dimers (i.e., ub*H2A/H2B or H2A/ub*H2B), but not to Ub or unmodified H2A/H2B (Figure 3.1C and Supplemental Fig. S1A). Nucleosome assembly protein-1 (Nap1) was used as a control as it showed no preference for unmodified or ubiquitinated histone dimers (Fierz et al., 2012a). Human Usp15 has 73% sequence similarity with another DUB, Usp4. Although Usp4 was not identified by mass spectrometry, when we immunoblotted for Usp4 in the pull-downs, we found that it behaved identically to Usp15 (Figure 3.1C).

Although histones are highly charged and aggregation-prone, among the numerous proteins present in the nuclear extract, Usp15 was one of the few proteins that bound exclusively to ubiquitinated but not unmodified histones. In order to quantify the affinity and specificity of the interactions between Usp15 and the ubiquitinated histones, we used the nonhydrolyzable ub*histone mimics in DUB activity assays as potential inhibitors of deubiquitination. Purified recombinant Usp15 can hydrolyze Ub-AMC, a minimal and general DUB substrate composed of Ub conjugated to 7-amino-4-methylcoumarin (AMC) (Figure 3.2). Upon addition of ub*H2A/H2B or H2A/ub*H2B dimers, Ub-AMC hydrolysis by Usp15 was inhibited in a dose-dependent manner (Figure 3.3A). In contrast, similar concentrations of unmodified H2A/H2B dimers did not inhibit Usp15 significantly. To address whether the artificial crosslink mediates unexpected interactions with the DUB, we prepared UbG76C crosslinked to glutathione via dichloroacetone. Whereas the IC50 values for inhibition by the ub*histone mimics were each about 0.1 mM, the IC50 for ub*GSH was

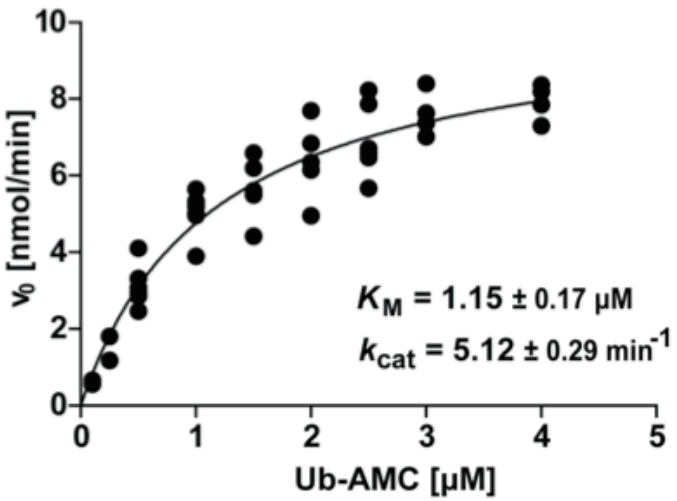

Figure 3.2. Usp15 hydrolyzes Ub-AMC. Purified recombinant GST-Usp15-His_6 (2 nM) was incubated with increasing concentrations of Ub-AMC and the initial rates of hydrolysis (V_0) were fitted with the Michaelis-Menten equation.

A

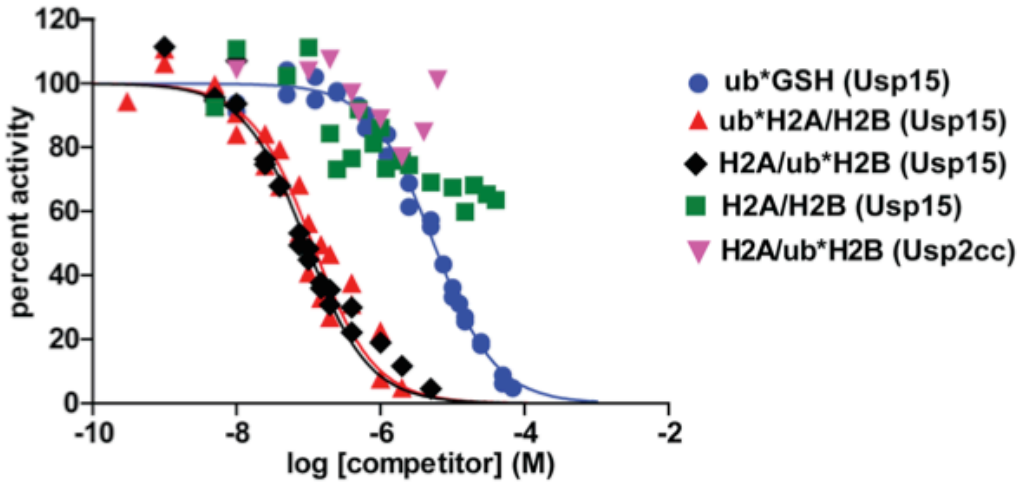

Usp15	ub*GSH	ub*H2A/H2B	H2A/ub*H2B
IC50 (nM)	5843 ± 217.2	113.7 ± 11.9	93.6 ± 7.57
R^2	0.990	0.932	0.959

B

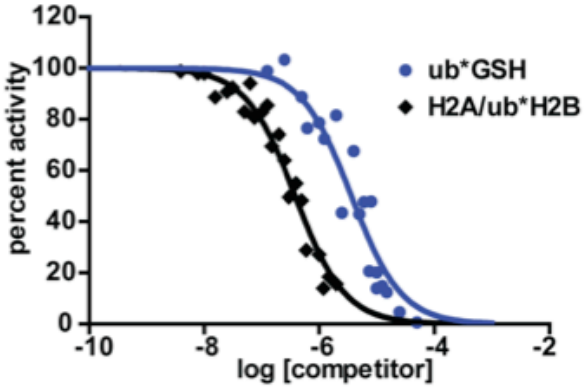

Usp4	ub*GSH	H2A/ub*H2B
IC50 (nM)	3660 ± 470	386± 29.4
R^2	0.899	0.962

C

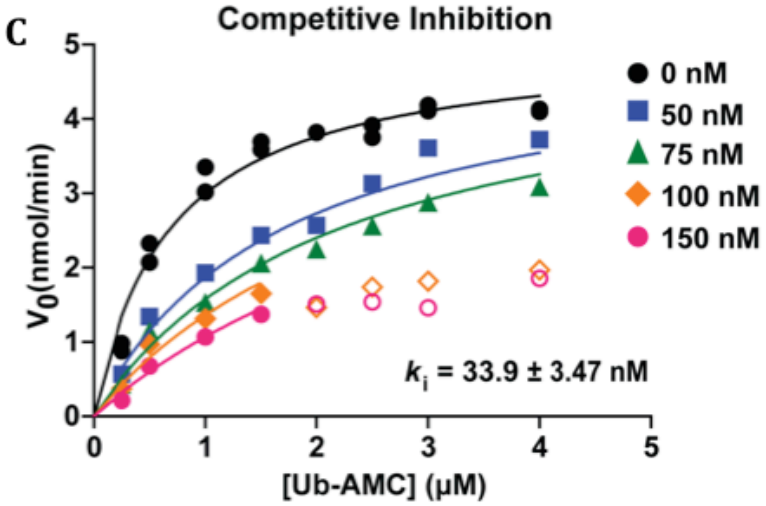

Model	R^2
Competitive	0.980
Noncompetitive	0.957
Uncompetitive	0.919

Figure 3.3. H2A/ub*H2B is a competitive inhibitor of Usp15 and Usp4. (A-B) Recombinant Usp15 and Usp4 bind to ubiquitinated H2A/H2B dimers with high affinity. The deubiquitinating activity of purified recombinant Usp15 or Usp2cc (A) or or Usp4 (B) was monitored by incubation with 1 mM Ub-AMC in the absence or presence of increasing amounts of potential competitive inhibitors, including ub*GSH, H2A/H2B, ub*H2A/H2B, or H2A/ub*H2B. The data were fit with a one-site binding model to determine the IC50 of each competitor. Unmodified H2A/H2B dimers below 1 mM did not inhibit, at concentrations >1 mM, non-specific inhibition was observed that is likely due to aggregation. **(C)** H2A/ub*H2B is a competitive inhibitor of Usp15. The rates of Ub-AMC hydrolysis by Usp15 were determined at indicated Ub-AMC and H2A/ub*H2B concentrations. These rates were plotted and fitted with competitive, noncompetitive, or uncompetitive inhibition models and the goodness of fit (R^2) for each model was shown in the table. Solid lines in the plot represent the fit with a competitive inhibition model. Using the Akaike's Information Criterion (AIC), there is 99.99% probability that the competitive inhibition model is correct. Due to aggregation issues at high concentrations of histones and Ub-AMC, open data points were excluded in all the fit.

nearly 60-fold higher (Figure 3.3A). Like Usp15, Usp4 was strongly inhibited by H2A/ub*H2B with an IC50 of 0.39 mM (Figure 3.3B). Further kinetic analysis showed that inhibition of Usp15 by H2A/ub*H2B was best described using a competitive binding model with a K_i of 34 nM (Figure 3.3C). These results demonstrate that the interactions between Usp15 and ubiquitinated histones are direct, specific, and of high affinity. Furthermore, because H2A/ub*H2B did not affect Ub-AMC hydrolysis by the Usp2 catalytic core domain (Usp2cc) (Figure 3.3A) (Ryu et al., 2006), this behavior is not a property shared among the USP family of DUBs.

3.3.2 Usp15 deubiquitinates free and nucleosomal histones with a strong preference for free histones

To test directly whether Usp15 deubiquitinates free histones or nucleosomes, we prepared acid-extracted histones from HEK293 cells and mononucleosomes purified from micrococcal nuclease-digested chromatin. As a positive control, we used the recombinant DUB module of the yeast SAGA complex ($SAGA^{DUB}$), which is known to deubiquitinate H2B *in vivo* and *in vitro* (Kohler et al., 2010; Samara et al., 2010). Figure 3.4A shows that both Usp15 and $SAGA^{DUB}$ deubiquitinated H2B as free histones or in nucleosomes. Because histones and nucleosomes purified from cells are heterogeneous, we sought to obtain a chemically-defined substrate. Using a strategy that combined solid phase peptide synthesis and native chemical ligation (Figure 3.5A) we obtained ubH2B that has a native Ub–histone isopeptide linkage and is free of other post-translational modifications (Figure 3.5B)(Haj-Yahya et al., 2012; Kumar et al., 2011). The ubH2B was successfully assembled with recombinant human H2A, H3.3 and H4 histones into octamers or mononucleosomes

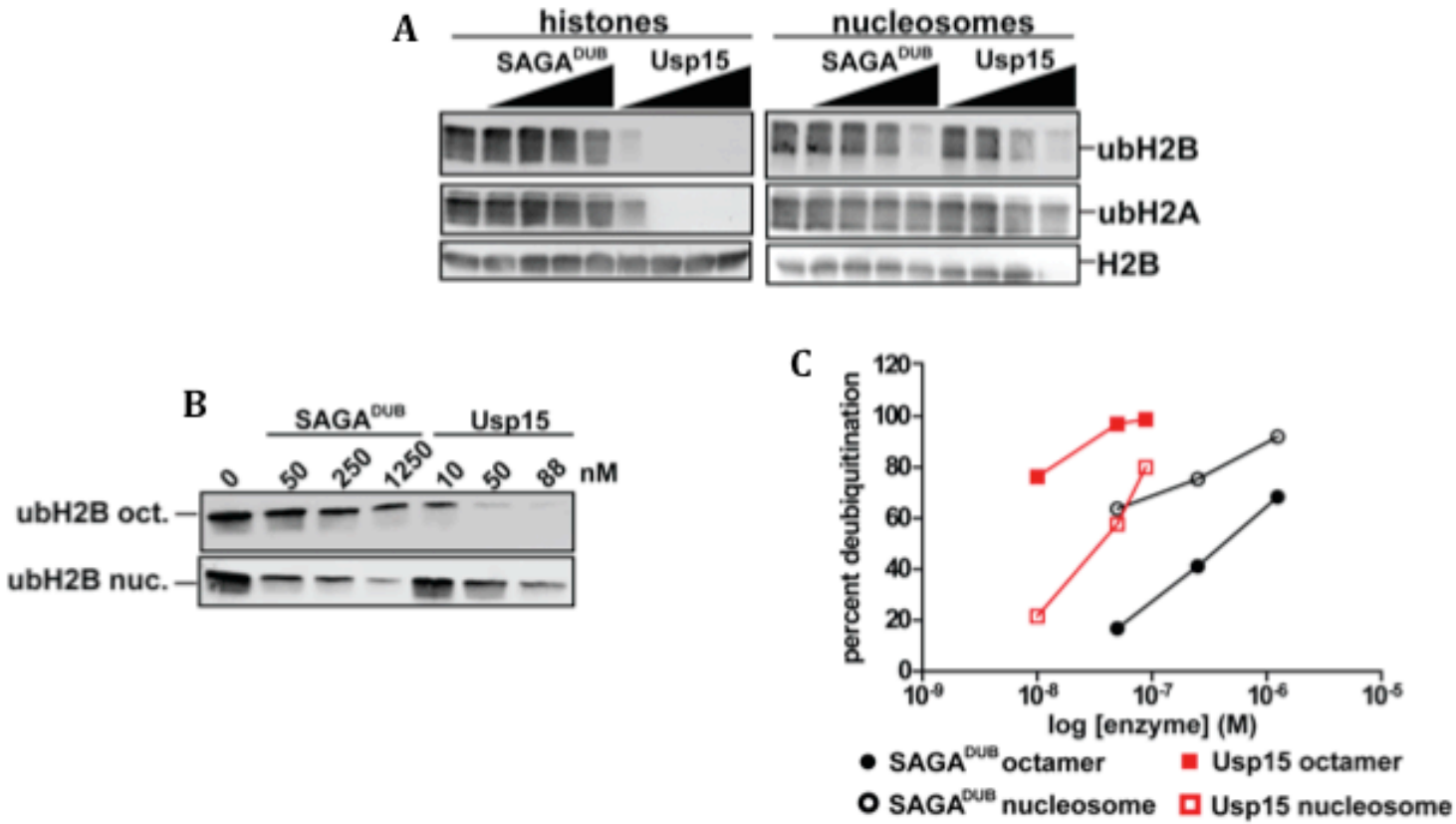

Figure 3.4. Usp15 preferentially deubiquitinates free histone substrates. (A) Usp15 and SAGA^{DUB} deubiquitinate ubH2B-containing histones and nucleosomes. 1, 10, 50, and 250 nM recombinant SAGA^{DUB} or MBP-Usp15 was incubated at 37 °C with acid-extracted histones (for 1 h) or mono-nucleosomes purified from cells (for 2 h). Each reaction contained approximately 500 nM ubH2A and 50 nM ubH2B. Deubiquitination was monitored by SDS-PAGE and immunoblotting with antibodies that specifically recognize H2A ubiquitinated at K119 (ubH2A) or H2B ubiquitinated at K120 (ubH2B). **(B)** Histone octamers or mononucleosomes were assembled from recombinant H2A, H3.3, H4, and semi-synthetic ubH2B. Each reaction, which contained 200 nM substrate and enzyme as indicated, was incubated at 37 °C for 2 h. Deubiquitination was monitored by SDS-PAGE and immunoblotting with the anti-ubH2B antibody. **(C)** Quantitation of the blot shown in (B).

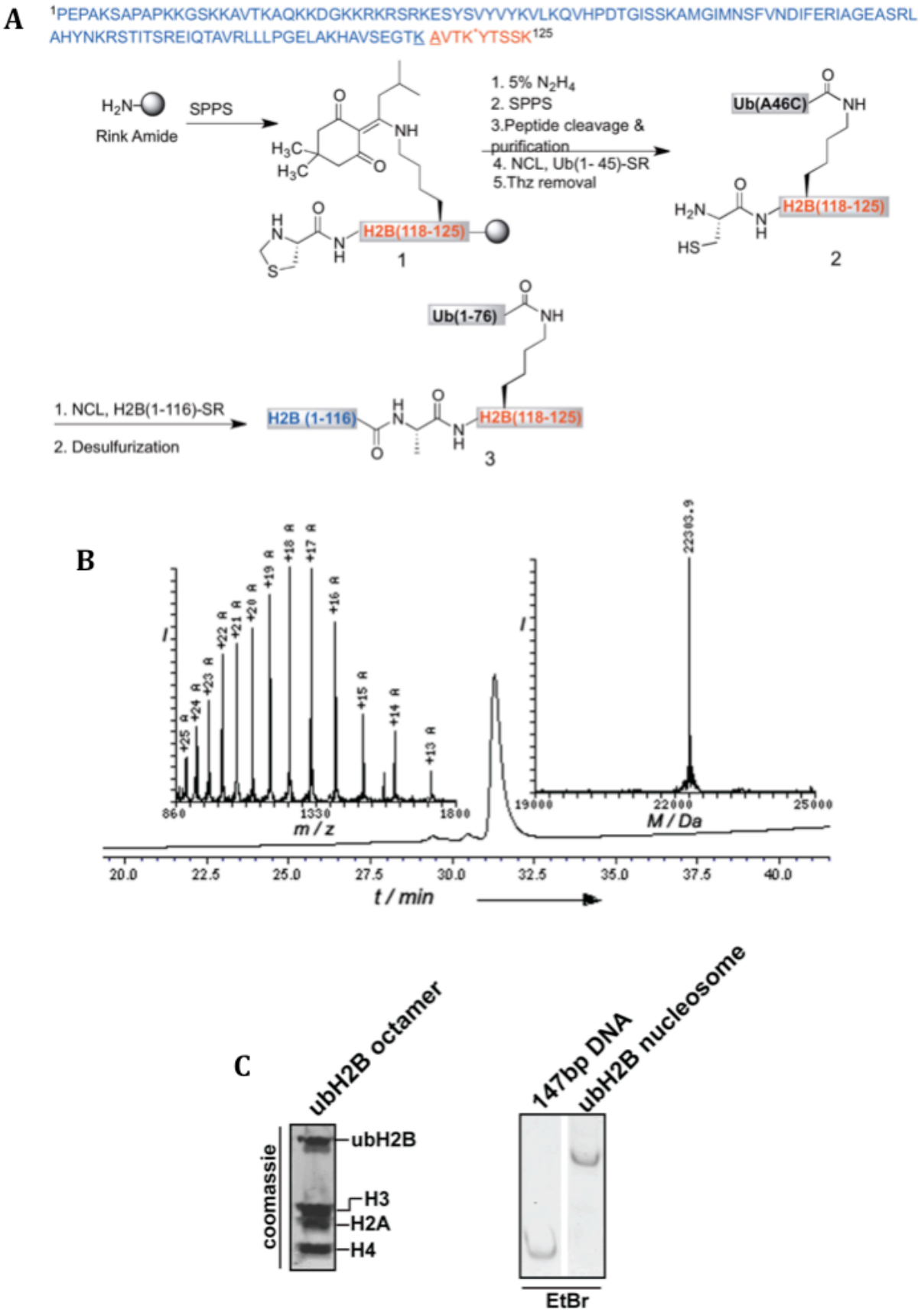
A
1PEPAKSAPAPKKGSKKAVTKAQKKDGKKRKRSRKESYSVYVYKVLKQVHPDTGISSKAMGIMNSFVNDIFERIAGEASRL
AHYNKRSTITSREIQTAVRLLLPGELAKHAVSEGTK AVTK*YTSSK125
H2N
Rink Amide
SPPS
1. 5% N2H4
2. SPPS
3.Peptide cleavage & purification
4. NCL, Ub(1- 45)-SR
5.Thz removal
Ub(A46C)
H2B(118-125)
1
2
Ub(1-76)
1. NCL, H2B(1-116)-SR
2. Desulfurization
H2B (1-116)
3
B
+25 A
+24 A
+23 A
+22 A
+21 A
+20 A
+19 A
+18 A
+17 A
+16 A
+15 A
+14 A
+13 A
22303.9
m / z
M / Da
t / min
C
ubH2B octamer
147bp DNA
ubH2B nucleosome
coomassie
ubH2B
H3
H2A
H4
EtBr

Figure 3.5. Semi-synthesis of ubH2B and reconstitution of ubH2B-containing mononucleosomes. (A) Scheme for semi-synthesis of ubH2B. The synthesis of ubiquitinated H2B was carried out using the expeditious synthesis approach to form fragment **2** as reported previously (Kumar et al., 2011). Thereafter, fragment **2** was ligated with the expressed fragment H2B(1–116)- thioester, followed by desulfurization to generate **3** in 20% yield (for four steps) (Haj-Yahya et al., 2012). **(B)** Characterization of semi-synthetic ubH2B. Analytical HPLC of the purified ubH2B and mass spectrometry analysis showed observed mass 22303.9 Da (calculated 22302.8 Da). **(C)** Reconstituted histone octamers and mono-nucleosomes containing semi-synthetic ubH2B. Recombinant human H2A, H3.3, H4 and semi-synthetic ubH2B were combined in equal molar to reconstitute histone octamers as described by Dyer et al., 2004. Purified histone octamers were analyzed by SDS-PAGE and coomassie staining. These octamers were used to assemble mono-nucleosomes on a 147 bp 601-positioning sequence by salt dilution (McGinty et al., 2008). Reconstitued nucleosomes were analyzed on a 6% polyacrylamide native gel and visualized by ethidium bromide staining.

(Figure 3.5C). Using these chemically-defined substrates, we found that both Usp15 and SAGA^{DUB} deubiquitinated H2B in the context of histone octamers or mononucleosomes (Figure 3.4B). However, with either the cell-derived or semi-synthetic substrates, Usp15 preferentially deubiquitinated the histones whereas SAGA^{DUB} preferred the ubH2B-containing nucleosomes. Recombinant Usp15 and SAGA^{DUB} have comparable activities against nucleosomal substrates, but Usp15 is ~10-fold more active against the histone substrates (Figure 3.4C).

3.3.3 Usp4 and Usp15 associate with RNF20/RNF40 and promote RNF40 stability

We established inducible stable cell lines that express full-length or truncated versions of Usp15 and Usp4. Previously, a large-scale effort by Sowa *et al.* had surveyed potential DUB-associated proteins by overexpressing HA-tagged DUBs in HEK293 cells, followed by anti-HA immunoprecipitation and identification of co-immuoprecipitated proteins by mass spectrometry (Sowa et al., 2009). Among the potential interactors of Usp15, RNF40, a subunit of the mammalian H2B E3 ligase, was identified with high confidence. Our cell lines have the advantage that, because of leaky expression in the absence of doxycycline (Dox) (Figure 3.6A), we could examine protein-protein interactions with a physiologically-relevant level of Flag-Usp15. We found that both endogenous RNF20 and RNF40 co-immunoprecipitated with Usp15 either with or without overexpression by induction with Dox (Figure 3.6B). Similarly, Flag-tagged Usp4 co-immunoprecipitated with endogenous RNF20 and RNF40, albeit less efficiently (Figure 3.6C).

The N-terminal portion (NTD) of Usp15 or Usp4 is comprised of two well-defined protein domains, a DUSP (Domain specific for USP) and a UBL (Ub-like) domain, whereas

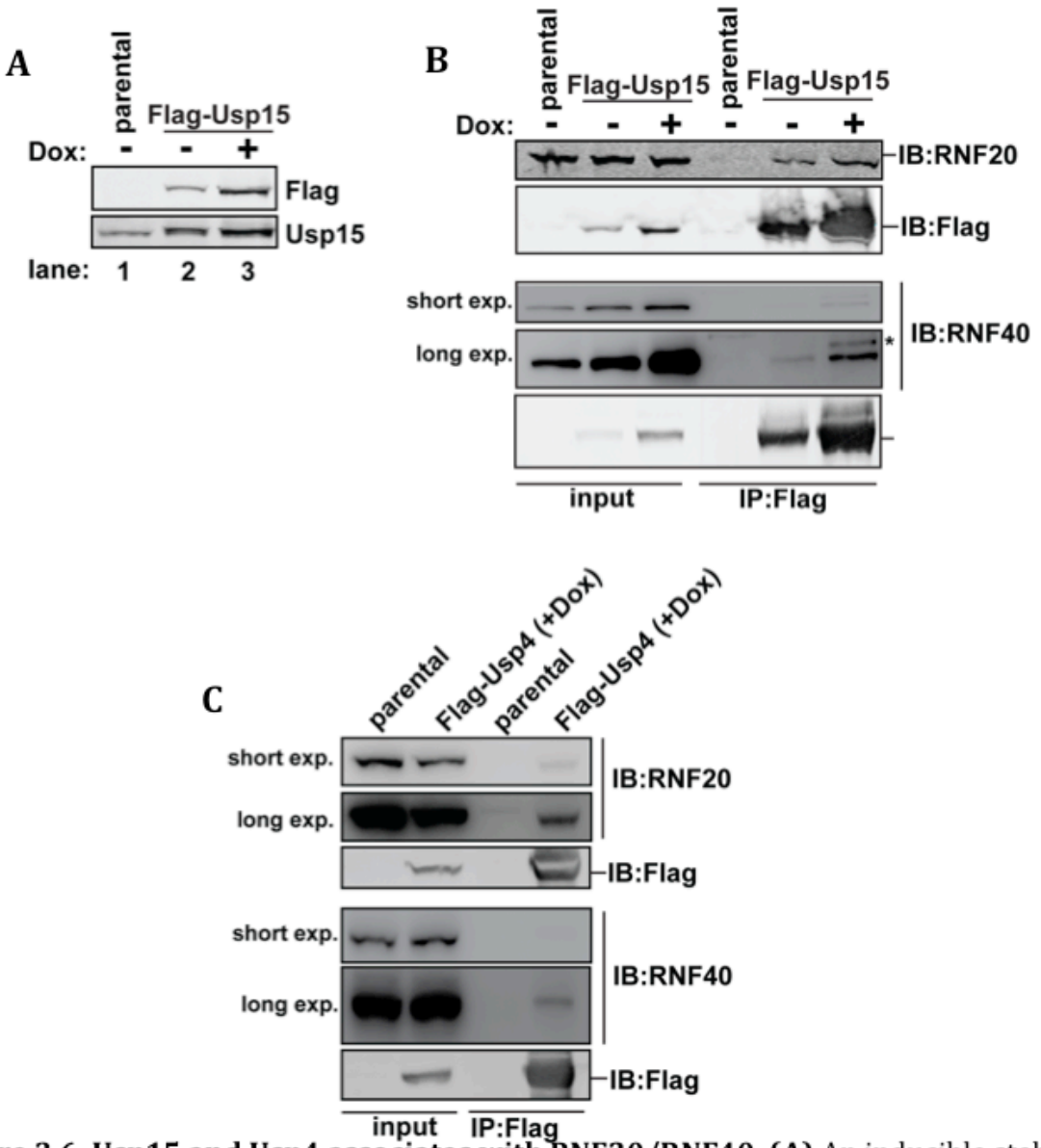

Figure 3.6. Usp15 and Usp4 associates with RNF20/RNF40. (A) An inducible stable cell line that expresses Flag-Usp15 in response to Doxycycline (Dox). The Flag-Usp15 inducible stable cells were treated with or without 1 mg/ml Dox for 48 h and cell lysates were analyzed by SDS-PAGE and immunoblotting along with parental cell lysates for comparison. In the absence of Dox, Flag-Usp15 was expressed at a similar level as endogenous Usp15 (compare lane 1 and 2 on the anti-Usp15 blot). Note that anti-Usp15 detects both endogenous and Flag-tagged Usp15, which migrate the same on this gel. **(B)** Endogenous RNF20 and RNF40 co-immunoprecipitate with Usp15. Extracts were prepared from the parental or Flag-Usp15-expressing cells with or without Dox treatment, incubated with anti-Flag agarose, and the bound proteins were detected by SDS-PAGE and immunoblotting with the indicated antibodies. Asterisk denotes a non-specific band. **(C)** Endogenous RNF20 and RNF40 co-immuoprecipitate with Usp4. Overexpressed Flag-Usp4 (+Dox) was immunoprecipitated with anti-Flag agarose as described in (B).

the large C-terminal portion (CTD) contains the catalytic residues (Figure 3.7A). The DUSP domain has been suggested to mediate protein-protein interactions. However, we found that the NTD of Usp15 did not associate with RNF20, whereas the full-length protein, or to a lesser extent, the CTD, bound to endogenous RNF20 (Figure 3.7B).

Other DUB–E3 associations have been reported previously (Clague et al., 2012; Sowa et al., 2009). The best-studied example is the Usp7–Mdm2 pair that regulates p53 ubiquitination. Depending on protein levels and other signals, Usp7 could either deubiquitinate p53 to promote substrate stability or deubiquitinate Mdm2 to stabilize the E3 ligase, thus leading to opposite downstream consequences (Li et al., 2004; Meulmeester et al., 2005). We sought to examine the function of the Usp15–RNF20/RNF40 pair in HeLa cells. Upon siRNA-mediated knockdown of Usp15 or Usp4, we did not observe significant changes of steady-state levels of either ubH2B or RNF20 (Figure 3.8A). The human genome encodes a paralogue of Usp15 and Usp4, Usp11 (Elliott et al., 2011). We attempted to knockdown Usp11 or a combination of all three DUBs, but we still did not observe significant changes of ubH2B or RNF20 levels (Figure 3.8A). By quantitative mRNA analysis, the knockdowns appeared to be effective (Figure 3.9A); however, due to lack of high-affinity antibodies, we could only monitor knockdown at the protein level for Usp15 (Figure 3.8A).

Steady-state protein levels are determined by both the rates of synthesis and degradation. To monitor directly the rate of degradation, we performed a cycloheximide chase in cells depleted of Usp15 and Usp4 (Figure 3.8B). In cells treated with control siRNA, both RNF20 and RNF40 were highly stable and showed no detectable changes of protein levels 4 hours after cycloheximide treatment. Depletion of Usp15 and Usp4 did not affect

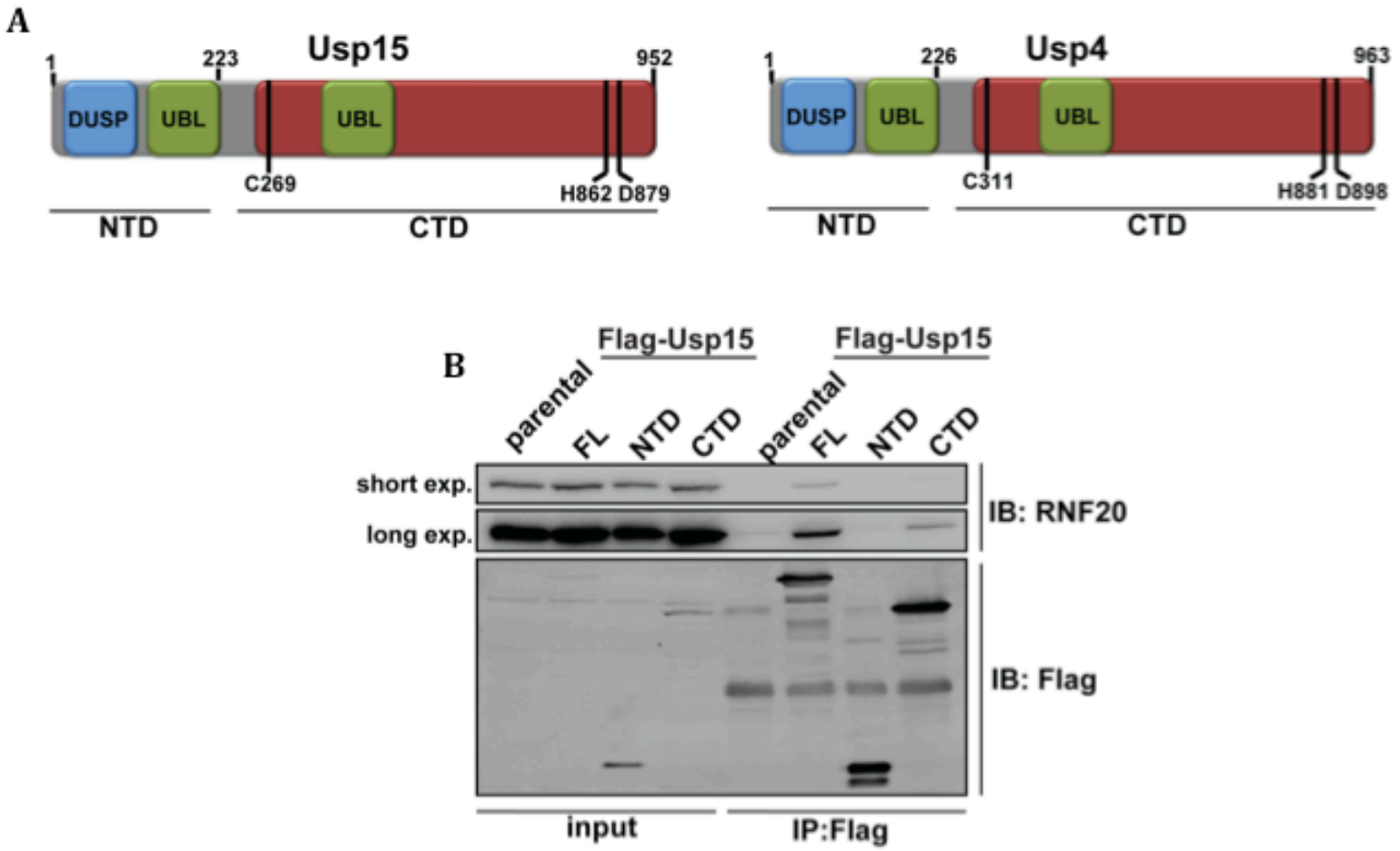

Figure 3.7. The CTD of Usp15 is required for interaction with RNF20. (A) Schematic of the domain structures of Usp4 and Usp15. Each N-terminal domain (NTD) consists of a domain specific to USP (DUSP) and a Ub-like domain (UBL). Each C-terminal domain (CTD) contains the catalytic residues and an additional UBL domain. **(B)** The NTD of Usp15 is not required for its association with RNF20. Stable cell lines expressing Flag-tagged full-length (FL), NTD or CTD of Usp15 were established; immuoprecipitations of cell lysates with anti-Flag agarose were performed as described in (Figure 3.4B).

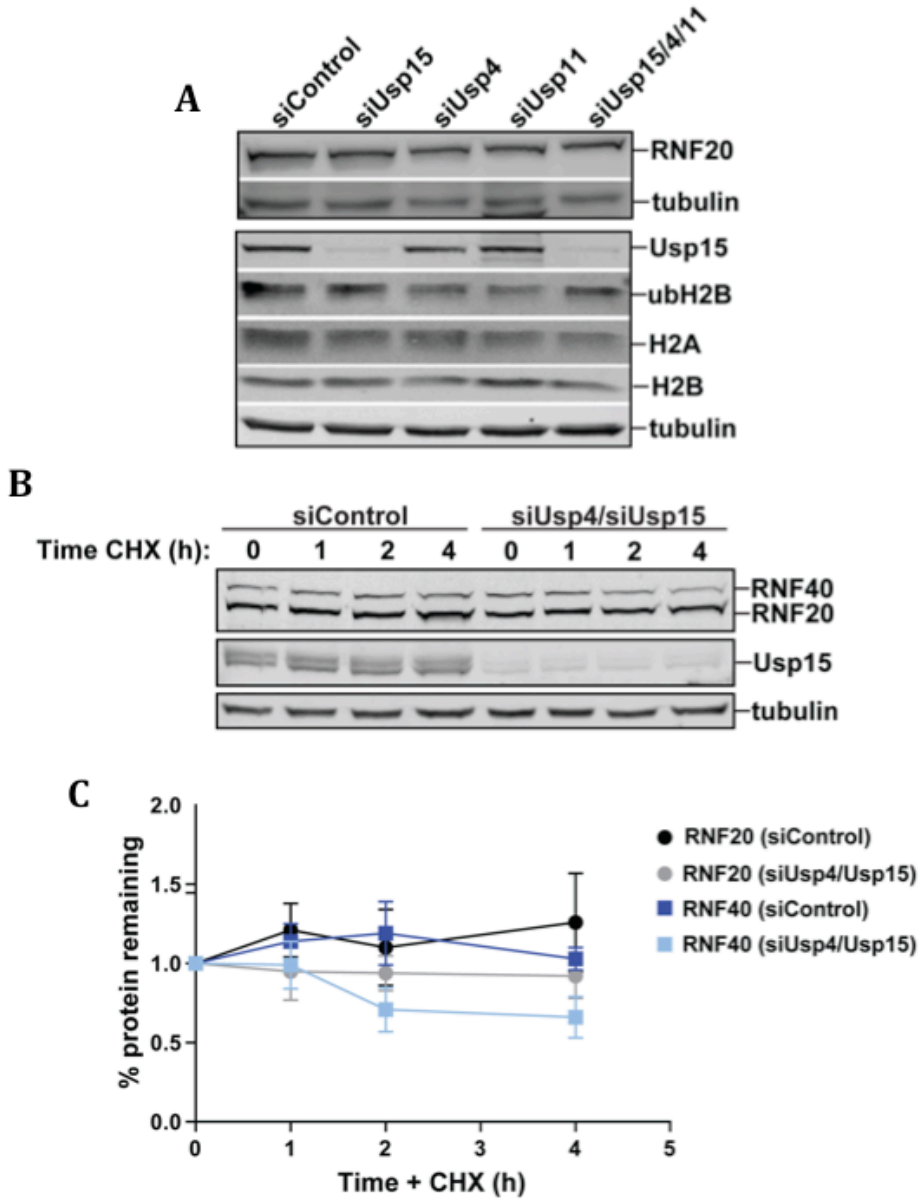

Figure 3.8. Usp15 and Usp4 regulate RNF40 stability. (A) Knockdown of Usp4, Usp15, Usp11, or all three together did not affect steady-state levels of RNF20, ubH2A or ubH2B. The DUBs were depleted from HeLa cells by transfection with 3.3 nM specific siRNAs. 72 h post transfection, total cell lysates were analyzed by SDS-PAGE and immunoblotting with the indicated antibodies. Tubulin was used as a loading control. **(B)** Usp4 and Usp15 depletion did not affect protein stability of RNF20 and moderately reduced the stability of RNF40. HeLa cells were transfected with 6.6 nM Control siRNA or a combination of Usp4 and Usp15 siRNAs at 3.3 nM each. 72 h post-transfection, cells were treated with cycloheximide (CHX) for the indicated times prior to harvesting. Protein levels were monitored by SDS-PAGE and quantitative immunoblotting. A representative experiment is shown. **(C)** Quantitation of blots shown in (B). Tubulin levels were used for normalization. Shown are the average changes (fold) from three independent experiments. Error bars represent standard deviations.

the stability of RNF20 but did accelerate turnover of RNF40. The effect on RNF40 half-life was moderate, but reproducible (Figure 3.8C shows quantitation from three independent experiments). Therefore, Usp15 and Usp4 play only a minor role in protecting the E3 ligase RNF40 from degradation, possibly by counteracting its auto-ubiquitination.

To test whether Usp15 directly interacts with RNF20 or RNF40, we co-expressed all three proteins in insect cells. We observed a 1:1 complex formed between RNF20 and RNF40, but failed to detect significant co-immunoprecipitation with Usp15 despite robust expression levels (data not shown). We note that co-immunoprecipitation of Usp15 and RNF20/RNF40 in mammalian cells was also inefficient (Figure 3.6A). These led us to conclude that Usp15's association with RNF20/RNF40 is likely to be indirect.

3.3.4 Usp15 directly associates with the U4/U6 recycling factor SART3

Previously, Song *et al.* reported that knockdown of Usp4 leads to cell cycle defects that are indicative of spindle checkpoint bypass. This was due to Usp4's role in facilitating pre-mRNA splicing through its interactions with the splicesosome tri-snRNP recycling factor, Squamous cell Antigen Recognized by T cells 3 (SART3) (also called p110 or Tip110) (Song et al., 2010). One important point of splicing regulation is the formation/recycling of the U4/U6.U5 tri-snRNP and this process is expedited by SART3 (Ghetti et al., 1995). In the early stage of spliceosome assembly, SART3 promotes the formation of the U4/U6 di-snRNP (Bell et al., 2002; Rader and Guthrie, 2002). As the spliceosome matures, the U4 snRNP is ejected, bound by SART3, and then recycled for the next round of assembly.

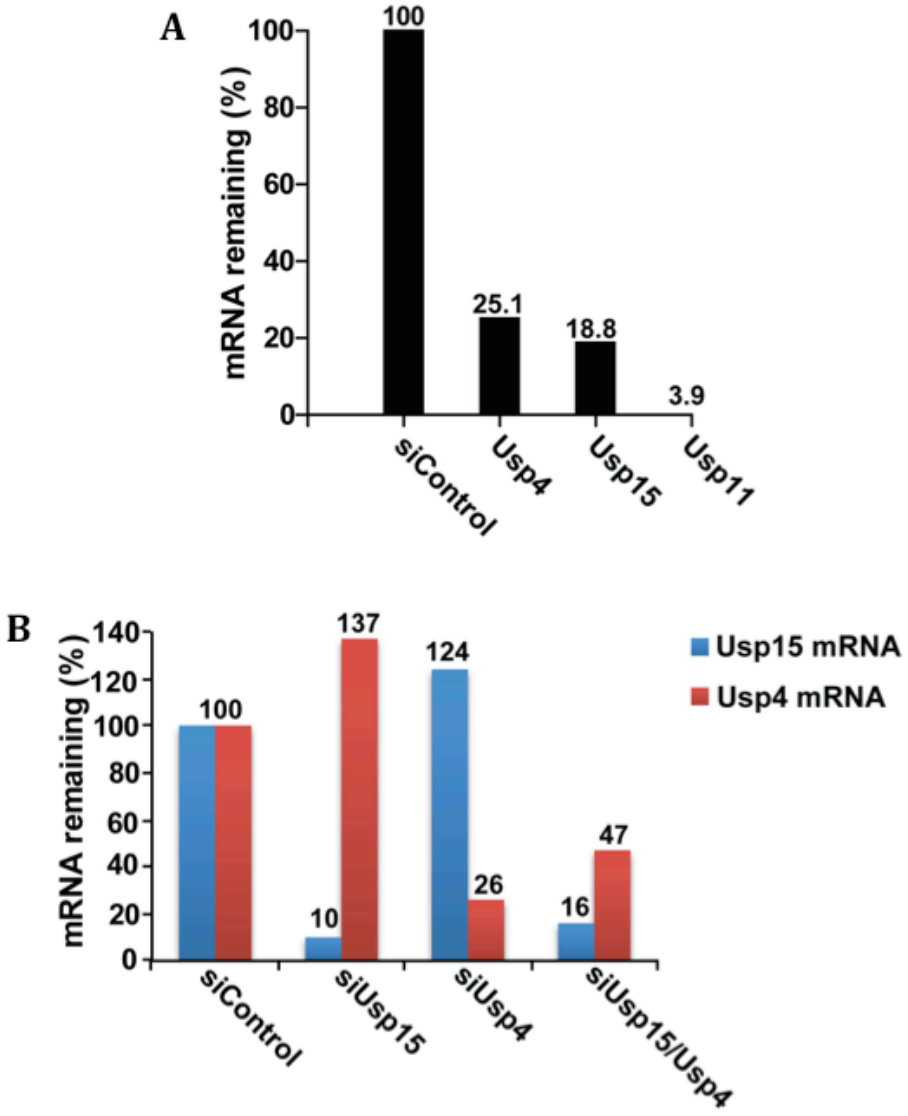

Figure 3.9. Knockdown efficiency of DUBs. (A) Usp4, Usp15, and Usp11 were depleted from cells by siRNA as described in Figure 3.6A. 72 h post transfection, total RNA was extracted from these cells and mRNA levels of each DUB were determined by quantitative RT-PCR. After normalization against GAPDH levels, percent mRNA remaining of each DUB was calculated based on its level in cells transfected with Control siRNA as 100%. **(B)** Usp4 and Usp15,were depleted from cells by siRNA as described in Figure 3.12B. 72 h post transfection, total RNA was extracted from these cells and mRNA levels of each DUB were determined by quantitative RT-PCR. Remaining mRNA was normalized and calculated as described in (A).

SART3 homologs can be found in eukaryotes ranging from *S. cerevisae* to human (Bell et al., 2002). The N-terminal domain is comprised of 7 HAT (Half A TPR) domains, which are critical for protein-protein interactions during U4/U6 recycling (Medenbach et al., 2004). SART3 also encodes a C-terminal LSM domain, which is required for interactions with the Lsm proteins associated with U4/U6 (Rader and Guthrie, 2002). Unlike other SART3 orthologs, the yeast ortholog Prp24 exists as an N-terminally truncated form of SART3 (Bell et al., 2002). It shares only 22% sequence identity and contains 4 RRMs compared to the 2 RRMs found in SART3. In addition to interacting with U4/U6-associated proteins, SART3 also interacts directly with the RNA component of the U6 snRNP (Bell et al., 2002). Notably, SART3 is not found in the tri-snRNP complex (U4/U6.U5) or associated with the spliceosome.

Within the cell, SART3 is localized in the nucleus but is highly concentrated in Cajal bodies (CBs) through an interaction with the CB-associated protein coilin (Novotny et al., 2011; Stanek and Neugebauer, 2006). CBs have been characterized as centers of spliceosome recycling, snRNP biogenesis, and histone mRNA processing. Within the CB, the tri-snRNP is recycled 10-times faster than the recycling rate outside of the CB (230 tri-SNPs formed per minute per CB) (Novotny et al., 2011).

SART3 also plays a role in the maintenance of pluripotency of ESCs by regulating the alternative splicing of *OCT4*. In the undifferentiated state, the high expression level of SART3 is maintained by CMYC and the OCT4A isoform is produced (Liu et al., 2011). Upon differentiation, CMYC and, consequently, SART3 levels decrease. As a result, *OCT4* undergoes alternative splicing and OCT4B is expressed, promoting cell differentiation (Liu et al., 2013).

Usp4 was shown to directly bind SART3, facilitating Usp4-mediated deubiquitination of Prp3, a component of the U4 snRNP, in order to facilitate the ejection of U4 and allow formation of the U2/U5/U6 active splicing complex (Song et al., 2010).

Because of the high homology between Usp15 and Usp4, we examined the association between Usp15 and SART3. Like Usp4, Usp15 co-immunoprecipitates via its NTD with endogenous SART3 (Figure 3.10A). Additionally, SART3 co-immunoprecipitates endogenous Usp15 through the N-terminal half of SART3 that contains the HAT repeats (Figures 3.10B-C). When we examined the cellular localization of Usp15, we found that endogenous Usp15 predominantly localizes to the cytoplasm with a small, but clearly detectable, fraction that is nuclear (Figure 3.11A). Interestingly, the Usp15 NTD or CTD expressed alone are primarily nuclear (Figure 3.11B); these observations suggest that intramolecular interactions within Usp15 modulate its localization. SART3 is exclusively nuclear with a small fraction that localizes to nuclear puncta that have been reported to be Cajal bodies (Stanek et al., 2003) where snRNP biogenesis and recycling is thought to occur (Figure 3.11C). Overexpression of SART3 strongly enhanced localization of Usp15 to the nucleoplasm, but did not recruit Usp15 to the Cajal bodies (Figure 3.11C).

The Usp15–SART3 interaction is direct, as purified recombinant Usp15 and SART3 bind to each other *in vitro* (Figure 3.8D). Using a ligand depletion assay, we estimated that the binding between the NTD of Usp15 and SART3 has a K_d of 42 nM (Figures 3.11E-F).

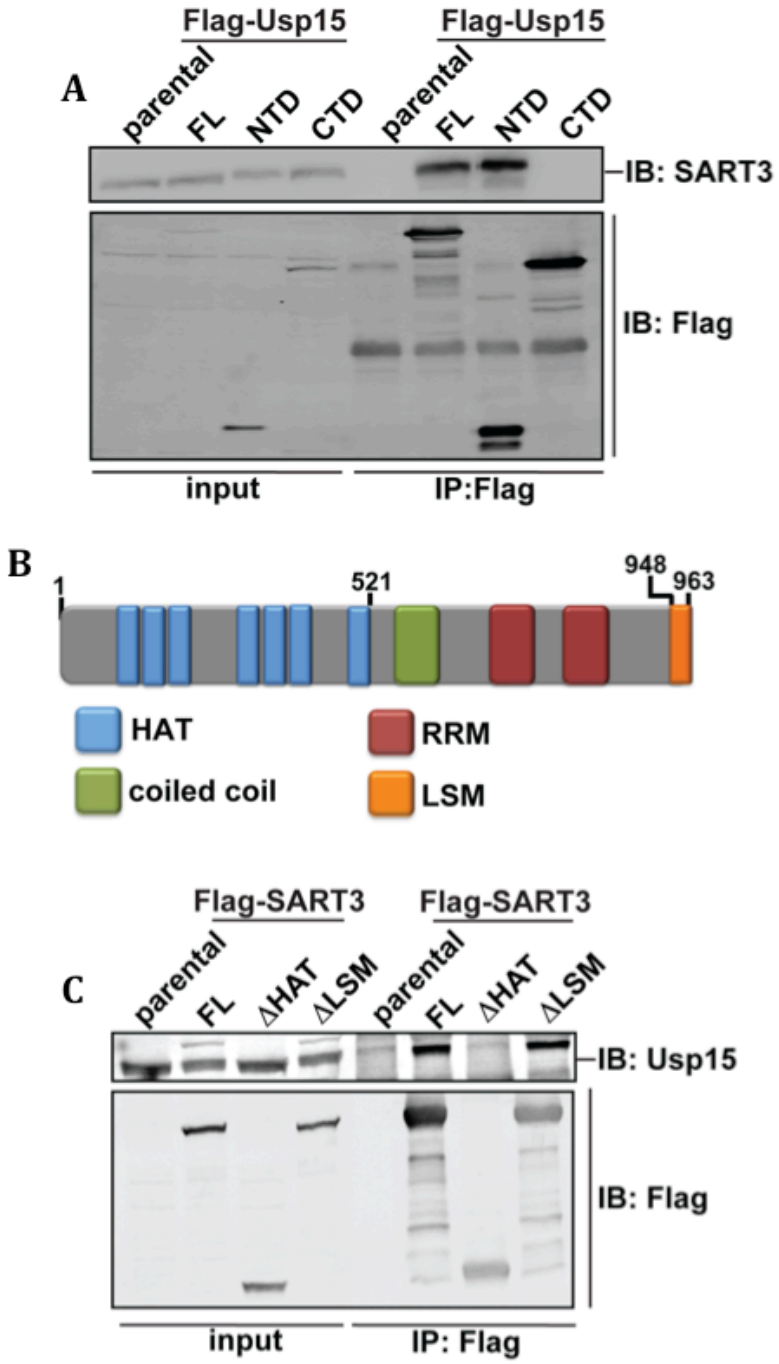

Figure 3.10. The NTD of Usp15 and SART3 are required for co-immunoprecipitation. (A) Usp15 NTD associates with SART3. Co-immunoprecipitations from stable cell lines were performed as described in Fig. 3.4A. **(B)** Schematic of SART3 domain structure. SART3 contains 7 HAT repeats, a coiled-coil domain, at least two RNA Recognition Motifs (RRMs), and a C-terminal LSM domain responsible for its association with U6 LSM proteins. **(C)** The N-terminal HAT repeats of SART3 are required for its association with Usp15. Stable cell lines expressing Flag-tagged full-length (FL), residues 521-963 (ΔHAT), or residues 1-948 (ΔLSM) of SART3 were established and immuoprecipitations with anti-Flag agarose were performed as described in Fig. 3.4A.

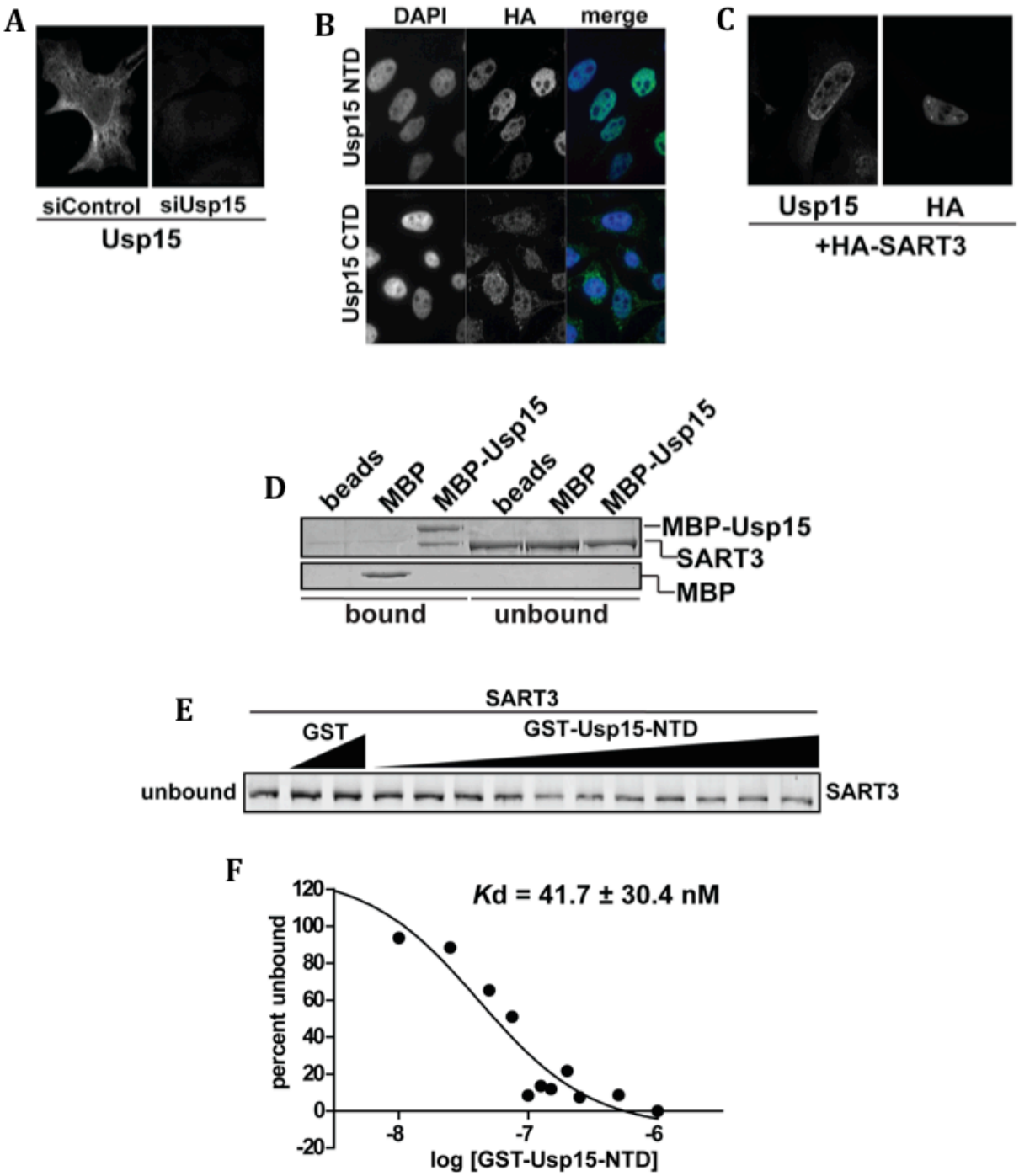
A
siControl
siUsp15
Usp15
B
DAPI
HA
merge
Usp15 NTD
Usp15 CTD
C
Usp15
HA
+HA-SART3
D
beads
MBP
MBP-Usp15
beads
MBP
MBP-Usp15
MBP-Usp15
SART3
MBP
bound
unbound
E
SART3
GST
GST-Usp15-NTD
unbound
SART3
F
Kd = 41.7 ± 30.4 nM
percent unbound
120
100
80
60
40
20
0
-20
-8
-7
-6
log [GST-Usp15-NTD]

Figure 3.11. Usp15 directly interacts with the U4/U6 recycling factor SART3 (A) Localization of Usp15 is regulated by intramolecular interactions. HeLa cells were transfected with control or Usp15 siRNA, and the localization of endogenous Usp15 was examined by anti-Usp15 immunofluorescence. **(B)** For the NTD and CTD fragments, HeLa Flp-In stable cell lines expressing HA-tagged NTD or CTD were induced with Dox for 48 h and stained with anti-HA antibody. **(C)** Overexpression of SART3 enhances nuclear localization of Usp15. HeLa cells overexpressing HA-SART3 by transient transfection were stained with anti-Usp15 and anti-HA antibodies. **(D)** Usp15 directly binds to SART3. 0.25 mM MBP or MBP-Usp15 were immobilized on amylose agarose and incubated with 1.25 mM purified recombinant Flag-SART3. Bound and unbound fractions were analyzed by SDS-PAGE and Coomassie staining. **(E-F)** Usp15 binds to SART3 with high affinity. Increasing amounts of GST or GST-Usp15-NTD (10 to 1000 nM) were immobilized on glutathione agarose and incubated with 100 nM Flag-SART3 for 2 h at 4 °C. The unbound fractions were rapidly removed, separated by SDS-PAGE and visualized by SYPRO-Ruby staining. The amounts of SART3 in these fractions were quantified by Image Quant and percent unbound was calculated assuming the first lane (GST only) was 100% unbound and the last lane (1 mM GST-Usp15-NTD) was 0% unbound. The data were plotted and fitted with a one-site binding model (F).

3.3.5 SART3 has histone chaperone-like activities and enhances H2B deubiquitination by Usp15

We noticed that SART3 was identified by mass spectrometry in our previous H2A/H2B histone dimer pull-down experiments. Immunoblotting analysis confirmed that SART3 bound to unmodified H2A/H2B, ub*H2A/H2B, or H2A/ub*H2B histone dimers (Figure 3.12A). Note that under the high salt condition of the nuclear extract, SART3 no longer associates with Usp15 (data not shown); thus, the association between SART3 and H2A/H2B is independent of Usp15 and insensitive to Ub modification of the histones. Because SART3 and some of its associated proteins interact with RNA, we wanted to test if its interactions with the histones were mediated by RNA. We treated the nuclear extract with RNase A and repeated the pull-down experiments. We found that RNase A treatment had no effect on SART3–H2A/H2B binding (Figure 3.12B).

Using purified recombinant proteins, we found that SART3 not only directly binds to H2A/H2B dimers, but also to H3/H4 tetramers and histone octamers (Figure 3.13A). In contrast, we observed no binding to mononucleosomes. These properties suggest that SART3 has histone chaperone-like activities. Classic histone chaperones, such as Nap1, promote nucleosome assembly by disaggregating free histones to allow productive histone–DNA interactions (Andrews et al., 2010; Elsasser and D'Arcy, 2012). This nucleosome assembly activity can be tested in an assay in which nucleosome formation on relaxed circular DNA leads to supercoiling (Lusser and Kadonaga, 2004). Using this assay, we found that SART3 promoted nucleosome formation in a dose-dependent manner (Figure 3.13B). In comparison with Nap1, SART3's ability to promote supercoiling is much weaker, which suggests that the physiological function of SART3 may not be to promote

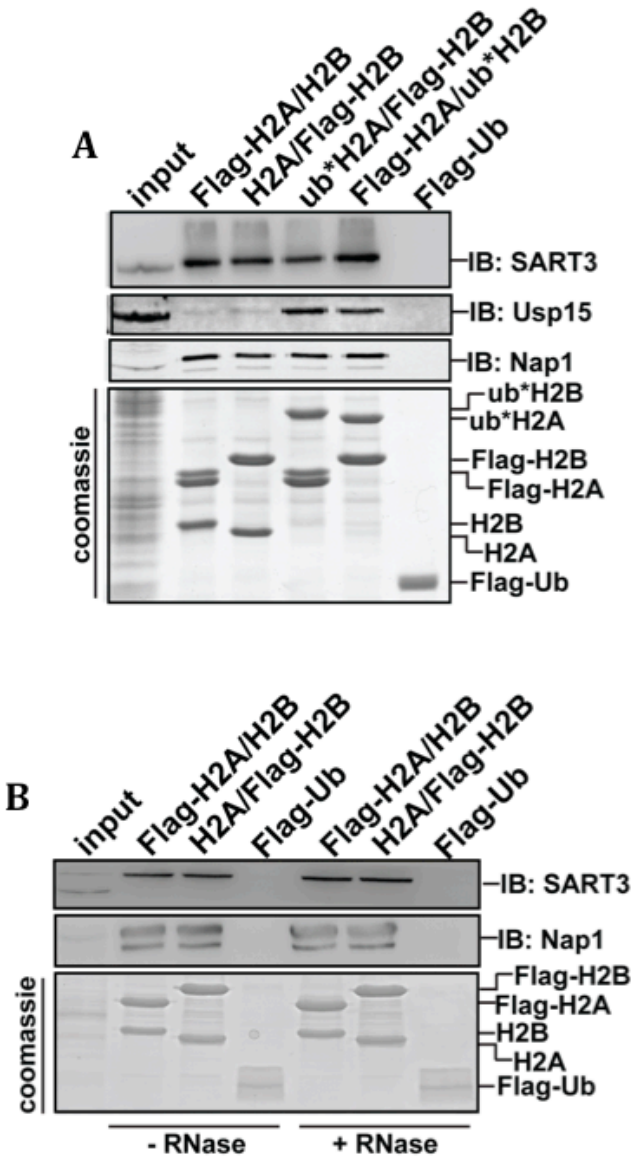

Figure 3.12. SART3 binds histone dimers independent of RNA. (A) SART3 binds to unmodified and ubiquitinated H2A/H2B dimers. Flag-tagged Ub, H2A/H2B, or ubiquitinated H2A/H2B were used in pull-down assays as described in Figure 3.1C except that NaCl concentration was adjusted to 300 mM in all steps. Note that Flag-H2A ran as a doublet on the gel when the bound fractions had been concentrated by TCA precipitation prior to SDS-PAGE. **(B)** SART3-histone interactions are not mediated by RNA. Pull-down assays were performed as described in (A). Where indicated, nuclear extract was treated with 20 mg/ml RNase A prior to incubation with immobilized proteins.

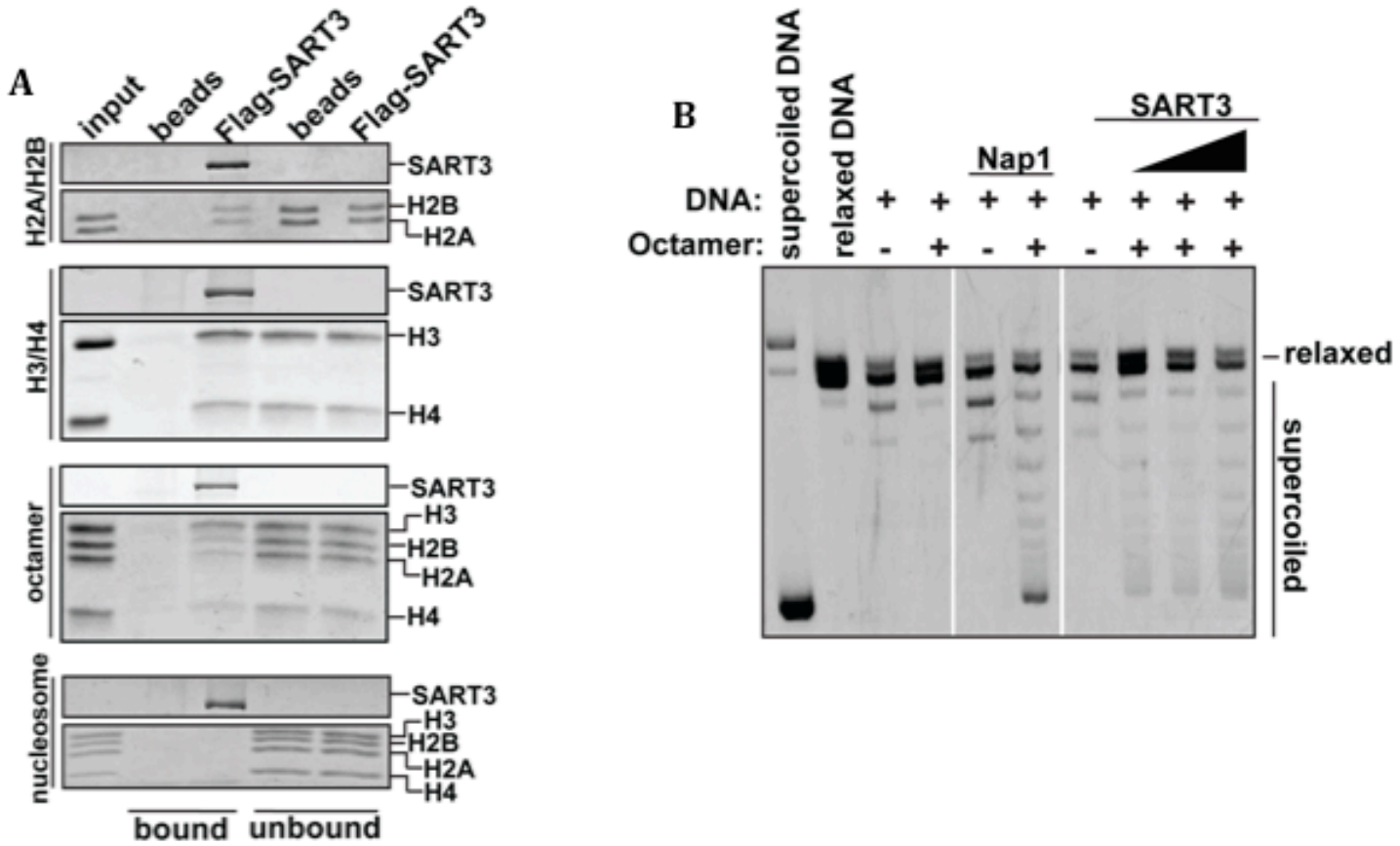

Figure 3.13. SART3 has histone chaperone-like activities. (A) SART3 binds to H2A/H2B, H3/H4, and histone octamers, but not to mononucleosomes. Purified recombinant Flag-SART3 was immobilized on anti-Flag agarose beads and incubated with 2 μM H2A/H2B, 0.5 μM H3/H4, 0.5 μM histone octamers, or 0.5 μM mononucleosomes at 37 °C for 1 h. Bound and unbound fractions were analyzed by SDS-PAGE and Coomassie staining. Anti-Flag agarose ("beads") was used as a negative control. **(B)** SART3 facilitates nucleosome assembly. Supercoiling assays (Dechassa et al., 2011) were performed with 0.3 μM Nap1 or increasing amounts of SART3 (0.14, 0.29, and 0.57 μM). Nucleosome assembly on the plasmid DNA was measured by formation of supercoils that promote faster migration on the gel.

nucleosome assembly on a large scale. However, we cannot rule out that certain types of post-translationally modified histones or other associating factors may enhance nucleosome assembly by SART3, or that SART3 might facilitate assembly at specific sites on chromatin.

Because SART3 and Usp15 interact, we explored the possibility that the interaction could affect the Usp15 deubiquitination activity. *In vitro,* SART3 did not affect Ub-AMC hydrolysis by Usp15 (Figure 3.14A). However, the H2A/ub*H2B dimer was a much stronger inhibitor of Usp15 in the presence of SART3, suggesting that SART3 could play a role in substrate recruitment (Figure 3.14B). Moreover, in contrast to SART3, addition of the Nap1 histone chaperone abolished the inhibition by H2A/ub*H2B. In experiments where we assayed for a direct, positive effect of SART3 on Usp15 activity, we found consistently that SART3 enhanced deubiquitination of ubH2B in the context of histone octamers, whereas Nap1 inhibited (Figure 3.14C). When ubH2B-containing nucleosomes were used as substrates, neither SART3 nor Nap1 affected deubiquitination (Figure 3.14D). These data strongly suggest that SART3 is a specialized histone chaperone that helps to recruit substrates to Usp15.

3.3.6 SART3 regulates global ubH2B levels

Despite that Usp15 binds to ubiquitinated histones with high affinity and efficiently deubiquitinates histones *in vitro*, knockdown of Usp15 alone or in combination with Usp4 did not affect global ubH2A or ubH2B levels (Figures 3.8A and 3.15B). One possibility is that other cellular DUBs have redundant functions in histone deubiquitination. However, to our surprise, depletion of SART3 resulted in a dramatic increase in ubH2B levels whereas

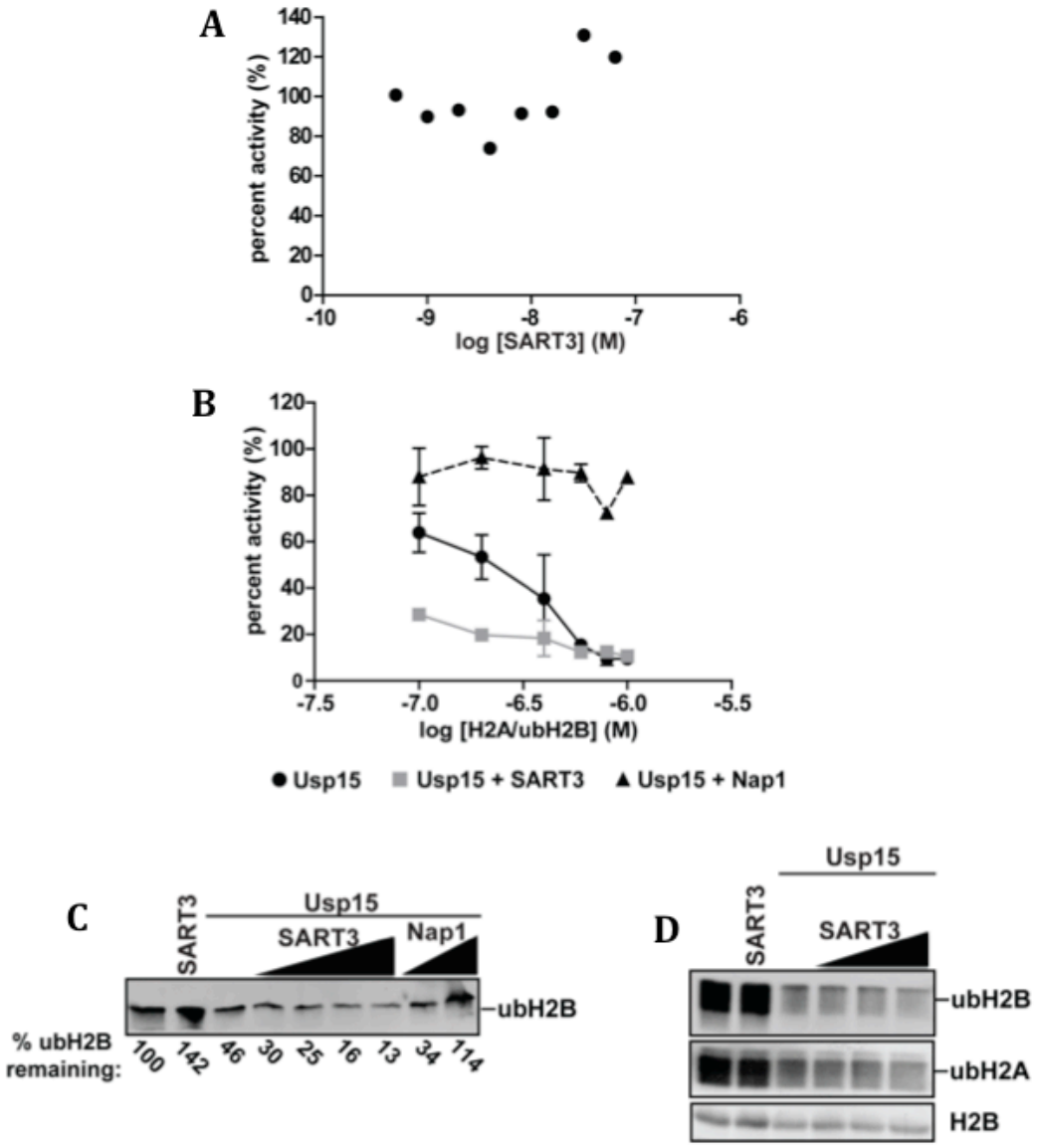

Figure 3.14. SART3 recruits substrates for Usp15. (A) SART3 does not affect Ub-AMC hydrolysis by Usp15. 2 nM MBP-Usp15 was incubated with 1 mM Ub-AMC in the presence of increasing amounts of SART3. Initial velocities of Ub-AMC hydrolysis were measured and normalized to the velocity in the absence of SART3. **(B)** SART3 enhances H2A/ub*H2B binding to Usp15 whereas Nap1 inhibits. Deubiquitinating assays were done as described in Figure 3.2A except that H2A/ub*H2B was added along with equal molar SART3 or Nap1. **(C)** SART3 and Nap1 have opposite effects on H2B deubiquitination by Usp15. Usp15 (5 nM) was incubated with 100 nM semi-synthetic ubH2B-containing histone octamer at 37 °C for 1 h. Where indicated, purified recombinant SART3 was added at 5, 25, 100, or 250 nM, and Nap1 was added at 5 or 250 nM. Reactions were terminated with SDS sample buffer and analyzed by SDS-PAGE and immunoblotting. **(D)** SART3 does not affect nucleosome deubiquitination by Usp15. MBP-Usp15 (250 nM) was incubated with mononucleosomes purified from cells as described in Figure 3.3A. Where indicated, SART3 was present at 0, 50, 100 and 250 nM, respectively.

there was no effect on ubH2A levels (Figure 3.15A). The increase in ubH2B was not caused by increased levels of either subunit of the H2B E3 ligase, RNF20 or RNF40. Also, knockdown of SART3 did not affect Usp4 or Usp15 protein levels. When we examined other histone modifications associated with active transcription, we found no changes in H3K36me3 or H3K4me3 levels. However, the increase of ubH2B was accompanied by a small increase in H3K79me2 (Figure 3.15A). Although both H3K4me3 and H3K79me2 are dependent on ubH2B (Ng et al., 2002; Sun and Allis, 2002), H3K4me3 primarily localizes to promoters and H3K79me2 is found in ORFs. Genome-wide, ubH2B localization correlates poorly with H3K4me3, but strongly with H3K79me2 (Jung et al., 2012). These observations suggest that the increase in ubH2B upon SART3 knockdown most likely occurs in gene bodies, which is consistent with the role of SART3 in co-transcriptional splicing.

The effect of SART3 knockdown on ubH2B levels is not restricted to HeLa cells. We observed similar phenotypes in MD-MBA-231 breast cancer cells (Figure 3.15B) and non-cancerous hTERT-RPE-1 cells (Figure 3.15C). Furthermore, to rule out off-target effects, we demonstrate that depletion of SART3 with two different siRNA oligonucleotides each led to increased ubH2B levels (Figure 3.7C). When we examined ubH2B levels by immunofluorescence, we found that ubH2B was increased in almost all of the cells that had SART3 depleted (Figures 3.15D-E), ruling out that this is a cell cycle-related phenotype. Because genetic and biochemical evidence have established a strong link between H2B ubiquitination and transcription elongation (Pirngruber et al., 2009b), we also examined the global pool of actively transcribing RNAPII. In SART3-depleted cells, we found no changes in RNAPII CTD Ser2 or Ser5 phosphorylation, which are hallmarks of the elongating polymerase (Figure 3.15F). Conversely, overexpression of SART3 by

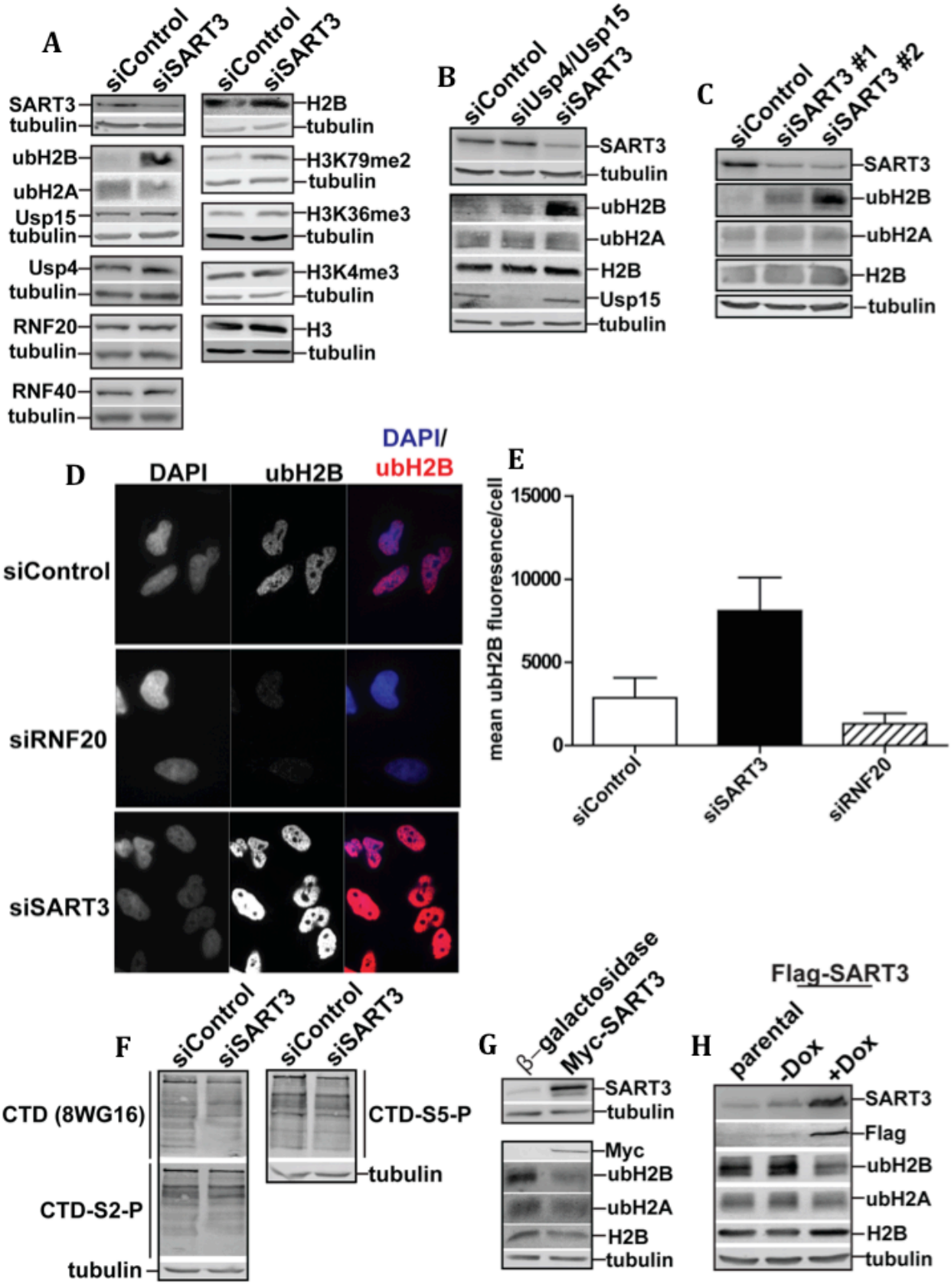
A
siControl
siSART3
siControl
siSART3
SART3
tubulin
ubH2B
ubH2A
Usp15
tubulin
Usp4
tubulin
RNF20
tubulin
RNF40
tubulin
H2B
tubulin
H3K79me2
tubulin
H3K36me3
tubulin
H3K4me3
tubulin
H3
tubulin
B
siControl
siUsp4/Usp15
siSART3
SART3
tubulin
ubH2B
ubH2A
H2B
Usp15
tubulin
C
siControl
siSART3 #1
siSART3 #2
SART3
ubH2B
ubH2A
H2B
tubulin
D
DAPI
ubH2B
DAPI/
ubH2B
siControl
siRNF20
siSART3
E
mean ubH2B fluoresence/cell
15000
10000
5000
0
siControl
siSART3
siRNF20
F
siControl
siSART3
siControl
siSART3
CTD (8WG16)
CTD-S2-P
tubulin
CTD-S5-P
tubulin
G
β–galactosidase
Myc-SART3
SART3
tubulin
Myc
ubH2B
ubH2A
H2B
tubulin
H
Flag-SART3
parental
-Dox
+Dox
SART3
Flag
ubH2B
ubH2A
H2B
tubulin

Figure 3.15. SART3 regulates global ubH2B levels. (A) SART3 depletion increases global ubH2B levels. HeLa cells were transfected with 3.3 nM Control or SART3 siRNA; 72 h post-transfection, cell lysates were harvested and analyzed by SDS-PAGE and immunoblotting. Tubulin was used as a loading control. Slices of immunoblots that came from the same gel are boxed together. ubH2A and ubH2B were detected on the same blot with monoclonal rabbit anti-ubH2A (Cell Signaling) and mouse anti-ubH2B (MediaMab) antibodies and two-color fluorescent secondary antibodies. **(B)** MDA-MB-231 cells were transfected with 6.6 nM Control or SART3 siRNA, or a combination of Usp4 and Usp15 siRNAs at 3.3 nM each. 72 h post-transfection protein levels were monitored as described in (A). **(C)** hTERT-RPE-1 cells were transfected with 3.3 nM Control siRNA or two different siRNAs that target SART3; 72 h post-transfection protein levels were monitored as described in (A). **(D)** Global ubH2B increase in SART3-depleted cells. HeLa cells transfected with Control, RNF20, or SART3 siRNA were stained with anti-ubH2B antibodies and DAPI. Depletion of RNF20 abolished almost all ubH2B staining, whereas depletion of SART3 led to increased ubH2B signals ubiquitously. **(E)** Fluorescence intensities of ubH2B signals from 100 cells in each condition as described in (C) were quantitated using SlideBook Reader. Error bars represent standard deviations. Using a paired student t-test, p-values of < 0.0001 were calculated for SART3 or RNF20 knockdown in comparison with the Control knockdown.
(F) Depletion of SART3 did not change RNAPII CTD phosphorylation levels globally. HeLa cells were transfected with Control or SART3 siRNA and cell lysates were analyzed as described in (A). **(G)** Overexpression of SART3 decreases global ubH2B levels. HEK293 cells were transfected with plasmids encoding either β-galactosidase or Myc-SART3. Cell lysates were prepared 48 h post-transfection and analyzed as in (A). **(H)** Cell lysates were prepared from parental or Flag-SART3 stable cells with or without Dox treatment and protein levels were monitored as described in (A).

transient transfection led to decreased ubH2B levels (Figure 3.15G). Similar phenotypes were observed with a stable cell line that overexpresses SART3 upon addition of Dox (Figure 3.15H).

Knockdown of Usp4 or SART3 leads to similar cell cycle defects (Sowa et al., 2009). The fact that ubH2B was only elevated in SART3 knockdown suggests that this phenotype is independent of the cell cycle defects. Consistently, when we examined ubH2B levels by immunofluorescence in cells treated with Control or SART3 siRNA, we found that ubH2B was increased in almost all of the cells that had SART3 depleted (Figure 3.15D). Because genetic and biochemical evidence have established a strong link between H2B ubiquitination and transcription elongation (Pirngruber et al., 2009a; Pirngruber et al., 2009b), we also sought to examine the global pool of actively transcribing RNAPII. In SART3 depleted cells, we found no changes in the levels of RNAPII CTD Ser2 or Ser5 phosphorylation, which are hallmarks of the elongating polymerase (Figure 3.15F).

Steady-state ubH2B levels are determined by the rates of both conjugation and deconjugation. Upon SART3 depletion, we found no global changes in either the RNF20/RNF40 E3 ligase levels or RNAPII CTD phosphorylation levels, both of which are determining factors in the rate of ubH2B conjugation. These observations suggested that the effect of SART3 knockdown on ubH2B might result from decreased deubiquitination. To deconvolute the possible contributions of conjugation and deconjugation, we treated cells with a highly specific E1 inhibitor (Chen et al., 2011) to block Ub conjugation and monitored ubH2A and ubH2B levels over time. Both ubH2A and ubH2B levels decreased over the course of one hour after E1 inhibition (Figures 3.16A-E). The ubH2B half-life was 15-20 min in both Control siRNA-treated and non-transfected cells. However, SART3 siRNA

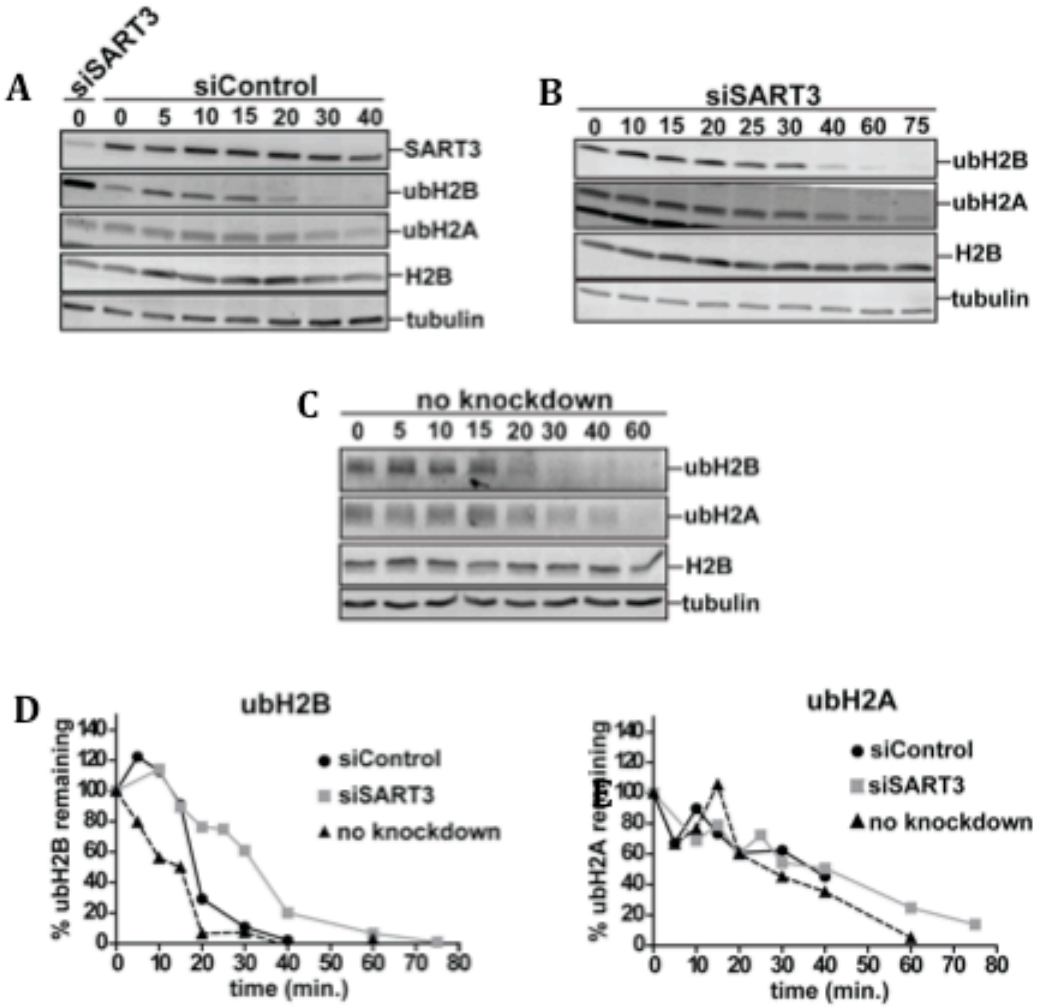

Figure 3.16. SART3 depletion affects ubH2B deconjugation (A-C) HeLa cells were transfected with Control or SART3 siRNA as described in (A). 72 h post transfection, 10 μM E1 inhibitor was added and cell lysates harvested at the indicated times. Treatment of untransfected cells was also performed as the "no knockdown" control. Protein levels were monitored by quantitative immunoblotting with fluorescent secondary antibodies.**(D-E)** Quantification of (A-C). Protein levels were quantified by Image Studio and normalized to H2B levels. Changes in ubH2B and ubH2A levels were plotted relative to the value at time 0 for each condition.

resulted in a doubling of the ubH2B half-life to about 35 min (Figure 3.16D). In contrast, no effect on the ubH2A half-life was observed (Figure 3.16E). Knockdown of Usp15 and Usp4 did not affect the half-lives of either ubH2A or ubH2B (data not shown). These data show that SART3 plays an important role in H2B deubiquitination. However, whereas our pull-down results and *in vitro* characterization strongly implicate Usp15 in this process, other DUB(s) might be involved as well.

3.4 Discussion

It is well established that ubiquitination of H2B is a highly conserved PTM that has important functions in the regulation of transcription, but how this modification supports these functions is uncertain and complex. The lack of knowledge of direct effectors of ubH2B is a major obstacle in understanding the underlying mechanisms. A related open question is whether H2A/H2B dimers or nucleosome complexes are the substrates for Ub attachment or removal *in vivo*. Ubiquitination of H2B is known to accompany transcription, a process during which nucleosomes are disassembled or remodeled to allow access for transcription activators and RNAPII; following passage of the transcribing RNAPII, nucleosomes are reassembled to prevent unwanted access to DNA. H2A/H2B dimers clearly are obligatory intermediates in this complex process, but their states with regard to ubiquitination or other PTMs are not well characterized.

The specificity of histone deubiquitination—In mammals, the PRC1 and RNF20/RNF40 complexes catalyze Ub conjugation to H2A residue K119 and H2B residue K120, respectively (Weake and Workman, 2008). In contrast, many histone DUBs identified to date are promiscuous towards these functionally distinct substrates (Frappier and

Verrijzer, 2011). The SAGA^{DUB}, Usp44 and Usp3 have all been reported to deubiquitinate both H2A and H2B (Fuchs et al., 2012; Lang et al., 2011; Mosbech et al., 2013; Nicassio et al., 2007), suggesting that targeting of these DUBs is the main factor in determining specificity. Because ubH2A and ubH2B may exist both inside and outside nucleosomes, another aspect of substrate specificity is whether these DUBs differentiate nucleosomal from free Ub–histone conjugates. This question had not been addressed for the three DUBs mentioned above. However, from qualitative activity assays, two other DUBs, Usp16 and Usp49 (Joo et al., 2007; Zhang et al., 2013), have been reported to preferentially deubiquitinate nucleosomal ubH2A and ubH2B, respectively.

To define rigorously the substrate specificities of these DUBs requires appreciable quantities of chemically-defined ubH2A and ubH2B. Through semi-chemical synthesis, we have produced ubH2B; we currently are developing methods to synthesize the complementary substrate, ubH2A. Nonetheless, using our nonhydrolyzable analogs, we were able to show that Usp4 and Usp15 bind to ub*H2A and ub*H2B-containing histone dimers with similar affinities. This observation is consistent with our results that used cell-derived ubH2A and ubH2B as substrates in assays that show Usp15 deubiquitinates both efficiently (Figure 3.4A). Interestingly, when we compared the synthetic ubH2B substrate in the histone octamer or nucleosomal form, Usp15 showed a strong preference for ubH2B-containing octamers, whereas SAGA^{DUB} preferred nucleosomal ubH2B (Figures 3.4B-C). Note that these DUB assay reactions contained 200 mM NaCl; in that salt condition, the histone octamers most likely dissociate into H2A/H2B dimers and H3/H4 tetramers. SAGA^{DUB} has a conserved arginine-rich surface whose mutation affects SAGA function in yeast (Kohler et al., 2010). It was postulated that this surface may mediate interactions

with nucleosomal DNA (Samara et al., 2010). Our data provides the first evidence for preferential deubiquitination of nucleosomal versus free histones by $SAGA^{DUB}$ and supports this idea. Usp15 by itself showed little specificity for binding to unmodified H2A/H2B dimers, yet it binds to ub*H2A or ub*H2B-containing dimers ~60-fold better than to Ub alone. This suggests that surfaces on histones and Ub might both contact Usp15, and that their combined effects contribute to specificity for Ub–histone conjugates. However, in the cell, histones that are not in nucleosomes are most likely complexed with histone chaperones; thus, physiologically, Usp15 might never encounter free histone substrates. This is in fact suggested by our observation that Nap1, a generic histone chaperone, blocked Usp15 binding to ub*H2B (Figure 3.14B). Our discovery that SART3 is a binding partner of Usp15 and has histone chaperone-like properties resolves this apparent conundrum. In contrast to Nap1, SART3 enhanced ub*H2B binding to Usp15 and also ubH2B hydrolysis by Usp15 (Figures 3.14B-C). These data strongly argue that free histones, rather than nucleosomes, are the likely substrates for the Usp15/SART3 complex.

Usp15 has been implicated in the deubiquitination of a wide variety of substrates, including proteins in the TGFb-signaling pathway and several E3 ligases (Eichhorn et al., 2012b; Faronato et al., 2013; Hayes et al., 2012; Hetfeld et al., 2005; Inui et al., 2011; Villeneuve et al., 2013). Although Usp4 and Usp15 sequences are very similar, they most likely perform overlapping, but non-identical, functions. Purified Usp4 binds to ub*H2B with 4-fold lower affinity than Usp15. When present in nuclear extract, Usp15 but not Usp4 was identified by mass spectrometry as bound to ubiquitinated histones. This suggests that, of these two DUBs, Usp15 is selective for histone substrates. On the other hand, knockdown of Usp4 but not Usp15 leads to cell cycle defects, thus Usp4 is primarily

responsible for deubiquitination of the splicing factor Prp3 (Sowa et al., 2009). Knockdown of Usp15, Usp4, or Usp15 and Usp4 together failed to change appreciably global ubH2A or ubH2B levels. This could be due to existence of other DUBs that deubiquitinate H2A or H2B. An alternative possibility is the depletion of Usp15 and Usp4 was not efficient enough to observe changes in ubH2B levels as the remaining protein was sufficient to deubiquitinate H2A and H2B. Quantitative RT-PCR showed that combinatorial knockdown of both Usp15 and Usp4 resulted in less efficient depletion of both DUBs (Figure 3.9B). Substantial redundancy has been observed for deubiquitination events associated with DNA DSB repair (Mosbech et al., 2013). Another possibility is that only a subset of ubH2A or ubH2B is regulated by Usp15 in specific cellular processes. Defining this subset will be the goal of our future work.

SART3 is a histone chaperone that functions in co-transcriptional splicing—In eukaryotes, transcription and mRNA processing are tightly coupled processes, both of which are regulated by dynamic chromatin disassembly and reassembly. SART3 is a recycling factor that assists pre-mRNA splicing by promoting formation of the U4/U6 di-snRNP. The CTD of SART3 is homologous to the protein encoded by *PRP24*, an essential gene in budding yeast whose protein product performs the same recycling function to ensure efficient splicing of mRNA encoding ribosomal proteins (Raghunathan and Guthrie, 1998). The NTD of SART3, although not present in Prp24, is present in its homologs in *S. pombe* and metazoans and it is responsible for binding to Usp4 or Usp15. Our discovery that SART3 binds to histones suggests that components of the splicing machinery may regulate aspects of chromatin dynamics. Capturing displaced histones during transcription to prevent exchange with the free histone pool could be one of the functions of SART3. An

emerging concept is that chromatin structure and the rate of transcription elongation regulate the efficiency of splicing and outcomes of alternative splicing (de Almeida and Carmo-Fonseca, 2012; Luco et al., 2011). Nucleosomes have higher occupancy in exons than in introns (Schwartz et al., 2009), and multiple histone PTMs, including H3K4Me3 and H3K36Me3, have been shown to recruit splicing factors (Luco et al., 2010; Sims et al., 2007). Conversely, it has been known for a long time that the presence of introns stimulates transcription and that inhibition of splicing can inhibit transcription. These observations indicate that the splicing machinery can somehow provide feedback to regulate transcription machinery and chromatin (Lin et al., 2008; Sims et al., 2007).

Our biochemical analyses suggest that one of the functions of SART3–histone interactions is to assist Usp15-mediated H2B deubiquitination. Evidence from multiple organisms indicates a conserved role for ubH2B in regulating co-transcriptional pre-mRNA splicing. ubH2B is enriched at the 5'-ends of actively transcribed genes and exon/intron boundaries (Jung et al., 2012; Shieh et al., 2011). In yeast, deletion of either *BRE1* (H2B E3 ligase) or *UBP8* (an H2B DUB) enhances the splicing defect of ribosomal protein genes when splicing is compromised by deletion of *NPL3*, which functions to promote recruitment of U1 and U2 snRNPs (Kress et al., 2008). Similarly, depletion of the *BRE1* counterpart, RNF20, suppresses exon skipping in human cells (Jung et al., 2012). It remains unclear whether ubH2B plays a direct role, such as recruiting splicing factors, or an indirect role in splicing through its function in transcription elongation. Regardless, the SART3–Usp15 complex is most likely responsible for erasing the Ub mark from histones that are evicted during transcription. This function may be particularly important to maintain low ubH2B levels in introns. Because ubH2B assists in nucleosome reassembly after RNAPII

passage, erasure of the mark may help to maintain low nucleosome occupancy in introns, thus enhancing the chromatin signatures that direct the next round of transcription and splicing (Figure 3.17). A recent report identified another DUB, Usp49, that specifically deubiquitinates H2B in nucleosomes (Zhang et al., 2013). Loss of Usp49 leads to a decrease in splicing efficiency in a subset of genes. Among a limited set of genes that we tested, genes whose splicing are affected by Usp49 were not affected by SART3 knockdown (L.L. and T.Y., unpublished results). Therefore, it is likely that SART3–Usp15 and Usp49 have different sets of target genes.

Using an inhibitor of the E1 Ub-activating enzyme, we report for the first time that in HeLa cells ubH2A and ubH2B have half-lives of 40 min and 15 min, respectively (Figures 3.16A-E). The half-life of ubH2B is very similar as what was observed upon inhibition of transcription (Pirngruber et al., 2009a), supporting the idea that ubH2B conjugation is largely co-transcriptional. It has been estimated that at steady state 10-15% of H2A is ubiquitinated, whereas only 1-5% of H2B is ubiquitinated. Our data suggest that the faster turnover of ubH2B is at least in part responsible for its lower abundance. Interestingly, knockdown of SART3 leads to a ~2-fold increase in ubH2B half-life with no effect on ubH2A, yet knockdown of Usp15 or Usp4 had no effect on global ubH2B or ubH2A levels. At this point, it is unclear whether the ubH2B increase we observed upon SART3 knockdown is a direct effect mediated by SART3-associated DUBs, or if it is an indirect effect mediated by other genes whose expression depend on SART3. Very little is known about the genes that SART3 regulates directly. Identification of these target genes in the future will be required to rule out indirect effects.

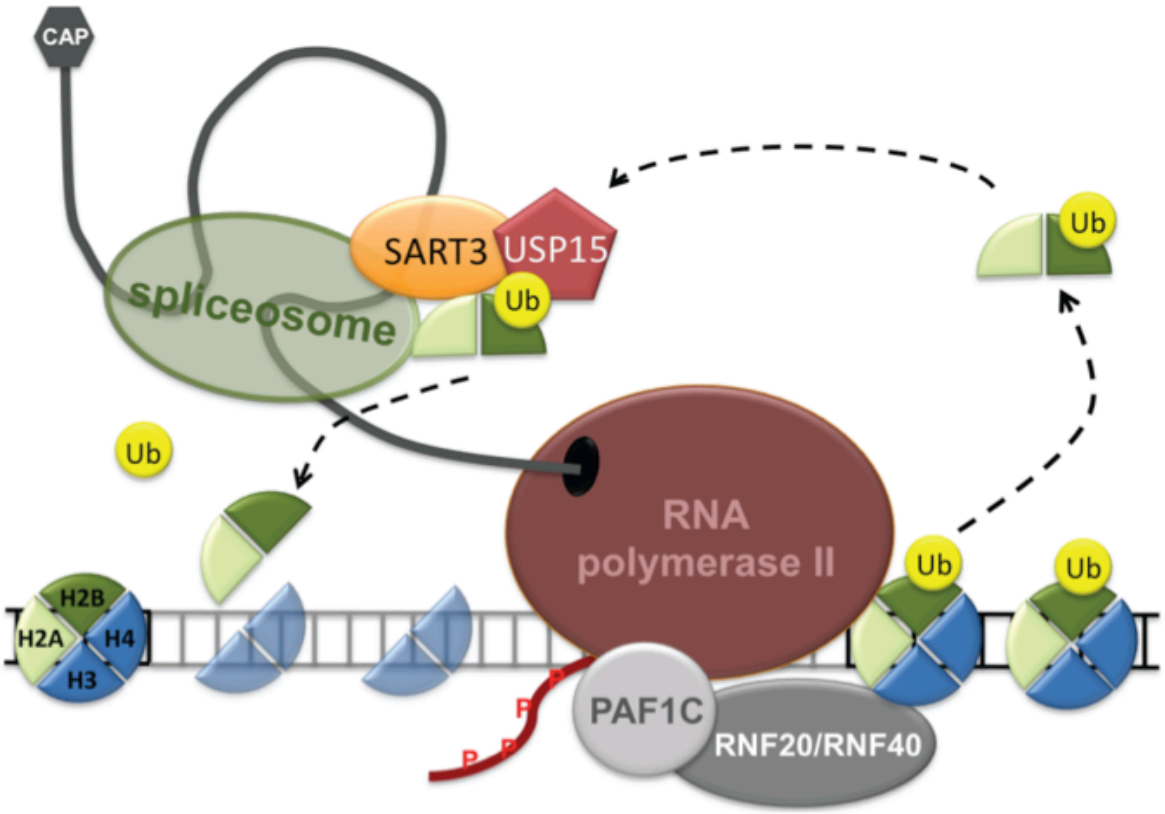

Figure 3.17. A model for co-transcriptional ubH2B deconjugation by the SART3-Usp15 complex. The RNF20/RNF40 heterodimer associates with the PAF complex (PAF1C), which directly binds to RNA polymerase II (RNAPII). This complex catalyzes H2B ubiquitination and stimulates transcription elongation. SART3 and other components of the splicing machinery are recruited to process nascent transcripts co-transcriptionally. During this process, histones are displaced from nucleosomes to allow RNAPII to access the DNA template. Evicted histones are bound by the SART3-Usp15 complex and Usp15 deconjugates Ub from histone dimers. Non-ubiquitinated histone dimers are now available for reassembly into nucleosomes in the wake of elongating RNAPII.

CHAPTER 4: ANALYSIS OF SART3-REGULATED GENES

4.1 Introduction

UbH2B plays a critical signaling role in the cell in various processes, including transcription and pre-mRNA splicing (Wright et al., 2012). During active transcription, the H2B E3 ligase, RNF20/RNF40 travels along with elongating RNAPII via associations with the Paf1 complex (Paf1C) (Wood et al., 2003b). Dynamic ubiquitination and deubiquitination of H2B is required for processive elongation of many genes (Henry et al., 2003). UbH2B is also required for proper nucleosome reassembly in the wake of elongating polymerase (Fleming et al., 2008; Kaplan et al., 2003; Pavri et al., 2006). In addition, ubH2B has also been demonstrated to play a role in the regulation of alternative splicing: 1) deletion of splicing components, such as components of the U1, U2, and U5 snRNPs, in an *htb-K123R* or *bre1*Δ yeast strain leads to sickness and/or lethality (Moehle et al., 2012; Shieh et al., 2011); 2) ubH2B is required for proper recruitment of splicing factors to nascent RNA transcripts (Herissant et al., 2014); 3) ubH2B levels are elevated at a subset of intron/exon junctions (Jung et al., 2012). The interactions between transcription and splicing machineries, and involvement of chromatin modifications possibly as messengers, have attracted rising interests in recent years (Luco et al., 2011).

We recently identified a previously uncharacterized histone DUB, Usp15, which directly interacts with the U4/U6 spliceosome recycling factor and histone chaperone, SART3. We found that H2B deubiquitination by Usp15 is enhanced by SART3 *in vitro*. Depletion of SART3 from cells results in a global increase in ubH2B levels due to a decreased rate of Ub deconjugation (Long et al., 2014). These observations led us to

investigate whether changes in ubH2B levels observed upon SART3 depletion could result in transcriptional and splicing defects.

To analyze changes in transcript levels and alternative splicing events upon SART3 knockdown, we depleted SART3 using two different methods and subjected the RNA to Next Generation Sequencing (NGS) analysis (RNA-seq). We identified a diverse set of genes that displayed aberrant transcriptional and splicing patterns upon SART3 depletion and validated a few of these transcriptional changes using qRT-PCR. ChIP analysis of a subset of genes whose transcript levels decreased in SART3 depleted cells revealed that SART3 is localized to these genes, suggesting the observed changes in transcript abundance are likely a direct consequence of SART3 loss. Interestingly, despite decreased transcript levels at these genes, RNAPII levels were only mildly affected; suggesting the reduction in transcript levels is due to defects in transcription elongation or RNA stability. We propose a splicing defect in SART3-depleted cells leads to defects in transcription elongation at particular genes.

4.2 Experimental Procedures

4.2.1 Generation of SART3 knockdown stable cell lines

Production of SART3 shRNA lentivirus: Lentiviruses were packaged and produced in 293T cells. Cells were plated in a 6 cm dish and transfected with 2 µg pPAX (encoding Gag-Pol), 1 µg PMD2.G (encoding VSV-G), and 2 µg of desired plasmid to be packaged (i.e. shSART3- or GFP-encoding vectors). DNA was mixed with 32 µL of 2 M $CaPO_4$ in a final volume of 260 µL. An equal volume of 2X HBS was added to the DNA mixture while vortexing. Following a 15-minute incubation, the transfection mixture was added drop wise

to cells. The following day, the media was replaced with 3 mL of fresh DMEM. 24 hours after replacing the media, virus-containing media was harvested and filtered through a 0.45 μm filter to remove residual 293T cells from the supernatant. Viruses were aliquoted and stored at -80 °C.

Generation of SART3 shRNA expression cell lines: Approximately $6x10^5$ HeLa cells were plated in a 6 cm dish. The following day (Day 1), cells were approximately 40-70% confluent and the media was exchanged with 3 mL of DMEM containing 34 μg Polybrene. HeLa cells were then infected using 1 mL of lentivirus-containing supernatant. After a 4-6 hour incubation, an additional 2 mL of DMEM was added to the transduction plate. On Day 2, cells were re-seeded to a confluency of 50%. Two days post-transduction (Day 3), the media was replaced with DMEM containing 10 μg/mL puromycin to select for cells that had integrated the virus. As a negative control, uninfected HeLa cells were subject to puromycin selection and complete cell death was observed in less than 24 hours. On Day 5, cells infected with a GFP-encoding virus were visualized using microscopy. We observed 100% of the viable cells fluoresced, implicating efficient transduction and successful selection by puromycin. After selection, cells were either harvested for protein or RNA analysis, frozen, or subjected to isolation of monoclonal cell lines.

Purification of RNA for RNA-seq and qRT-PCR: Cells were either transfected with siRNA as described in Section 3.2.2 or transduced cells were plated in a 6-well dish and grown to confluency. Approximately $1.0x10^6$ cells were lysed in 1 mL TRIzol® Reagent (Life Technologies), and RNA was extracted according to manufacturer's instructions. RNA pellets were resuspended in 40 μL of RNase-free water and stored at -20 °C.

4.2.2 Generation of the HA-SART3 inducible stable cell line

Stable cell lines were generated with pcDNA5 FRT/TO constructs using the parental Flp-In HeLa cell lines (Life Technologies) as described by Yao et al. (Yao et al., 2006). SART3 constructs encoded N-terminal Flag-Flag-HA epitope tags.

4.2.3 Chromatin immunoprecipitation (ChIP) assay

Prepare and harvest cells: For ChIP analysis under control and SART3 knockdown conditions, $1.8x10^6$ cells were transfected using 19.8 nM siRNA and 48 µL RNAiMax. 72-hours post-transfection, cells were fixed and harvested as described below. Approximately $3.3x10^6$ and $7.4x10^6$ cells were present per each 10 cm dish for siControl and siSART3, respectively because transfection of Control siRNA resulted in greater cell death when compared to transfection with SART3 siRNA. A minimum of $2.5x10^6$ and $0.9x10^6$ cells was used for immunoprecipitation of ubH2B and H2B, respectively. For ChIP analysis of HA-SART3 stable cell lines, cells were plated at 25% confluency (approximately $3x10^6$ cells/dish) in 10 cm dishes and induced with Doxycycline (Dox) at 1 µg/mL for 48 hours before fixing and harvesting. Typically, we harvested $1.2x10^7$ cells per 10 cm dish, and, therefore, approximately 0.5 to 1 confluent 10 cm dishes were used for each IP.

Cross-linking: Confluent plates were washed with PBS before cross-linking with 1% formaldehyde/PBS at room temperature for 10 minutes. Cross-linking reactions were stopped upon the addition of 120 mM sterile glycine at room temperature for 5 minutes. Fixed cells were washed and harvested in chilled 1xPBS, 1 mM PMSF. Cells were pelleted for 5 minutes at 4 °C at 2000 rpm and either stored at -80 °C or lysed and sonicated.

Lysis and sonication: Cell pellets were thawed on ice and resuspended in 1 mL of cell lysis buffer (5 mM PIPES, pH 8, 85 mM KCl, 1% NP-40, PIC) per $1.2x10^7$-$1.4x10^7$ cells.

Resuspended cells were transferred to sonication tubes and incubated on ice for 20 minutes. The chromatin-containing fraction was pelleted at 5000 rpm at 4°C for 5 minutes and resuspended in 200 µL of 0.5% SDS lysis buffer (50 mM Tris, pH 8, 10 mM EDTA, 0.5% SDS) per $1.2x10^7$-$1.4x10^7$ cells. Chromatin was sonicated for 45 minutes in a cyclic fashion where a 30 second sonication was followed by a 30 second rest period. Samples were quickly centrifuged every 15 minutes to pellet the liquid that accumulated on the sides of the tubes. After sonication, cells were centrifuged at 13,200 rpm for 10 minutes at 15 °C, and the supernatant was transferred into fresh tubes. Chromatin concentration was measured by mixing 5 µL sonicated chromatin with 495 µL 0.1 M NaOH and measuring the OD_{260}. Typically, an OD_{260} between 0.4 and 0.5 is achieved. The concentrations of different sample types are normalized based upon the OD_{260} reading by the addition of 0.5% SDS lysis buffer.

Sonication analysis: To monitor the efficiency of chromatin fragmentation by sonication, a small sample is processed to remove the DNA-bound proteins and visualize the DNA on an agarose gel. In this process, 5 µL of sonicated chromatin is diluted in 45 µL elution buffer (1% SDS, 0.1M $NaHCO_3$, made freshly). The cross-link is reversed though the addition of 2 µL of 5 M NaCl at 95 °C for 15 minutes. Samples are cooled to room temperature before adding RNase A at 0.2 mg/mL for 15-30 minutes at 37 °C. DNA is extracted with 50 µL of Phenol/Chloroform/Isoamylalcohol (PCI) and ethanol precipitated with 100 µL ice cold 100% EtOH. Pellets are washed with 70% EtOH, dried, and gently resuspended in 40 µL nuclease-free water. Sucrose is added to a final concentration of 2% to 2 µg of DNA. The DNA is separated on a 2% agarose gel and visualized by ethidium

bromide staining. An ideal sonication produces DNA fragments from 200 to 600 base pairs in length.

Immunoprecipitation: For each immunoprecipitation (IP), 10 µL of Protein G Dynabead slurry is washed twice with 500 µL IP dilution buffer (16.7 mM Tris, pH 8, 1.2 mM EDTA, 167 mM NaCl, 1.1% Triton X-100, 0.01% SDS). 1 µg of the appropriate antibody is diluted in 500 µL of IP dilution buffer and incubated with the washed Protein G beads for 2 hours at 4°C while rotating. Lysates are diluted 1:10 in IP dilution buffer to reduce the SDS concentration to 0.05%. The unconjugated antibody is removed and up to 1.5 mL of the diluted lysates are incubated with the antibody-bound beads overnight at 4°C while rotating. The next day, IP samples are sequentially washed with for 5 minutes at 4 °C with 1 mL of Low salt buffer (20 mM Tris, pH 8, 2 mM EDTA, 150 mM NaCl, 1% Triton X-100, 0.1% SDS), High salt buffer (20 mM Tris, pH 8, 2 mM EDTA, 500 mM NaCl, 1% Triton X-100, 0.1% SDS) and, LiCl buffer (10 mM Tris, pH 8, 1 mM EDTA, 0.25 M LiCl, 1% NP-40, 1% NaDOC). These wash steps are followed by 2 additional washes using TE buffer (10 mM Tris, pH 8, 1 mM EDTA). IP samples are transferred to low-binding tubes as detergent-free solutions cause mild adhesion of Dynabeads to the tube surface. IP samples are incubated with 250 µL of fresh elution buffer at 65°C for 5 minutes, followed by rotation at room temperature for 15 minutes. Eluates are transferred from the bead-containing tubes into Sure-lock tubes. The elution step is repeated and eluates are combined. Reverse cross-linking is mediated by the addition of 20 µL of 5 M NaCl and incubation at 65 °C overnight.

DNA purification: After reversing the cross-link, 20 uL of 1 M Tris-HCl, pH 6.5, 10 µL 0.5 mM EDTA, pH 8, and 1 uL of 20 mg/mL Proteinase K are added to the elution fractions and incubated at 45 °C for 1 hour. DNA is extracted using 550 µL PCI. Glycogen (2 µL of a 20

mg/mL stock solution) is added to the extracted DNA along with 1 mL of 100% EtOH to enhance visualization of the DNA pellet. Samples are incubated at -20 °C for at least 2 hours. DNA is pelleted, washed with 70% EtOH, dried, and resuspended in 50-100 µL nuclease free water.

Input processing: For input samples, 250 µL of the sample lysate (which has already been diluted 1:10 in IP dilution buffer) is mixed with 250 uL water and 20 µL of 5 M NaCl at 65 °C overnight. The next day, 20 µL of 1 M Tris-HCl, pH 6.5, 10 µL 0.5 M EDTA, Ph 8, 2.5 µL 20 mg/mL Proteinase K, and 2 µL of 10 mg/mL RNase A is added and incubated at 55 °C for 2 hours. The DNA is extracted as described above for the IP samples and dissolved in 40 µL nuclease-free water.

Quantitative real-time PCR (qRT-PCR): QRT-PCR reactions were comprised of 7.5 µL 2x Sybr Green RT-PCR mix, 0.75 µL of 10 µM forward and reverse primers, 3 µL of water, and 3 µL of IP DNA. Input DNA was diluted 1:40 prior to qRT-PCR analysis. For each primer set, standard curves were generated to calculate the amount of ChIP DNA at each amplified region.

4.3 Results

4.3.1 Generation of cell lines stably depleted of SART3 using shRNA

To comprehensively investigate the role of SART3 in transcription and splicing, we decided to perform RNA-seq analysis of RNA harvested from control and SART3-depleted cells. Because SART3 is involved in splicing and because SART3 depletion affects ubH2B levels, which has also been implicated in transcription and alternative splicing, we proposed that RNA-seq data would reveal transcription and/or splicing defects at SART3-

regulated genes. Typically, studies involving genome-wide analysis of knockdown samples deplete the protein of interest using two different RNAi sequences, and high confidence data points are changes that are observed in both knockdown samples. We took a slightly different approach to this method in that, in one case, we chose to deplete SART3 using siRNA and in the other case, we generated cell lines with SART3 stably depleted using shRNA. One advantage to using this approach is that transcriptional changes observed in both data sets would be more likely caused by depletion of SART3 rather than due to off-target effects of the RNAi or the method of RNAi introduction (transfection vs. transduction).

To generate cell lines stably depleted of SART3, we packaged SART3 shRNA encoding a puromycin resistance cassette into lentiviruses, infected HeLa cells, and selected for puromycin-resistant cells. For the initial screen of SART3 depletion efficiency, 12 SART3 shRNA plasmids, each encoding a unique sequence to target SART3 for depletion, were assayed (Table A2.2). These plasmids were packaged into lentiviruses and on Day 1, HeLa cells were infected with each virus. Lentivirus packaged with a plasmid encoding GFP was used as a positive control for infection (as this could be visualized by microscopy) and was used as a negative control for SART3 depletion. On Day 3, cells were subjected to selection by 10 μg/ml puromycin treatment. Cell lysates were harvested for western blot analysis on Day 6. Western blotting analysis showed each shRNA construct depleted SART3 to different degrees. The efficiency of SART3 depletion using plasmids 1, 2, and 10 seemed comparable to SART3 depletion using siRNA (Figure 4.1A). For this reason, we chose to further characterize SART3 depletion using these three lentiviral-packaged shRNA plasmids.

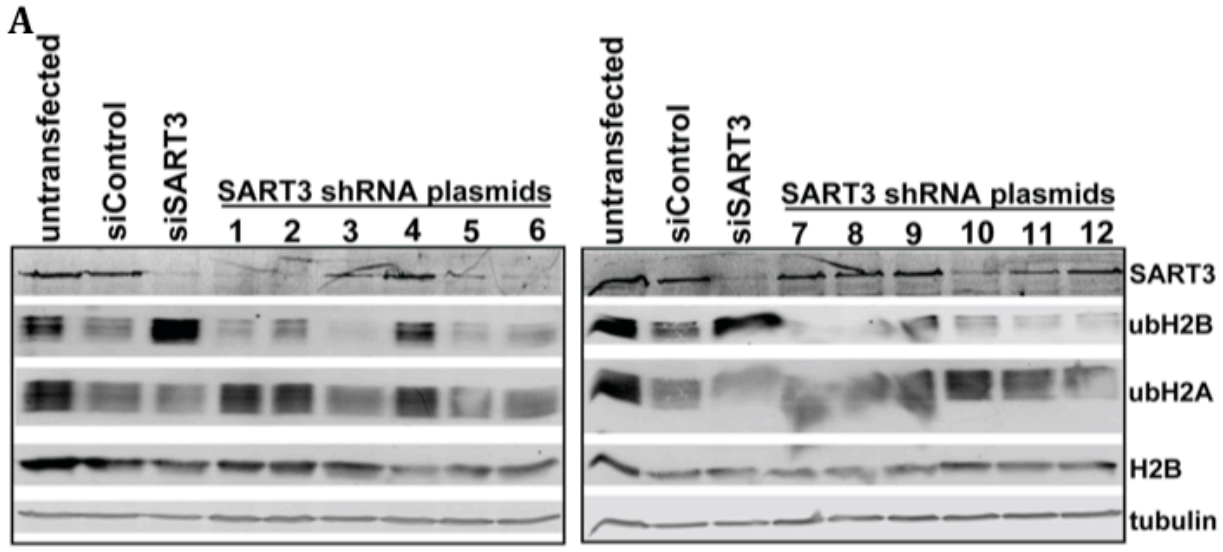
A
untransfected
siControl
siSART3
SART3 shRNA plasmids
1 2 3 4 5 6
untransfected
siControl
siSART3
SART3 shRNA plasmids
7 8 9 10 11 12
SART3
ubH2B
ubH2A
H2B
tubulin

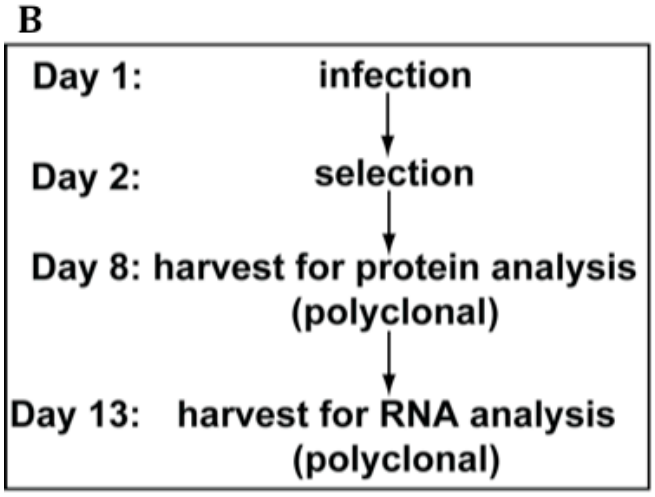
B
Day 1: infection
Day 2: selection
Day 8: harvest for protein analysis (polyclonal)
Day 13: harvest for RNA analysis (polyclonal)

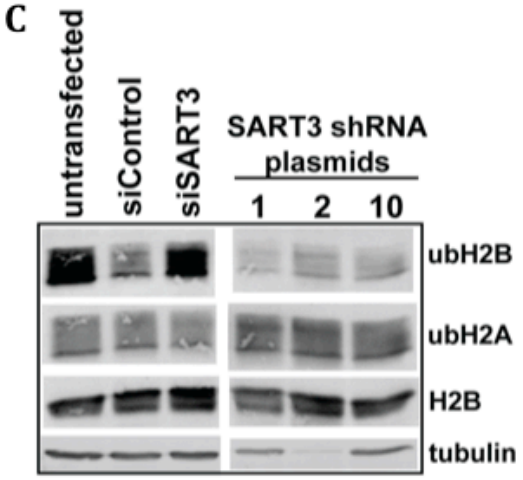
C
untransfected
siControl
siSART3
SART3 shRNA plasmids
1 2 10
ubH2B
ubH2A
H2B
tubulin

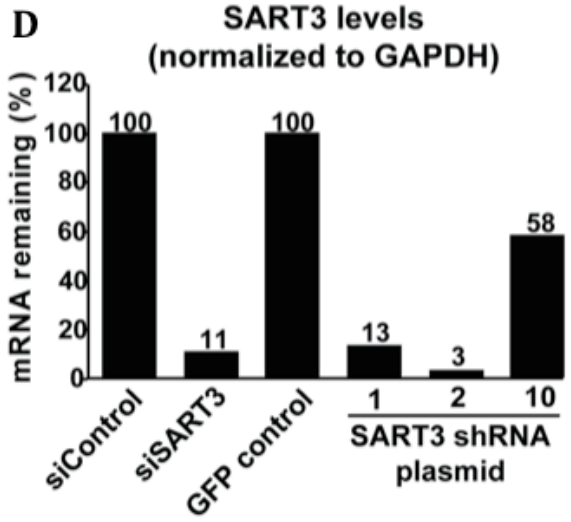
D
SART3 levels (normalized to GAPDH)
mRNA remaining (%)
120
100
80
60
40
20
0
100
11
100
13
3
58
siControl
siSART3
GFP control
1
2
10
SART3 shRNA plasmid

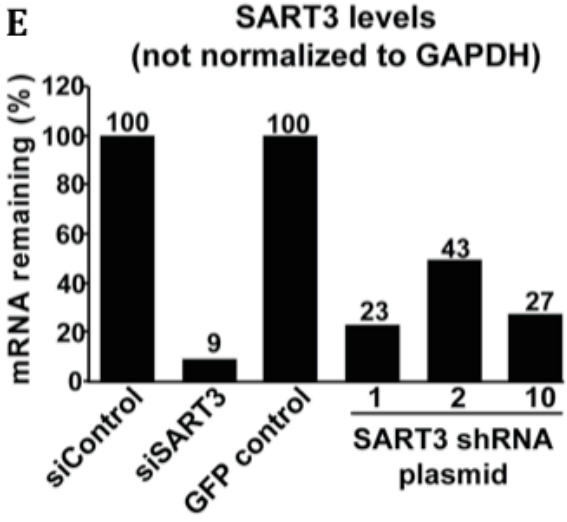
E
SART3 levels (not normalized to GAPDH)
mRNA remaining (%)
120
100
80
60
40
20
0
100
9
100
23
43
27
siControl
siSART3
GFP control
1
2
10
SART3 shRNA plasmid

Figure 4.1. Generation of cell lines stably depleted of SART3 using shRNA. (A) SART3 shRNA plasmids deplete SART3 protein at various efficiencies. HeLa cells were infected with 12 unique SART3 shRNA-containing lentiviruses (labeled 1-12, Table A2.2). Puromycin selection was applied 48 hours post-transduction (Day 3) and total cell lysates (polyclonal) were harvested on Day 6. Proteins were visualized using SDS-PAGE and immunoblotting. **(B)** Experimental scheme for generation of shSART3 cell lysates for western blot and RNA-seq analysis. **(C)** SART3 depletion by shRNA does not increase ubH2B levels. HeLa cells were infected with lentivirus that packaged shSART3 plasmids 1, 2, and 10 as described in (B). Lysates were separated by SDS-PAGE and proteins were detected by western blotting. Untransfected HeLa cells were used as an additional control. **(D)** RNA from Day 13 shSART3 cells was extracted and isolated using Trizol reagent. Equal amounts of total RNA for each sample was reverse transcribed using iScript (BioRad). SART3 and GAPDH levels were measured using qRT-PCR. Primers that detected total GAPDH transcripts (both unspliced and spliced) were used to normalize total cDNA content. **(E)** Transcript levels were analyzed using the same data as presented in (D), but normalization to GAPDH was not employed.

To identify the best candidate for RNA-seq analysis, HeLa cells were treated according to the schematic depicted in Figure 4.1B. On Day 1, cells were infected with lentivirus packaged with plasmids encoding GFP or shSART3 sequences 1, 2, or 10. Puromycin selection was employed on Day 2 and cell lysates were harvested for western blot analysis on Day 8. Cells were passaged until Day 13 when total RNA was harvested from cells using the Trizol reagent.

Cell lysates harvested on Day 8 were separated by SDS-PAGE and subjected to analysis by immunoblotting. As was previously observed, ubH2B levels did not increase upon depletion of SART3 using shRNA (Figures 4.1C and 4.1A). Notably, shSART3 plasmid 2 showed a large reduction in tubulin levels, indicating SART3 depletion for an extended amount of time using shSART3 plasmid 2 might have global effects.

RNA harvested on Day 13 was reverse transcribed into cDNA and SART3 transcript levels were measured using quantitative real-time PCR (qRT-PCR). GAPDH transcript levels were used for normalization and the efficiency of SART3 knockdown was compared to either siControl or lentivirus GFP (for siSART3, and shSART3 plasmids 1, 2, and 10, respectively). SART3 was most efficiently depleted using siSART3 (Figure 4.1D). At first glance, shSART3 plasmid 2 seemed to exhibit the most efficient SART3 depletion when compared to plasmids 1 and 10 (3% SART3 transcripts remaining versus 13% and 58% SART3 transcripts remaining, respectively). Because western blot analysis showed similar SART3 depletion at the protein level for each of these shSART3 plasmids (Figure 4.1A), it seemed unusual that there would be such a large discrepancy between the transcript and the protein levels for each shSART3 sample. Additionally, despite the fact that equal amounts of total RNA for each sample type were reverse transcribed into cDNA, we noticed

the GAPDH transcript levels for shSART3 plasmid 2 were unusually high. This was accompanied by the strange observation that tubulin protein levels were also reduced in this sample (Figure 4.1C, lane 5). Therefore, SART3 transcript levels were also analyzed without normalization to GAPDH and compared to control knockdown samples (Figure 4.1E). Using this analysis method and the GAPDH normalization method, we found shSART3 plasmid 1 most efficiently depleted SART3 transcript levels when compared to plasmids 2 and 10. For this reason, RNA extracted from GFP- and shSART3 plasmid 1-infected cells 13 days post-infection and siControl- and siSART3 cells 3 days post-transfection were sent for RNA-seq analysis.

4.3.2 RNA-seq analysis revealed changes in transcript levels and splicing defects in SART3-depleted cells

RNA samples were submitted to the Colorado State University Next Generation Sequencing Core for analysis. Ribosomal RNA depletion, reverse transcription, and additional sample processing was performed at the core facility. Because one of our objectives was to identify intron inclusion and alternative splicing patterns upon SART3 depletion, obtaining sequence reads at the unspliced intron/exon and spliced exon/exon junctions was critical. For this and other reasons, we chose to use the Ion Torrent sequencing platform over the Illumina sequencing platform as the average read length is substantially longer (up to 250 base pairs versus up to 150 base pairs per read) and the chances of mapping reads corresponding to spliced exon/exon junctions and unspliced intron/exon junctions are enhanced. Data processing were carried out by the Core personnel using Nextgene to trim reads with a quality score lower than 13 and filter out

reads with length less than 35 bp, followed by expression analysis using AvardisNGS. Sequence reads were normalized using either total read count (TC) or DESeq normalization methods. Notably, both normalization methods gave very similar results.

Using the TC normalization method and excluding fold-changes <2 and adjusted p-value > 0.05, we found 1181 genes had increased transcript levels upon SART3 depletion using the siRNA depletion method (Figure 4.2A). A comparatively equal number of genes (1175) exhibited decreased transcript levels upon siSART3 transfection. In stark contrast, only 272 genes displayed increased transcript levels upon depletion of SART3 using shRNA while 1959 genes showed decreased transcript levels. This large discrepancy between the number of genes with increased and decreased transcript levels is alarming. We think that the long-term SART3 knockdown (13 days) in the shSART3 samples possibly led to total collapse of splicing, transcription and other function of the cell. Therefore, many of the observed changes in transcription are likely due to secondary effects of long-term SART3 depletion. In contrast, SART3 depletion by siRNA was carried out in 3 days. Additionally, there are only a small overlap between the genes affected by shSART3 knockdown and those affected by siSART3 knockdown. For these reasons, we chose to continue analysis using only the data obtained from the siControl and siSART3 samples.

To validate the observed fold-changes identified in the RNA-seq analysis, at least 5 genes from each category (transcript abundance either increased or decreased upon SART3 depletion) were chosen. Transcript levels were determined with qRT-PCR using primers designed to amplify a region within a single exon, thus eliminating changes in transcript levels due to changes in splicing (Table A2.3). Transcript levels were normalized

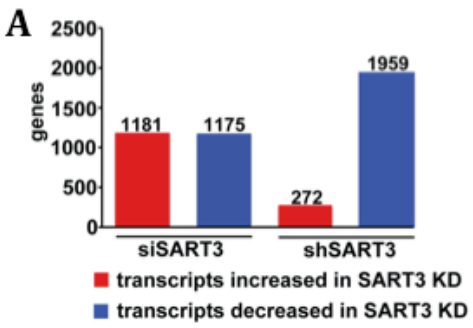

B

Gene	NGS	qRT-PCR
MFAP5	↑47.8	21.7
LAMP3	↑25.8	38.0
MEG3	↑5.74	9.53
CDKN1A	↑5.58	16.9
GRAM1BD	↑5.42	4.48
F11R	↓89.4	5.89
SPINT1	↓15.1	7.77
PDGFB	↓17.4	9.83
USP18	↓10.6	2.71
CTR9	↓4.42	3.20

Figure 4.2. RNA-seq analysis revealed changes in transcript levels and alternative splicing in SART3-depleted cells. (A) RNA-seq analysis of fold-changes observed in transcript levels. Transcripts identified in RNA-seq analysis were aligned to the annotated human genome, normalized using the total count (TC) method, and fold-change of transcript levels between control and SART3-depleted samples (using SART3 siRNA or shRNA) was quantitated. The number of genes that displayed a transcript level change of 2.0-fold or greater and a corresponding p-value of 0.05 or less are plotted. **(B)** Validation of RNA-seq analysis. Specific genes from (A) were selected for validation by qRT-PCR. A portion of siControl and siSART3 RNA that was submitted for RNA-seq analysis was reverse transcribed using iScript (BioRad) and primers amplifying a region of the indicated gene was used for qRT-PCR analysis. Primers were designed to amplify a region within a single exon that was common between all splice variants to prevent convoluting results due to aberrant or alternative splicing. Red arrows indicate genes with increased transcription upon SART3 depletion and blue arrows indicate genes with decreased transcription upon SART3 depletion. qRT-PCR quantities were normalized to GAPDH transcript levels. Fold-changes reported in the Next Generation Sequencing (NGS) and the qRT-PCR analyses are reported. **(C)** Alternatively spliced genes do not seem to correlate with genes with increased or decreased transcript levels upon SART3 depletion. RNA-seq data was aligned to the annotated human genome (hg18) and normalization with the DESeq method was used to calculate fold-change in transcript level. Genes with a fold-change of greater than 2.0 were selected without a p-value constraint. Next, Avadis software was used to identify genes with alternative splicing patterns in siControl and siSART3 cells. A ven diagram was used to compare the overlap between alternatively spliced genes and genes with an increased or decreased transcript level upon SART3 depletion.

to GAPDH as previously described. The fold-change observed in the Next Generation Sequencing (NGS) data set and the fold-change observed in the qRT-PCR validation are listed in Figure 4.2B. In each case, the observed trend in the NGS results agreed with the trend obtained in the qRT-PCR validation results (either increased or decreased transcript level in the siSART3 sample, indicated by the red and blue arrows) (Figure 4.2B). In many cases, the degree of fold-change observed in the NGS and qRT-PCR validation was not identical, but this can most likely be attributed to differences in sample preparation, reverse transcription, amplification, and normalization methods.

Because SART3 is a U4/U6 spliceosome recycling factor, we analyzed the RNA-seq data to look for genes that displayed alternative splicing patterns upon SART3 depletion using the AvardisNGS software on a trial basis. In this analysis, the data were normalized using the DESeq normalization method. Additionally, expression and splicing changes were not restricted to a p-value of less than 0.05 as was previously described (Figure 4.2A). Using these parameters, we observed 1115 genes that displayed differential splicing patterns upon SART3 depletion (Figure 4.2C). A fraction of these alternatively spliced genes also displayed an increase or decrease in transcript level in SART3 knockdown cells (157 versus 130 genes, respectively) (Figure 4.2C). These differential splicing events have not been confirmed by qRT-PCR. The bioinformatic analysis also needs to be repeated in the future to ensure appropriate parameters were chosen in the process.

4.3.3 SART3 localizes to genes that are down-regulated upon SART3 depletion

Using RNA-seq and validation by qRT-PCR, we identified many genes whose transcript abundance were either increased or decreased upon SART3 depletion. To

identify if the changes in transcription are directly modulated through the action of SART3, we used Chromatin Immunoprecipitation (ChIP) to detect the presence of SART3 at these particular genes. For these initial studies, we chose to focus on a subset of genes whose transcript level decreased upon SART3 depletion.

For ChIP analysis of SART3, we used a HeLa Flp-In stable cell line that, upon the addition of doxycycline (Dox), induces the expression of HA-tagged SART3. An anti-HA antibody was used to immunoprecipitate (IP) HA-SART3 (Figure 4.3, red bars). Negative controls include IP using normal IgG antibodies in Dox-induced cells and IP using anti-HA antibodies in uninduced cells (Figure 4.3, black bars and blue bars, respectively). Localization of SART3 was monitored using two or three primer sets for CTR9, F11R, and FAT3. For each gene, we designed primers to amplify a region within the first exon or to amplify the intron/exon junction at the 3' end of intron 1 and the 5' end of exon 2 (Figure 4.3). In the case of the FAT3 genes, an additional primer set was designed to amplify the exon/intron junction region at the 3' end of exon 1 and the 5' end of intron 1. Unfortunately the resolution obtained in ChIP analysis is not enough to accurately localize SART3 between exon 1 and the first exon/intron junction in CTR9 and F11R as the length of the first exon is relatively short.

Nevertheless, we found high levels of SART3 at these particular genomic regions when compared to negative controls (IgG and HA (–Dox)), suggesting that changes in CTR9, F11R, and FAT3 transcript levels in SART3-depleted cells could be a direct effect, rather than an indirect effect of SART3 loss (Figure 4.3). While SART3 levels increase at the intron/exon junction of CTR9 (amplicon 1 vs. amplicon 2), we observed a decrease in SART3 levels at the FAT3 intron/exon junction (amplicon 1 vs. amplicon 3). Meanwhile,

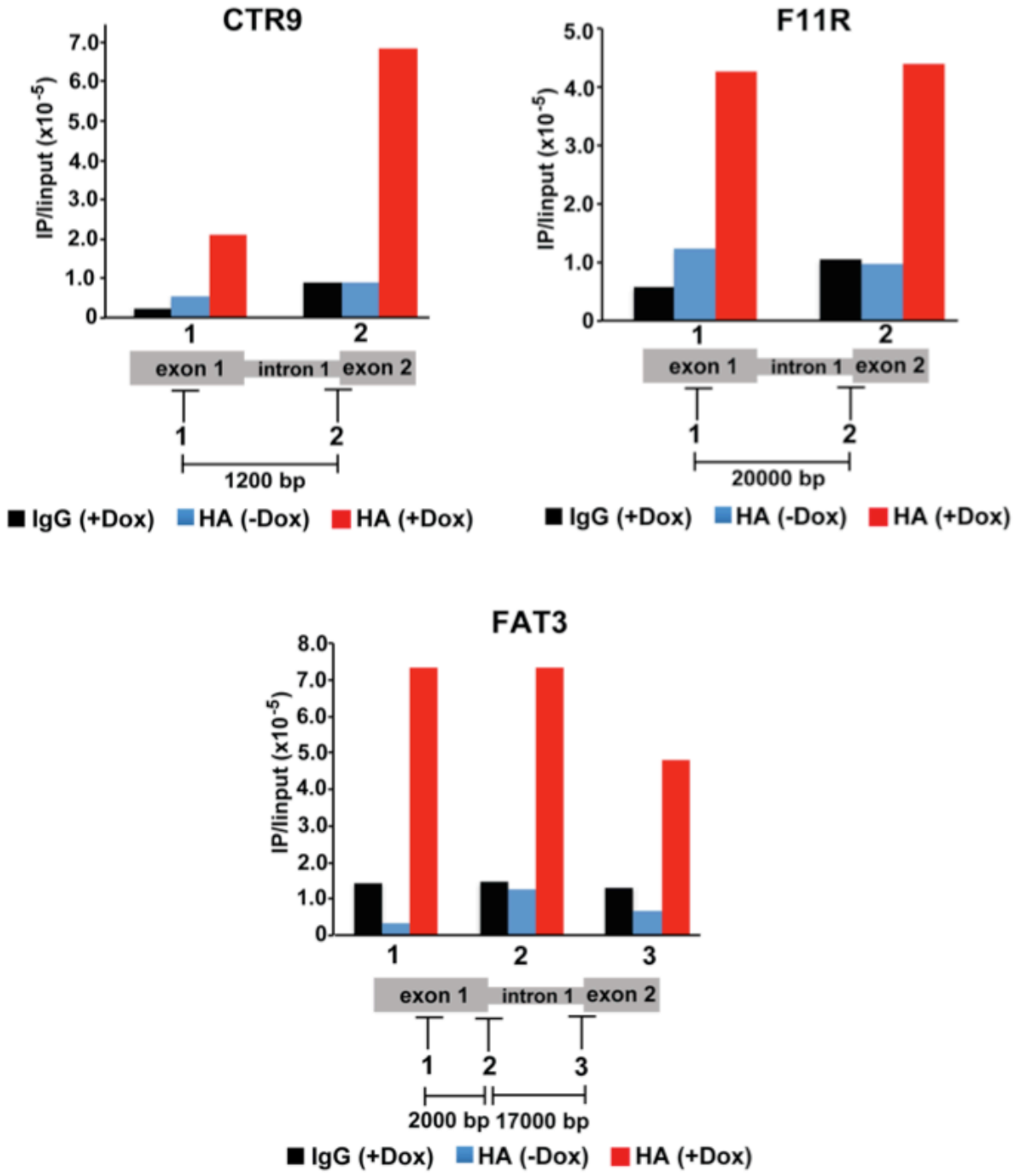

Figure 4.3. SART3 localizes to genes that are down-regulated upon SART3 depletion. A 48 hour doxycycline (Dox) treatment was used to induce expression in stable HeLa HA-SART3 cell lines. ChIP analysis was performed using IgG or anti-HA antibodies (black or red bars, respectively). As a negative control, ChIP analysis using anti-HA was also performed on uninduced samples (blue bars). Specific regions within CTR9, F11R, and FAT3 were amplified using qRT-PCR to quantitate SART3 localization (Table A2.4). Primer amplification regions and distances between amplicons (in base pairs) are indicated. For each sample, IP signal was normalized to input signal.

SART3 is detected at the F11R exon 1 and intron/exon junction positions at similar levels. The reason for the different patterns of SART3 localization is unclear, but one possible explanation is that the size of the intron could affect the level of SART3 occupancy (compare CTR9 vs. F11R and FAT3). A more comprehensive analysis of SART3 localization throughout multiple genes is necessary to discern any pattern.

Typically, an additional normalization parameter is applied to ChIP data analysis where ChIP signal is normalized to the signal detected within a region void of the target protein (in this case, HA-SART3). Classically, for normalization of proteins involved in transcription, these primers are designed to amplify a transcriptionally silent region. Because little is known about the function of SART3, in the future, primers designed to amplify different silent regions of chromatin such as the centromeric DNA have to be tested in order to identify suitable negative controls.

4.3.4 RNAPII localization in SART3-depleted cells

Because depletion of SART3 causes a decrease in transcript level of multiple genes, we sought to assay RNAPII patterns at these genes. We performed ChIP analysis with 8WG16 antibodies in siControl and siSART3 cells and used the previously described primer sets to assay the localization of RNAPII. Despite the observed decrease in transcript level upon SART3 depletion, only minor changes in RNAPII levels were detected (Figure 4.4). Furthermore, in the case of F11R, we observed a slight increase in RNAPII at the intron/exon junctions in SART3-depleted cells. These data suggest that RNAPII may be piling up at the F11R intron/exon junction, possibly due to a defect in splicing, leading to less processive transcription.

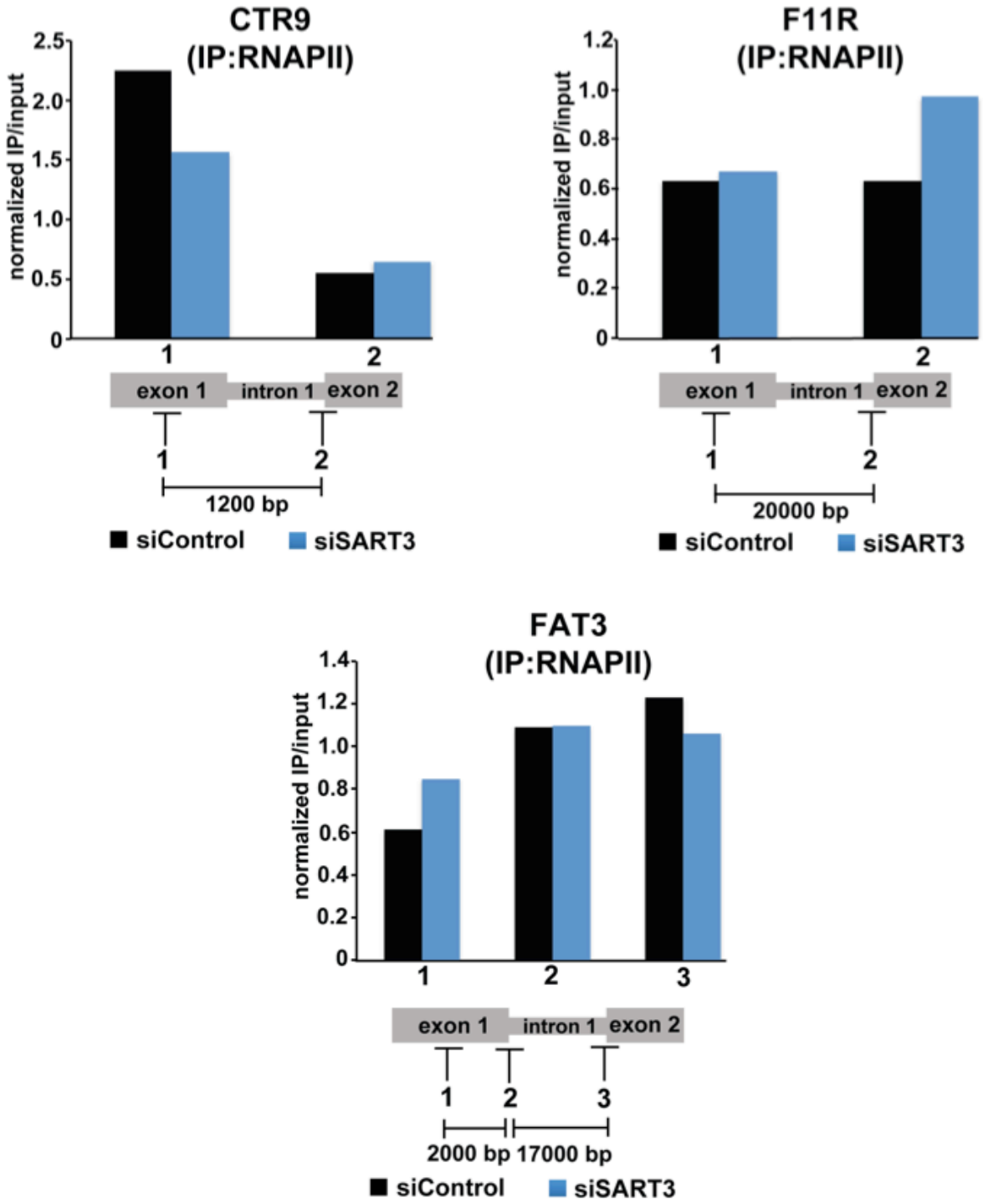

Figure 4.4. RNAPII accumulates at intron/exon junctions in SART3-depleted cells. HeLa cells were transfected with either control or SART3 siRNA 72 hours prior to ChIP analysis using the 8WG16 antibody. IgG antibody was used as a negative control in a previous experiment under the same ChIP conditions (not shown). Primers sets described in Figure 4.3 were used. For each sample, IP signal was normalized to both input signal and to ChIP signal at a transcriptionally silent, intergenic region of the genome.

In the case of CTR9, the levels of RNAPII did not change at the intron/exon junction upon SART3 knockdown, but it is important to note that the fold-change of RNAPII levels between exon 1 and the intron/exon junction is greater in the siControl sample than the siSART3 sample (3.46-fold vs. 2.17-fold, respectively). Future ChIP-seq studies analyzing global RNAPII occupancy coupled with CTD phosphorylation status will be needed to obtain better understanding of whether and how SART3 communicates with the transcription machinery.

4.4 Discussion

In this study, we used RNA-seq analysis to identify changes in transcript levels and splicing patterns in SART3-depleted cells. We used qRT-PCR to validate the observed changes in transcript levels from NGS analysis for 10 different genes and found that 100% of the tested genes displayed consistent trend in transcript level change (either an increase or decrease in transcript levels). Presumably, at least a fraction of these genes are directly regulated by SART3 as ChIP analysis revealed SART3 localization to regions within the CTR9, F11R, and FAT3 genes. Despite significant decrease in transcript levels of these genes, we found RNAPII levels did not decrease at 5' end of each gene. On the contrary, our preliminary data suggest RNAPII may be piling up at intron/exon junctions, possibly due to defects in splicing in the absence of SART3.

SART3 depletion using shRNA does not increase ubH2B levels—Upon transfection, ubH2B levels are reduced when compared to untransfected HeLa cells (Figure 4.1A, compare lanes 1 and 2). Others and we have consistently observed this phenomenon using a variety of control siRNA sequences. For this reason, untransfected HeLa cell lysate was

used as a standard to monitor changes in ubH2B levels in cells depleted of SART3 using shRNA. Note that ubH2B levels in the GFP control were comparable to ubH2B levels in the untransfected HeLa cell lysate (data not shown).

We found that both ubH2A and ubH2B levels changed to various degrees with each shRNA plasmid 6 days post-transduction, but we did not observe an increase in ubH2B under any condition (Figure 4.1A). Furthermore, the observed changes in ubH2A and ubH2B levels did not seem to correlate with the efficiency of SART3 depletion. One explanation is that, when compared to SART3 knockdown using siRNA, stable depletion of SART3 using lentiviral shRNA occurs over a longer period of time (3 days vs. 6-8 days) and cells may undergo further changes in response to the depletion of SART3 over an extended amount of time. One of these adaptation mechanisms may involve the reorganization, redistribution, and changes in global levels of ubH2B.

RNAPII occupancy—Despite a decrease in transcript levels of CTR9, F11R, and FAT3 upon SART3 knockdown, we observed only a mild decrease in RNAPII levels at exon 1 in CTR9. Meanwhile, RNAPII levels in exon 1 of F11R and FAT3 either remained unchanged or slightly increased. These data suggest transcript levels are not reduced due to a decrease in RNAPII recruitment to the 5' end of the gene. Recent studies have shown SART3 is recruited to the HIV promoter and enhances P-TEFb recruitment to the promoter, which leads to increased Serine 2 phosphorylation (Ser2P) of the RNAPII CTD (Zhao et al., 2014). This Ser2P enhances processive elongation and is required for efficient synthesis of full-length transcripts. Like our findings, this study also observed that total RNAPII CTD levels did not change, suggesting the phosphorylation status of the RNAPII CTD, and not recruitment of RNAPII itself, may be changed upon SART3 depletion. Therefore, ChIP

analysis of different phosphorylated forms of RNAPII could provide further insight into the relationship between SART3 and the transcription apparatus. Notably, global levels of Ser2P and Ser5P of the CTD are unaffected in SART3-depleted cells, but this type of global analysis may not reveal changes of CTD phosphorylation at specific genes (Figure 3.12F).

It is also important to note that the afore mentioned ChIP studies analyzing the presence of SART3, P-TEFb, and RNAPII CTD-Ser2P utilized a reporter gene system whereby transcription of the reporter gene (Luciferase) was driven by the HIV promoter (Zhao et al., 2014). Because the reporter gene does not contain an intron, the function of SART3 in splicing may not be recapitulated in this system. These data also suggest SART3 could affect transcription in a splicing-independent manner. Future analysis of transcription and splicing machinery at SART3-regulated genes is necessary to provide mechanistic insight into the function of SART3 in transcription and splicing.

CHAPTER 5: DISCUSSION AND PERSPECTIVES

5.1 Co-transcriptional pre-mRNA splicing

Generally speaking, most splicing events of mammalian genes occur co-transcriptionally. This is evidenced, in part, by the fact that most c-Src and fibronectin mRNA introns are removed prior to release from the chromatin (Pandya-Jones and Black, 2009). Additionally, many splicing factors are recruited to and directly bind the RNAPII CTD, and this recruitment is dependent upon processive pre-mRNA synthesis (Misteli and Spector, 1999; Sapra et al., 2009). An intimate relationship between transcription and splicing has also been demonstrated in that the RNAPII CTD is required for proper pre-mRNA splicing and processing. Specifically, substituting RNAPI, RNAPIII, or a RNAPII CTD deletion mutant in place of *wild-type* RNAPII results in defects in pre-mRNA processing due to the inability to properly and efficiently recruit the splicing machinery (McCracken et al., 1997; Misteli and Spector, 1999). Furthermore, perturbation of transcription rates affect alternative splicing (Luco et al., 2011). An example of this relationship was demonstrated via modulation of the RNAPII elongation rate. In this study, implementation of a mutant RNAPII with an abnormally slow elongation rate resulted in inclusion of alternative exons into the final pre-mRNA product (de la Mata et al., 2003). Conversely, increasing the rate of RNAPII transcription elongation results in inefficient splicing and intron retention (Braberg et al., 2013). In the first case, intron removal is presumably more efficient because the slowed RNAPII elongation rate allows temporal recruitment of splicing factors that may normally not be recruited under normal rates of RNAPII elongation. Alternatively, when the elongation rate of RNAPII is increased, intron removal is presumably less efficient due to

inefficient recruitment of splicing factors. This model by which the elongation rate of RNAPII directly modulates splicing efficiency is referred to as the "kinetic" model.

5.2 Chromatin structure affects alternative splicing

Additionally, chromatin architecture and chromatin remodeling factors have been demonstrated to affect alternative splicing patterns. Characterization of nucleosome positioning using genome-wide mapping techniques revealed that nucleosomes are enriched at intron-exon junctions (Schwartz et al., 2009). Nucleosome positioning extends beyond simply defining exons as chromatin architecture as alternative splicing is also regulated by chromatin. This was demonstrated by the observation that: 1) *included* alternatively spliced exons have a higher nucleosome density when compared to the nucleosome density observed in *excluded* alternatively spliced exons and 2) weaker splice sites have more well-positioned nucleosomes (Spies et al., 2009; Tilgner et al., 2009). Hypothetically, this enrichment of nucleosome density functions as a physical barrier to slow the rate of RNAPII elongation, thus allowing time for splicing factors to be recruited and enhancing the inclusion of particular exons in the final transcript product. Notably, there is at least one instance where chromatin remodeling regulates alternative splicing without affecting the elongation rate of RNAPII (Auboeuf et al., 2002). Therefore, it is unlikely that the kinetic transcription model of splicing regulation is a completely accurate model under all circumstances.

5.3 The role of histone post-translational modifications in pre-mRNA splicing

In addition to chromatin architecture marking intron/exon junctions, specific post-translational modifications of nucleosomal histones also play a role in exon definition. Specifically, H3K36me3, H3K4me3, H3K27me2, and H3K27me3 are elevated in exons, even after normalization to nucleosome density, and enrichment of these marks is decreased in alternatively spliced exons (when compared to constitutively included exons) (Andersson et al., 2009; Dhami et al., 2010; Luco et al., 2010; Spies et al., 2009). In addition, ubH2B is particularly elevated at intron/exon junctions in highly expressed exons in mammalian cells (Jung et al., 2012). Conversely, some histone marks, such as H3K9me3 are notably absent from exon regions (Spies et al., 2009).

Because both active transcription (H3K36me3, H3K4me3, and ubH2B) and repressive transcription (H3K27me2, H3K27me3, and ubH2B) marks regulate alternative splicing, it is unlikely these histone PTMs regulate splicing using a mechanism by altering RNAPII elongation rates to manipulate the inclusion or exclusion of exons. Rather, some studies have found that certain histone modification-binding proteins act as a bridge between chromatin and specific splicing factors (Gunderson and Johnson, 2009; Herissant et al., 2014; Loomis et al., 2009; Luco et al., 2010; Piacentini et al., 2009; Sims et al., 2007). For example, the chromatin remodeler, CHD1, binds both H3K4me3 and the U2 snRNP to enhance pre-mRNA splicing efficiency (Sims et al., 2007).

UbH2B, in particular, was reported to stimulate recruitment of U1 and U2 onto nascent RNA (Herissant et al., 2014). In this study, nascent mRNPs were purified from *wild-type* or *htbK123R* yeast strains and bound proteins were detected using quantitative mass spectrometry. Results showed that components of the U1 and U2 snRNPs were less

abundant in the mRNPs isolated from the *htbK123R* strain, thus identifying a role for ubH2B in recruitment of splicing factors. Whether any of the splicing factors directly interact with ubH2B remains unclear. As ubH2B plays a critical role in transcription elongation, another possibility is that ubH2B may affect alternative splicing through modulation of RNAPII elongation rates. There is evidence that increasing global levels of ubH2B in mammalian cells results in increased intron retention in the final pre-mRNA product (Zhang et al., 2013). In this study, depletion of the histone DUB, Usp49 resulted in increased ubH2B levels, increased exon skipping in alternatively spliced genes, and a decrease in complete pre-mRNA splicing. Under these circumstances, it's possible that elevated ubH2B levels increase the RNAPII elongation rate, thus disfavoring proper temporal recruitment of splicing factors and cause inefficient splicing.

5.4 Future directions

As illustrated in our model (Figure 3.17), our *in vitro* and *in vivo* data suggest Usp15 and SART3 work together in a coordinated fashion to deubiquitinate evicted histones during transcription prior to their reassembly onto DNA behind elongating RNAPII. Deubiquitinating histones prior to reassembly would "reset" the chromatin template, thereby allowing histone PTM patterning to be redefined for the next round of transcription. Thus, deregulation of SART3 could cause transcriptional and pre-mRNA processing aberrations. Based upon this model, we hope to answer three main questions: 1) Does SART3 affect transcription and/or pre-mRNA splicing? 2) If so, *how* is SART3 affecting transcript levels? and 3) Does Usp15 play a role in SART3-mediated regulation of

transcript and ubH2B levels *in vivo*. Specific experiments designed to address these questions are detailed below.

5.4.1 Does SART3 affect transcription and/or pre-mRNA splicing?

Upon SART3 depletion, we identified many genes with increased transcript levels, decreased transcript levels, or differentially spliced transcripts. Because these transcript changes could be an indirect effect of SART3 depletion, we hope to identify changes that are directly mediated through the action of SART3. Thus, we plan to use the HeLa HA-SART3 stable cell line utilized in Figure 3.3 to perform ChIP-seq analysis (using anti-HA for IP) to define regions of the genome to which HA-SART3 is localized. Analysis of SART3 ChIP-seq data will include a comparison with our RNA-seq data to look for a correlation between those genes whose transcription was affected by SART3 depletion and genes at which SART3 is localized. If there is a high correlation between changes in transcript levels in SART3 depleted cells and SART3 localization, we can be more confident the transcript changes observed are a direct effect of SART3 function. As was previously mentioned, we have yet to identify a genomic region where SART3 is absent. This ChIP-seq analysis could provide useful information in identifying SART3-depleted regions of the genome.

5.4.2 How is SART3 affecting transcript levels?

The changes in transcript abundance we observed in SART3-depleted cells are most likely caused by changes in either transcription or RNA stability. As SART3 and ubH2B have been implicated to play roles in the transcription pathway, we plan to first investigate the

possibility that changes in transcription are responsible for the observed changes in transcript levels.

First, we plan to examine RNAPII localization on a global level in SART3-depleted cells using ChIP-seq. If changes in RNAPII levels are observed at genes affected by SART3 depletion, this would support the idea that transcript abundance changes in SART3-depleted cells are primarily caused by changes in transcription and not RNA stability. Preliminary analysis of RNAPII occupancy at 3 genes revealed RNAPII levels are not substantially affected by SART3 depletion. Nonetheless, it is possible that, although RNAPII localization is unaffected by SART3 depletion, the phosphorylation status of the RNAPII CTD may be affected, indicating changes in transcription are not due to defects in RNAPII recruitment, but rather due to defects in transcription initiation or elongation. Thus, we also plan to use ChIP to examine the Ser5P and Ser2P patterning of RNAPII at SART3-affected genes.

There is evidence supporting the model that RNAPII pauses at 3' splice sites (intron/exon junctions) to facilitate proper temporal recruitment of the splicing machinery before transcription elongation is allowed to proceed (Alexander et al., 2010). Specifically, studies in yeast using ChIP analysis showed the timing of splicing factor recruitment is slightly delayed in relationship to the timing of RNAPII pausing at splice sites and inhibition of splicing disrupts RNAPII pausing patterns (i.e. RNAPII no longer pauses at 3' splice sites). Furthermore, RNAPII pausing at the most 5' intron/exon junction within a gene is required for efficient Ser2 phosphorylation of the RNAPII CTD. Based upon these studies, we expect to observe changes in RNAPII and RNAPII CTD phosphorylation patterning at SART3-affected genes.

If the observed changes in transcript abundance in SART3 depleted cells is a consequence of deregulated transcription, it's possible the mechanism of transcriptional reprogramming is caused by changes in ubH2B levels or patterning. Because SART3 depletion resulted in a global increase in ubH2B levels, we are interested to learn if ubH2B levels and patterning on SART3-affected genes is changed upon SART3 depletion. First, we hope to analyze ubH2B localization using publicly available ChIP data to look for particular ubH2B patterning in SART3-affected genes, such as elevated levels within exons or at intron/exon junctions. Secondly, we plan to monitor changes in ubH2B at SART3-regulated genes upon SART3 depletion to assess a possible relationship between changes in transcript levels and changes in ubH2B localization. Thirdly, we plan to analyze changes in ubH2B levels and localization at genes with differential splicing patterns upon SART3 depletion to see if there is a correlation between ubH2B patterning and changes in alternative splicing. UbH2B levels will be normalized to H2B ChIP signal to account for changes in nucleosome density.

We observed that SART3 has mild histone chaperone activity *in vitro*. We are interested in investigating if the histone chaperone activity of SART3 is required for the regulation of global ubH2B levels and proper transcriptional control of SART3-regulated genes. To do this, we propose to use mutational dissection of SART3 to disrupt SART3-histone binding as measured by *in vitro* histone binding and supercoiling assays. Secondly, we propose to deplete SART3 from HeLa cells and rescue the SART3 depletion by expressing *wild-type* SART3, the SART3 mutant defective for histone binding, or GFP as a control. If the histone binding property of SART3 is required for ubH2B and transcriptional maintenance, we expect to see ubH2B and transcript levels restored in cells transfected

with *wild-type* SART3 and not those rescued with the SART3 mutant. Furthermore, ChIP studies analyzing the localization of mutant SART3, RNAPII, and ubH2B could highlight specific regulation steps at which the histone binding property of SART3 is paramount. We must also consider the possibility that mutating SART3 residues could not only disrupt histone binding, but could also disrupt interactions between SART3 and other binding partners.

5.4.3 Does Usp15 play a role in SART3-mediated regulation of transcript and ubH2B levels *in vivo*?

Our model proposes that Usp15 is recruited to sites of active transcription via SART3 and deubiquitinates histones prior to their re-deposition onto DNA behind elongating RNAPII (Figure 3.14). We are interested to see if Usp15 can also be detected at SART3-regulated genes using ChIP analysis. Furthermore, we plan to investigate whether SART3 and Usp15 localization overlap, based upon ChIP analysis. Along these lines, it is possible to deplete SART3 from cells and rescue with a *wild-type* or SART3 N-terminal domain deletion mutant (which does not bind Usp15) and investigate changes in transcript levels and ubH2B patterning at SART3-affected genes. Again, these data must be analyzed with the understanding that deletion of the SART3 NTD could abrogate interactions between SART3 and other proteins.

Depletion of Usp15 and its closest homologs, Usp4 and Usp11, did not result in global changes of ubH2B levels (Figure 3.12B). Nevertheless, it is possible that Usp15 may deubiquitinate a subset of H2B and this small change may not be discernible in the context of total cellular ubH2B. Therefore, if Usp15 can be detected at particular genes using ChIP

analysis, we plan to examine changes in ubH2B at these gene loci upon perturbation of Usp15 (either by depletion of Usp15 or overexpression of the catalytically inactive mutant, Usp15C269A). These data could provide further insight into the biological function of Usp15 in transcription and splicing.

5.5 Perspectives

Many questions remain unanswered in the field of co-transcriptional splicing. For example, an increase in ubH2B is observed at intron/exon junctions, but it is unclear how this ubH2B patterning is achieved. Because RNAPII pauses at 3' splice sites and because the H2B E3 ligase (RNF20/RNF40) associates with the elongating RNAPII complex, it's possible ubH2B levels are elevated at these RNAPII pause sites simply due to an increased residency time of RNAPII at these intron/exon junctions (Alexander et al., 2010; Wood et al., 2003b). Alternatively, it's possible RNF20/RNF40 non-discriminately ubiquitinates H2B and, rather, ubH2B patterning within genes is established through directed H2B deubiquitination.

Not only is it not well understood why ubH2B levels are elevated at intron/exon junctions, but the precise role of ubH2B in splicing not known. Herissant et al. showed ubH2B is required for efficient recruitment of splicing factors onto nascent RNA, but the mechanism of ubH2B-mediated splicing factor recruitment has not been characterized (Herissant et al., 2014). Although it is possible ubH2B directly recruits splicing factors to splice sites, it's also possible that an undefined factor acts as a bridging factor between ubH2B and the splicing machinery. This bridging mechanism as a means of cross-talk between the chromatin and splicing machinery has been described in multiple cases (see

Section 5.3). Although SART3 interacts with both histones and the splicing components, it's unlikely that SART3 is acting as the primary bridging factor as our histone dimer pull-down assays indicate SART3 non-preferentially binds unmodified and ubiquitinated histone dimers (Figure 3.12A). Along these lines, it's also possible ubH2B is not playing a direct role in splicing, but rather regulates splicing via modulation of transcription elongation rates.

To achieve processive transcription elongation, it's clear that both ubiquitination and deubiquitination of H2B are required. What remains unclear is in which context (free histones vs. nucleosomal histones) H2B is ubiquitinated or deubiquitinated, and how are these processes regulated. According to our model, we propose RNF20/RNF40 associated with elongating RNAPII ubiquitinates nucleosomal H2B as ubiquitination after assembly onto chromatin would be the most intuitive way to establish ubH2B patterning on genes.

Our work also sheds light on the mechanistic question concerning which histone substrates are deubiquitinated, free histone or nucleosomal histones. Based upon our *in vitro* deubiquitinating assay, we found that both free histones and nucleosomal histones are deubiquitinated, but the different histone DUBs (namely $SAGA^{DUB}$ and Usp15) exhibit different degrees of substrate specificity (Figure 3.4B-C). These data indicate H2B deubiquitination dynamics is regulated by multiple factors including histone DUBs and the context in which the DUB encounters the histone substrate, thus increasing the complexity of H2B deconjugation regulation. Further studies are needed to elucidate details concerning histone DUB regulation during processes such as transcription, DNA replication, and DNA damage repair.

REFERENCES

Abmayr, S.M., Yao, T., Parmely, T., and Workman, J.L. (2006). Preparation of nuclear and cytoplasmic extracts from mammalian cells. Current protocols in pharmacology / editorial board, S.J. Enna *Chapter 12*, Unit12 13.

Alexander, R.D., Innocente, S.A., Barrass, J.D., and Beggs, J.D. (2010). Splicing-dependent RNA polymerase pausing in yeast. Mol Cell *40*, 582-593.

Amerik, A.Y., and Hochstrasser, M. (2004). Mechanism and function of deubiquitinating enzymes. Biochim Biophys Acta *1695*, 189-207.

Andersson, R., Enroth, S., Rada-Iglesias, A., Wadelius, C., and Komorowski, J. (2009). Nucleosomes are well positioned in exons and carry characteristic histone modifications. Genome Res *19*, 1732-1741.

Andrews, A.J., Chen, X., Zevin, A., Stargell, L.A., and Luger, K. (2010). The histone chaperone Nap1 promotes nucleosome assembly by eliminating nonnucleosomal histone DNA interactions. Mol Cell *37*, 834-842.

Annunziato, A.T. (2013). Assembling chromatin: the long and winding road. Biochim Biophys Acta *1819*, 196-210.

Arnaudo, A.M., and Garcia, B.A. (2013). Proteomic characterization of novel histone post-translational modifications. Epigenetics Chromatin *6*, 24.

Auboeuf, D., Honig, A., Berget, S.M., and O'Malley, B.W. (2002). Coordinate regulation of transcription and splicing by steroid receptor coregulators. Science *298*, 416-419.

Baker, R.T., Catanzariti, A.M., Karunasekara, Y., Soboleva, T.A., Sharwood, R., Whitney, S., and Board, P.G. (2005). Using deubiquitylating enzymes as research tools. Methods Enzymol *398*, 540-554.

Barbera, A.J., Chodaparambil, J.V., Kelley-Clarke, B., Joukov, V., Walter, J.C., Luger, K., and Kaye, K.M. (2006). The nucleosomal surface as a docking station for Kaposi's sarcoma herpesvirus LANA. Science *311*, 856-861.

Bartke, T., Vermeulen, M., Xhemalce, B., Robson, S.C., Mann, M., and Kouzarides, T. (2010). Nucleosome-interacting proteins regulated by DNA and histone methylation. Cell *143*, 470-484.

Batta, K., Zhang, Z., Yen, K., Goffman, D.B., and Pugh, B.F. (2011). Genome-wide function of H2B ubiquitylation in promoter and genic regions. Genes Dev *25*, 2254-2265.

Bei, S.Z., Li, Y.A., Li, L., Pan, Z.Y., Li, G.X., Lan, B.X., Bao, Y.H., Yan, Q.Y., and Wang, Q. (1983). Electron microscopic studies on the chromatin of blastoderm nuclei and yolk granules

beneath blastoderm of fertilized and unincubated chicken eggs. Scientia Sinica. Series B, Chemical, biological, agricultural, medical & earth sciences / Chung-kuo k'o hsueh yuan, chu pan *26*, 708-715.

Bell, M., Schreiner, S., Damianov, A., Reddy, R., and Bindereif, A. (2002). p110, a novel human U6 snRNP protein and U4/U6 snRNP recycling factor. EMBO J *21*, 2724-2735.

Bergink, S., Salomons, F.A., Hoogstraten, D., Groothuis, T.A., de Waard, H., Wu, J., Yuan, L., Citterio, E., Houtsmuller, A.B., Neefjes, J.*, et al.* (2006). DNA damage triggers nucleotide excision repair-dependent monoubiquitylation of histone H2A. Genes Dev *20*, 1343-1352.

Bienko, M., Green, C.M., Crosetto, N., Rudolf, F., Zapart, G., Coull, B., Kannouche, P., Wider, G., Peter, M., Lehmann, A.R.*, et al.* (2005). Ubiquitin-binding domains in Y-family polymerases regulate translesion synthesis. Science *310*, 1821-1824.

Bottomley, M.J. (2004). Structures of protein domains that create or recognize histone modifications. EMBO Rep *5*, 464-469.

Braberg, H., Jin, H., Moehle, E.A., Chan, Y.A., Wang, S., Shales, M., Benschop, J.J., Morris, J.H., Qiu, C., Hu, F.*, et al.* (2013). From structure to systems: high-resolution, quantitative genetic analysis of RNA polymerase II. Cell *154*, 775-788.

Cao, R., Tsukada, Y., and Zhang, Y. (2005). Role of Bmi-1 and Ring1A in H2A ubiquitylation and Hox gene silencing. Mol Cell *20*, 845-854.

Carlile, C.M., Pickart, C.M., Matunis, M.J., and Cohen, R.E. (2009). Synthesis of free and proliferating cell nuclear antigen-bound polyubiquitin chains by the RING E3 ubiquitin ligase Rad5. J Biol Chem *284*, 29326-29334.

Chandrasekharan, M.B., Huang, F., and Sun, Z.W. (2009). Ubiquitination of histone H2B regulates chromatin dynamics by enhancing nucleosome stability. Proc Natl Acad Sci U S A *106*, 16686-16691.

Chen, A., Kleiman, F.E., Manley, J.L., Ouchi, T., and Pan, Z.Q. (2002). Autoubiquitination of the BRCA1*BARD1 RING ubiquitin ligase. J Biol Chem *277*, 22085-22092.

Chen, J.J., Tsu, C.A., Gavin, J.M., Milhollen, M.A., Bruzzese, F.J., Mallender, W.D., Sintchak, M.D., Bump, N.J., Yang, X., Ma, J.*, et al.* (2011). Mechanistic studies of substrate-assisted inhibition of ubiquitin-activating enzyme by adenosine sulfamate analogues. J Biol Chem *286*, 40867-40877.

Chen, M., and Manley, J.L. (2009). Mechanisms of alternative splicing regulation: insights from molecular and genomics approaches. Nature reviews. Molecular cell biology *10*, 741-754.

Clague, M.J., Coulson, J.M., and Urbe, S. (2012). Cellular functions of the DUBs. J Cell Sci *125*, 277-286.

Daniel, J.A., Torok, M.S., Sun, Z.W., Schieltz, D., Allis, C.D., Yates, J.R., 3rd, and Grant, P.A. (2004). Deubiquitination of histone H2B by a yeast acetyltransferase complex regulates transcription. J Biol Chem *279*, 1867-1871.

de Almeida, S.F., and Carmo-Fonseca, M. (2012). Design principles of interconnections between chromatin and pre-mRNA splicing. Trends Biochem Sci *37*, 248-253.

de la Mata, M., Alonso, C.R., Kadener, S., Fededa, J.P., Blaustein, M., Pelisch, F., Cramer, P., Bentley, D., and Kornblihtt, A.R. (2003). A slow RNA polymerase II affects alternative splicing in vivo. Mol Cell *12*, 525-532.

Dechassa, M.L., Wyns, K., Li, M., Hall, M.A., Wang, M.D., and Luger, K. (2011). Structure and Scm3-mediated assembly of budding yeast centromeric nucleosomes. Nature communications *2*, 313.

Dhalluin, C., Carlson, J.E., Zeng, L., He, C., Aggarwal, A.K., and Zhou, M.M. (1999). Structure and ligand of a histone acetyltransferase bromodomain. Nature *399*, 491-496.

Dhami, P., Saffrey, P., Bruce, A.W., Dillon, S.C., Chiang, K., Bonhoure, N., Koch, C.M., Bye, J., James, K., Foad, N.S.*, et al.* (2010). Complex exon-intron marking by histone modifications is not determined solely by nucleosome distribution. PLoS One *5*, e12339.

Dyer, P.N., Edayathumangalam, R.S., White, C.L., Bao, Y., Chakravarthy, S., Muthurajan, U.M., and Luger, K. (2004). Reconstitution of nucleosome core particles from recombinant histones and DNA. Methods Enzymol *375*, 23-44.

Eichhorn, P.J., Rodon, L., Gonzalez-Junca, A., Dirac, A., Gili, M., Martinez-Saez, E., Aura, C., Barba, I., Peg, V., Prat, A.*, et al.* (2012a). USP15 stabilizes TGF-beta receptor I and promotes oncogenesis through the activation of TGF-beta signaling in glioblastoma. Nat Med.

Eichhorn, P.J., Rodon, L., Gonzalez-Junca, A., Dirac, A., Gili, M., Martinez-Saez, E., Aura, C., Barba, I., Peg, V., Prat, A.*, et al.* (2012b). USP15 stabilizes TGF-beta receptor I and promotes oncogenesis through the activation of TGF-beta signaling in glioblastoma. Nat Med *18*, 429-435.

Eletr, Z.M., and Wilkinson, K.D. (2014). Regulation of proteolysis by human deubiquitinating enzymes. Biochim Biophys Acta *1843*, 114-128.

Elliott, P.R., Liu, H., Pastok, M.W., Grossmann, G.J., Rigden, D.J., Clague, M.J., Urbe, S., and Barsukov, I.L. (2011). Structural variability of the ubiquitin specific protease DUSP-UBL double domains. FEBS Lett *585*, 3385-3390.

Elsasser, S.J., and D'Arcy, S. (2012). Towards a mechanism for histone chaperones. Biochim Biophys Acta *1819*, 211-221.

Emre, N.C., Ingvarsdottir, K., Wyce, A., Wood, A., Krogan, N.J., Henry, K.W., Li, K., Marmorstein, R., Greenblatt, J.F., Shilatifard, A.*, et al.* (2005). Maintenance of low histone

ubiquitylation by Ubp10 correlates with telomere-proximal Sir2 association and gene silencing. Mol Cell *17*, 585-594.

Fang, J., Chen, T., Chadwick, B., Li, E., and Zhang, Y. (2004). Ring1b-mediated H2A ubiquitination associates with inactive X chromosomes and is involved in initiation of X inactivation. J Biol Chem *279*, 52812-52815.

Faronato, M., Patel, V., Darling, S., Dearden, L., Clague, M.J., Urbe, S., and Coulson, J.M. (2013). The deubiquitylase USP15 stabilizes newly synthesized REST and rescues its expression at mitotic exit. Cell Cycle *12*, 1964-1977.

Fierz, B., Chatterjee, C., McGinty, R.K., Bar-Dagan, M., Raleigh, D.P., and Muir, T.W. (2010). Histone H2B ubiquitylation disrupts local and higher-order chromatin compaction. Nat Chem Biol *7*, 113-119.

Fierz, B., Kilic, S., Hieb, A.R., Luger, K., and Muir, T.W. (2012a). Stability of nucleosomes containing homogenously ubiquitylated H2A and H2B prepared using semisynthesis. Journal of the American Chemical Society *134*, 19548-19551.

Fierz, B., Kilic, S., Hieb, A.R., Luger, K., and Muir, T.W. (2012b). Stability of nucleosomes containing homogenously ubiquitylated H2A and H2B prepared using semisynthesis. J Am Chem Soc *134*, 19548-19551.

Fleming, A.B., Kao, C.F., Hillyer, C., Pikaart, M., and Osley, M.A. (2008). H2B ubiquitylation plays a role in nucleosome dynamics during transcription elongation. Mol Cell *31*, 57-66.

Frappier, L., and Verrijzer, C.P. (2011). Gene expression control by protein deubiquitinases. Curr Opin Genet Dev *21*, 207-213.

Fuchs, G., Shema, E., Vesterman, R., Kotler, E., Wolchinsky, Z., Wilder, S., Golomb, L., Pribluda, A., Zhang, F., Haj-Yahya, M.*, et al.* (2012). RNF20 and USP44 regulate stem cell differentiation by modulating H2B monoubiquitylation. Mol Cell *46*, 662-673.

Gatti, M., Pinato, S., Maspero, E., Soffientini, P., Polo, S., and Penengo, L. (2012). A novel ubiquitin mark at the N-terminal tail of histone H2As targeted by RNF168 ubiquitin ligase. Cell Cycle *11*, 2538-2544.

Gearhart, M.D., Corcoran, C.M., Wamstad, J.A., and Bardwell, V.J. (2006). Polycomb group and SCF ubiquitin ligases are found in a novel BCOR complex that is recruited to BCL6 targets. Mol Cell Biol *26*, 6880-6889.

Ghetti, A., Company, M., and Abelson, J. (1995). Specificity of Prp24 binding to RNA: a role for Prp24 in the dynamic interaction of U4 and U6 snRNAs. Rna *1*, 132-145.

Goldknopf, I.L., Taylor, C.W., Baum, R.M., Yeoman, L.C., Olson, M.O., Prestayko, A.W., and Busch, H. (1975). Isolation and characterization of protein A24, a "histone-like" non-histone chromosomal protein. J Biol Chem *250*, 7182-7187.

Gunderson, F.Q., and Johnson, T.L. (2009). Acetylation by the transcriptional coactivator Gcn5 plays a novel role in co-transcriptional spliceosome assembly. PLoS Genet *5*, e1000682.

Haj-Yahya, M., Eltarteer, N., Ohayon, S., Shema, E., Kotler, E., Oren, M., and Brik, A. (2012). N-methylation of isopeptide bond as a strategy to resist deubiquitinases. Angew Chem Int Ed Engl *51*, 11535-11539.

Harper, S., Besong, T.M., Emsley, J., Scott, D.J., and Dreveny, I. (2011). Structure of the USP15 N-terminal domains: a beta-hairpin mediates close association between the DUSP and UBL domains. Biochemistry *50*, 7995-8004.

Harper, S., Gratton, H.E., Cornaciu, I., Oberer, M., Scott, D.J., Emsley, J., and Dreveny, I. (2014). Structure and catalytic regulatory function of ubiquitin specific protease 11 N-terminal and ubiquitin-like domains. Biochemistry.

Hatch, C.L., Bonner, W.M., and Moudrianakis, E.N. (1983). Minor histone 2A variants and ubiquinated forms in the native H2A:H2B dimer. Science *221*, 468-470.

Hayes, S.D., Liu, H., MacDonald, E., Sanderson, C.M., Coulson, J.M., Clague, M.J., and Urbe, S. (2012). Direct and indirect control of mitogen-activated protein kinase pathway-associated components, BRAP/IMP E3 ubiquitin ligase and CRAF/RAF1 kinase, by the deubiquitylating enzyme USP15. J Biol Chem *287*, 43007-43018.

Henry, K.W., Wyce, A., Lo, W.S., Duggan, L.J., Emre, N.C., Kao, C.F., Pillus, L., Shilatifard, A., Osley, M.A., and Berger, S.L. (2003). Transcriptional activation via sequential histone H2B ubiquitylation and deubiquitylation, mediated by SAGA-associated Ubp8. Genes Dev *17*, 2648-2663.

Herissant, L., Moehle, E.A., Bertaccini, D., Van Dorsselaer, A., Schaeffer-Reiss, C., Guthrie, C., and Dargemont, C. (2014). H2B Ubiquitylation Modulates Spliceosome Assembly and Function in Budding Yeast. Biology of the cell / under the auspices of the European Cell Biology Organization.

Hetfeld, B.K., Helfrich, A., Kapelari, B., Scheel, H., Hofmann, K., Guterman, A., Glickman, M., Schade, R., Kloetzel, P.M., and Dubiel, W. (2005). The zinc finger of the CSN-associated deubiquitinating enzyme USP15 is essential to rescue the E3 ligase Rbx1. Curr Biol *15*, 1217-1221.

Hong, L., Schroth, G.P., Matthews, H.R., Yau, P., and Bradbury, E.M. (1993). Studies of the DNA binding properties of histone H4 amino terminus. Thermal denaturation studies reveal that acetylation markedly reduces the binding constant of the H4 "tail" to DNA. J Biol Chem *268*, 305-314.

Hoppe, T. (2005). Multiubiquitylation by E4 enzymes: 'one size' doesn't fit all. Trends Biochem Sci *30*, 183-187.

Hu, M., Gu, L., Li, M., Jeffrey, P.D., Gu, W., and Shi, Y. (2006). Structural basis of competitive recognition of p53 and MDM2 by HAUSP/USP7: implications for the regulation of the p53-MDM2 pathway. PLoS Biol *4*, e27.

Inui, M., Manfrin, A., Mamidi, A., Martello, G., Morsut, L., Soligo, S., Enzo, E., Moro, S., Polo, S., Dupont, S.*, et al.* (2011). USP15 is a deubiquitylating enzyme for receptor-activated SMADs. Nat Cell Biol *13*, 1368-1375.

Jacobs, S.A., and Khorasanizadeh, S. (2002). Structure of HP1 chromodomain bound to a lysine 9-methylated histone H3 tail. Science *295*, 2080-2083.

Jason, L.J., Finn, R.M., Lindsey, G., and Ausio, J. (2005). Histone H2A ubiquitination does not preclude histone H1 binding, but it facilitates its association with the nucleosome. J Biol Chem *280*, 4975-4982.

Joo, H.Y., Jones, A., Yang, C., Zhai, L., Smith, A.D.t., Zhang, Z., Chandrasekharan, M.B., Sun, Z.W., Renfrow, M.B., Wang, Y.*, et al.* (2011). Regulation of histone H2A and H2B deubiquitination and Xenopus development by USP12 and USP46. J Biol Chem *286*, 7190-7201.

Joo, H.Y., Zhai, L., Yang, C., Nie, S., Erdjument-Bromage, H., Tempst, P., Chang, C., and Wang, H. (2007). Regulation of cell cycle progression and gene expression by H2A deubiquitination. Nature *449*, 1068-1072.

Jung, I., Kim, S.K., Kim, M., Han, Y.M., Kim, Y.S., Kim, D., and Lee, D. (2012). H2B monoubiquitylation is a 5'-enriched active transcription mark and correlates with exon-intron structure in human cells. Genome Res *22*, 1026-1035.

Kanno, T., Kanno, Y., Siegel, R.M., Jang, M.K., Lenardo, M.J., and Ozato, K. (2004). Selective recognition of acetylated histones by bromodomain proteins visualized in living cells. Mol Cell *13*, 33-43.

Kao, C.F., Hillyer, C., Tsukuda, T., Henry, K., Berger, S., and Osley, M.A. (2004). Rad6 plays a role in transcriptional activation through ubiquitylation of histone H2B. Genes Dev *18*, 184-195.

Kaplan, C.D., Laprade, L., and Winston, F. (2003). Transcription elongation factors repress transcription initiation from cryptic sites. Science *301*, 1096-1099.

Kim, J., Guermah, M., McGinty, R.K., Lee, J.S., Tang, Z., Milne, T.A., Shilatifard, A., Muir, T.W., and Roeder, R.G. (2009). RAD6-Mediated transcription-coupled H2B ubiquitylation directly stimulates H3K4 methylation in human cells. Cell *137*, 459-471.

Kim, J., Hake, S.B., and Roeder, R.G. (2005). The human homolog of yeast BRE1 functions as a transcriptional coactivator through direct activator interactions. Mol Cell *20*, 759-770.

Kim, J., and Roeder, R.G. (2009). Direct Bre1-Paf1 complex interactions and RING finger-independent Bre1-Rad6 interactions mediate histone H2B ubiquitylation in yeast. J Biol Chem *284*, 20582-20592.

Kim, J., and Roeder, R.G. (2011). Nucleosomal H2B ubiquitylation with purified factors. Methods *54*, 331-338.

Kim, W., Bennett, E.J., Huttlin, E.L., Guo, A., Li, J., Possemato, A., Sowa, M.E., Rad, R., Rush, J., Comb, M.J., *et al.* (2011). Systematic and quantitative assessment of the ubiquitin-modified proteome. Mol Cell *44*, 325-340.

Kohler, A., Schneider, M., Cabal, G.G., Nehrbass, U., and Hurt, E. (2008). Yeast Ataxin-7 links histone deubiquitination with gene gating and mRNA export. Nat Cell Biol *10*, 707-715.

Kohler, A., Zimmerman, E., Schneider, M., Hurt, E., and Zheng, N. (2010). Structural basis for assembly and activation of the heterotetrameric SAGA histone H2B deubiquitinase module. Cell *141*, 606-617.

Kouzarides, T. (2007). Chromatin modifications and their function. Cell *128*, 693-705.

Kress, T.L., Krogan, N.J., and Guthrie, C. (2008). A single SR-like protein, Npl3, promotes pre-mRNA splicing in budding yeast. Mol Cell *32*, 727-734.

Kumar, K.S., Spasser, L., Ohayon, S., Erlich, L.A., and Brik, A. (2011). Expeditious chemical synthesis of ubiquitinated peptides employing orthogonal protection and native chemical ligation. Bioconjugate chemistry *22*, 137-143.

Lang, G., Bonnet, J., Umlauf, D., Karmodiya, K., Koffler, J., Stierle, M., Devys, D., and Tora, L. (2011). The tightly controlled deubiquitination activity of the human SAGA complex differentially modifies distinct gene regulatory elements. Mol Cell Biol *31*, 3734-3744.

Laribee, R.N., Krogan, N.J., Xiao, T., Shibata, Y., Hughes, T.R., Greenblatt, J.F., and Strahl, B.D. (2005). BUR kinase selectively regulates H3 K4 trimethylation and H2B ubiquitylation through recruitment of the PAF elongation complex. Curr Biol *15*, 1487-1493.

Lee, J.S., Garrett, A.S., Yen, K., Takahashi, Y.H., Hu, D., Jackson, J., Seidel, C., Pugh, B.F., and Shilatifard, A. (2012). Codependency of H2B monoubiquitination and nucleosome reassembly on Chd1. Genes Dev *26*, 914-919.

Lee, J.S., Shukla, A., Schneider, J., Swanson, S.K., Washburn, M.P., Florens, L., Bhaumik, S.R., and Shilatifard, A. (2007). Histone crosstalk between H2B monoubiquitination and H3 methylation mediated by COMPASS. Cell *131*, 1084-1096.

Lee, K.K., Florens, L., Swanson, S.K., Washburn, M.P., and Workman, J.L. (2005). The deubiquitylation activity of Ubp8 is dependent upon Sgf11 and its association with the SAGA complex. Mol Cell Biol *25*, 1173-1182.

Li, M., Brooks, C.L., Kon, N., and Gu, W. (2004). A dynamic role of HAUSP in the p53-Mdm2 pathway. Mol Cell *13*, 879-886.

Lin, S., Coutinho-Mansfield, G., Wang, D., Pandit, S., and Fu, X.D. (2008). The splicing factor SC35 has an active role in transcriptional elongation. Nature structural & molecular biology *15*, 819-826.

Liu, Y., Timani, K., Mantel, C., Fan, Y., Hangoc, G., Cooper, S., He, J.J., and Broxmeyer, H.E. (2011). TIP110/p110nrb/SART3/p110 regulation of hematopoiesis through CMYC. Blood *117*, 5643-5651.

Liu, Y., Timani, K., Ou, X., Broxmeyer, H.E., and He, J.J. (2013). C-MYC controlled TIP110 protein expression regulates OCT4 mRNA splicing in human embryonic stem cells. Stem cells and development *22*, 689-694.

Long, L., Thelen, J.P., Furgason, M., Haj-Yahya, M., Brik, A., Cheng, D., Peng, J., and Yao, T. (2014). The U4/U6 Recycling Factor SART3 Has Histone Chaperone Activity and Associates with USP15 to Regulate H2B Deubiquitination. J Biol Chem *289*, 8916-8930.

Loomis, R.J., Naoe, Y., Parker, J.B., Savic, V., Bozovsky, M.R., Macfarlan, T., Manley, J.L., and Chakravarti, D. (2009). Chromatin binding of SRp20 and ASF/SF2 and dissociation from mitotic chromosomes is modulated by histone H3 serine 10 phosphorylation. Mol Cell *33*, 450-461.

Luco, R.F., Allo, M., Schor, I.E., Kornblihtt, A.R., and Misteli, T. (2011). Epigenetics in alternative pre-mRNA splicing. Cell *144*, 16-26.

Luco, R.F., Pan, Q., Tominaga, K., Blencowe, B.J., Pereira-Smith, O.M., and Misteli, T. (2010). Regulation of alternative splicing by histone modifications. Science *327*, 996-1000.

Luger, K., Mader, A.W., Richmond, R.K., Sargent, D.F., and Richmond, T.J. (1997). Crystal structure of the nucleosome core particle at 2.8 A resolution. Nature *389*, 251-260.

Lusser, A., and Kadonaga, J.T. (2004). Strategies for the reconstitution of chromatin. Nature methods *1*, 19-26.

Mattiroli, F., Vissers, J.H., van Dijk, W.J., Ikpa, P., Citterio, E., Vermeulen, W., Marteijn, J.A., and Sixma, T.K. (2012). RNF168 ubiquitinates K13-15 on H2A/H2AX to drive DNA damage signaling. Cell *150*, 1182-1195.

McBryant, S.J., Lu, X., and Hansen, J.C. (2010). Multifunctionality of the linker histones: an emerging role for protein-protein interactions. Cell research *20*, 519-528.

McBryant, S.J., Park, Y.J., Abernathy, S.M., Laybourn, P.J., Nyborg, J.K., and Luger, K. (2003). Preferential binding of the histone (H3-H4)2 tetramer by NAP1 is mediated by the amino-terminal histone tails. J Biol Chem *278*, 44574-44583.

McCracken, S., Fong, N., Yankulov, K., Ballantyne, S., Pan, G., Greenblatt, J., Patterson, S.D., Wickens, M., and Bentley, D.L. (1997). The C-terminal domain of RNA polymerase II couples mRNA processing to transcription. Nature *385*, 357-361.

McGinty, R.K., Kim, J., Chatterjee, C., Roeder, R.G., and Muir, T.W. (2008). Chemically ubiquitylated histone H2B stimulates hDot1L-mediated intranucleosomal methylation. Nature *453*, 812-816.

Medenbach, J., Schreiner, S., Liu, S., Luhrmann, R., and Bindereif, A. (2004). Human U4/U6 snRNP recycling factor p110: mutational analysis reveals the function of the tetratricopeptide repeat domain in recycling. Mol Cell Biol *24*, 7392-7401.

Meulmeester, E., Maurice, M.M., Boutell, C., Teunisse, A.F., Ovaa, H., Abraham, T.E., Dirks, R.W., and Jochemsen, A.G. (2005). Loss of HAUSP-mediated deubiquitination contributes to DNA damage-induced destabilization of Hdmx and Hdm2. Mol Cell *18*, 565-576.

Minsky, N., and Oren, M. (2004). The RING domain of Mdm2 mediates histone ubiquitylation and transcriptional repression. Mol Cell *16*, 631-639.

Minsky, N., Shema, E., Field, Y., Schuster, M., Segal, E., and Oren, M. (2008). Monoubiquitinated H2B is associated with the transcribed region of highly expressed genes in human cells. Nat Cell Biol *10*, 483-488.

Misteli, T., and Spector, D.L. (1999). RNA polymerase II targets pre-mRNA splicing factors to transcription sites in vivo. Mol Cell *3*, 697-705.

Moehle, E.A., Ryan, C.J., Krogan, N.J., Kress, T.L., and Guthrie, C. (2012). The yeast SR-like protein Npl3 links chromatin modification to mRNA processing. PLoS Genet *8*, e1003101.

Mosbech, A., Lukas, C., Bekker-Jensen, S., and Mailand, N. (2013). The deubiquitylating enzyme USP44 counteracts the DNA double-strand break response mediated by the RNF8 and RNF168 ubiquitin ligases. J Biol Chem *288*, 16579-16587.

Moyal, L., Lerenthal, Y., Gana-Weisz, M., Mass, G., So, S., Wang, S.Y., Eppink, B., Chung, Y.M., Shalev, G., Shema, E.*, et al.* (2011). Requirement of ATM-dependent monoubiquitylation of histone H2B for timely repair of DNA double-strand breaks. Mol Cell *41*, 529-542.

Nakagawa, T., Kajitani, T., Togo, S., Masuko, N., Ohdan, H., Hishikawa, Y., Koji, T., Matsuyama, T., Ikura, T., Muramatsu, M.*, et al.* (2008). Deubiquitylation of histone H2A activates transcriptional initiation via trans-histone cross-talk with H3K4 di- and trimethylation. Genes Dev *22*, 37-49.

Nakamura, K., Kato, A., Kobayashi, J., Yanagihara, H., Sakamoto, S., Oliveira, D.V., Shimada, M., Tauchi, H., Suzuki, H., Tashiro, S.*, et al.* (2011). Regulation of homologous recombination by RNF20-dependent H2B ubiquitination. Mol Cell *41*, 515-528.

Narita, T., Yung, T.M., Yamamoto, J., Tsuboi, Y., Tanabe, H., Tanaka, K., Yamaguchi, Y., and Handa, H. (2007). NELF interacts with CBC and participates in 3' end processing of replication-dependent histone mRNAs. Mol Cell *26*, 349-365.

Nathan, D., Ingvarsdottir, K., Sterner, D.E., Bylebyl, G.R., Dokmanovic, M., Dorsey, J.A., Whelan, K.A., Krsmanovic, M., Lane, W.S., Meluh, P.B.*, et al.* (2006). Histone sumoylation is a negative regulator in Saccharomyces cerevisiae and shows dynamic interplay with positive-acting histone modifications. Genes Dev *20*, 966-976.

Ng, H.H., Xu, R.M., Zhang, Y., and Struhl, K. (2002). Ubiquitination of histone H2B by Rad6 is required for efficient Dot1-mediated methylation of histone H3 lysine 79. J Biol Chem *277*, 34655-34657.

Nicassio, F., Corrado, N., Vissers, J.H., Areces, L.B., Bergink, S., Marteijn, J.A., Geverts, B., Houtsmuller, A.B., Vermeulen, W., Di Fiore, P.P.*, et al.* (2007). Human USP3 is a chromatin modifier required for S phase progression and genome stability. Curr Biol *17*, 1972-1977.

Nielsen, P.R., Nietlispach, D., Mott, H.R., Callaghan, J., Bannister, A., Kouzarides, T., Murzin, A.G., Murzina, N.V., and Laue, E.D. (2002). Structure of the HP1 chromodomain bound to histone H3 methylated at lysine 9. Nature *416*, 103-107.

Novotny, I., Blazikova, M., Stanek, D., Herman, P., and Malinsky, J. (2011). In vivo kinetics of U4/U6.U5 tri-snRNP formation in Cajal bodies. Mol Biol Cell *22*, 513-523.

Ong, S.E., and Mann, M. (2006). A practical recipe for stable isotope labeling by amino acids in cell culture (SILAC). Nature protocols *1*, 2650-2660.

Orphanides, G., Wu, W.H., Lane, W.S., Hampsey, M., and Reinberg, D. (1999). The chromatin-specific transcription elongation factor FACT comprises human SPT16 and SSRP1 proteins. Nature *400*, 284-288.

Osley, M.A. (2006). Regulation of histone H2A and H2B ubiquitylation. Brief Funct Genomic Proteomic *5*, 179-189.

Pandya-Jones, A., and Black, D.L. (2009). Co-transcriptional splicing of constitutive and alternative exons. Rna *15*, 1896-1908.

Patel, D.J., and Wang, Z. (2013). Readout of epigenetic modifications. Annu Rev Biochem *82*, 81-118.

Pauli, E.K., Chan, Y.K., Davis, M.E., Gableske, S., Wang, M.K., Feister, K.F., and Gack, M.U. (2014). The ubiquitin-specific protease USP15 promotes RIG-I-mediated antiviral signaling by deubiquitylating TRIM25. Science signaling *7*, ra3.

Pavri, R., Zhu, B., Li, G., Trojer, P., Mandal, S., Shilatifard, A., and Reinberg, D. (2006). Histone H2B monoubiquitination functions cooperatively with FACT to regulate elongation by RNA polymerase II. Cell *125*, 703-717.

Pham, A.D., and Sauer, F. (2000). Ubiquitin-activating/conjugating activity of TAFII250, a mediator of activation of gene expression in Drosophila. Science *289*, 2357-2360.

Piacentini, L., Fanti, L., Negri, R., Del Vescovo, V., Fatica, A., Altieri, F., and Pimpinelli, S. (2009). Heterochromatin protein 1 (HP1a) positively regulates euchromatic gene expression through RNA transcript association and interaction with hnRNPs in Drosophila. PLoS Genet *5*, e1000670.

Pickart, C.M., and Eddins, M.J. (2004). Ubiquitin: structures, functions, mechanisms. Biochim Biophys Acta *1695*, 55-72.

Pinder, J.B., Attwood, K.M., and Dellaire, G. (2013). Reading, writing, and repair: the role of ubiquitin and the ubiquitin-like proteins in DNA damage signaling and repair. Frontiers in genetics *4*, 45.

Pirngruber, J., Shchebet, A., and Johnsen, S.A. (2009a). Insights into the function of the human P-TEFb component CDK9 in the regulation of chromatin modifications and co-transcriptional mRNA processing. Cell Cycle *8*, 3636-3642.

Pirngruber, J., Shchebet, A., Schreiber, L., Shema, E., Minsky, N., Chapman, R.D., Eick, D., Aylon, Y., Oren, M., and Johnsen, S.A. (2009b). CDK9 directs H2B monoubiquitination and controls replication-dependent histone mRNA 3'-end processing. EMBO Rep *10*, 894-900.

QIAGEN (2003). The QIAexpressionist, Vol Fifth Edition, 5th edn.

Rader, S.D., and Guthrie, C. (2002). A conserved Lsm-interaction motif in Prp24 required for efficient U4/U6 di-snRNP formation. Rna *8*, 1378-1392.

Raghunathan, P.L., and Guthrie, C. (1998). A spliceosomal recycling factor that reanneals U4 and U6 small nuclear ribonucleoprotein particles. Science *279*, 857-860.

Robzyk, K., Recht, J., and Osley, M.A. (2000). Rad6-dependent ubiquitination of histone H2B in yeast. Science *287*, 501-504.

Rodriguez-Navarro, S. (2009). Insights into SAGA function during gene expression. EMBO Rep *10*, 843-850.

Rogakou, E.P., Redon, C., Boon, C., Johnson, K., and Bonner, W.M. (2000). Rapid histone extraction for electrophoretic analysis. BioTechniques *28*, 38-40, 42, 46.

Ryu, K.Y., Baker, R.T., and Kopito, R.R. (2006). Ubiquitin-specific protease 2 as a tool for quantification of total ubiquitin levels in biological specimens. Analytical biochemistry *353*, 153-155.

Samara, N.L., Datta, A.B., Berndsen, C.E., Zhang, X., Yao, T., Cohen, R.E., and Wolberger, C. (2010). Structural insights into the assembly and function of the SAGA deubiquitinating module. Science *328*, 1025-1029.

Sanso, M., Lee, K.M., Viladevall, L., Jacques, P.E., Page, V., Nagy, S., Racine, A., St Amour, C.V., Zhang, C., Shokat, K.M*., et al.* (2012). A positive feedback loop links opposing functions of P-TEFb/Cdk9 and histone H2B ubiquitylation to regulate transcript elongation in fission yeast. PLoS Genet *8*, e1002822.

Sapra, A.K., Anko, M.L., Grishina, I., Lorenz, M., Pabis, M., Poser, I., Rollins, J., Weiland, E.M., and Neugebauer, K.M. (2009). SR protein family members display diverse activities in the formation of nascent and mature mRNPs in vivo. Mol Cell *34*, 179-190.

Scheuermann, J.C., de Ayala Alonso, A.G., Oktaba, K., Ly-Hartig, N., McGinty, R.K., Fraterman, S., Wilm, M., Muir, T.W., and Muller, J. (2010). Histone H2A deubiquitinase activity of the Polycomb repressive complex PR-DUB. Nature *465*, 243-247.

Schor, I.E., Lleres, D., Risso, G.J., Pawellek, A., Ule, J., Lamond, A.I., and Kornblihtt, A.R. (2012). Perturbation of chromatin structure globally affects localization and recruitment of splicing factors. PLoS One *7*, e48084.

Schwabish, M.A., and Struhl, K. (2004). Evidence for eviction and rapid deposition of histones upon transcriptional elongation by RNA polymerase II. Mol Cell Biol *24*, 10111-10117.

Schwartz, S., Meshorer, E., and Ast, G. (2009). Chromatin organization marks exon-intron structure. Nature structural & molecular biology *16*, 990-995.

Shanbhag, N.M., Rafalska-Metcalf, I.U., Balane-Bolivar, C., Janicki, S.M., and Greenberg, R.A. (2010). ATM-dependent chromatin changes silence transcription in cis to DNA double-strand breaks. Cell *141*, 970-981.

Shchebet, A., Karpiuk, O., Kremmer, E., Eick, D., and Johnsen, S.A. (2012). Phosphorylation by cyclin-dependent kinase-9 controls ubiquitin-conjugating enzyme-2A function. Cell Cycle *11*, 2122-2127.

Shema, E., Kim, J., Roeder, R.G., and Oren, M. (2011). RNF20 inhibits TFIIS-facilitated transcriptional elongation to suppress pro-oncogenic gene expression. Mol Cell *42*, 477-488.

Shema, E., Tirosh, I., Aylon, Y., Huang, J., Ye, C., Moskovits, N., Raver-Shapira, N., Minsky, N., Pirngruber, J., Tarcic, G*., et al.* (2008). The histone H2B-specific ubiquitin ligase RNF20/hBRE1 acts as a putative tumor suppressor through selective regulation of gene expression. Genes Dev *22*, 2664-2676.

Shema-Yaacoby, E., Nikolov, M., Haj-Yahya, M., Siman, P., Allemand, E., Yamaguchi, Y., Muchardt, C., Urlaub, H., Brik, A., Oren, M*., et al.* (2013). Systematic identification of proteins binding to chromatin-embedded ubiquitylated H2B reveals recruitment of SWI/SNF to regulate transcription. Cell reports *4*, 601-608.

Shieh, G.S., Pan, C.H., Wu, J.H., Sun, Y.J., Wang, C.C., Hsiao, W.C., Lin, C.Y., Tung, L., Chang, T.H., Fleming, A.B.*, et al.* (2011). H2B ubiquitylation is part of chromatin architecture that marks exon-intron structure in budding yeast. BMC Genomics *12*, 627.

Shiio, Y., and Eisenman, R.N. (2003). Histone sumoylation is associated with transcriptional repression. Proc Natl Acad Sci U S A *100*, 13225-13230.

Shukla, A., and Bhaumik, S.R. (2007). H2B-K123 ubiquitination stimulates RNAPII elongation independent of H3-K4 methylation. Biochem Biophys Res Commun *359*, 214-220.

Siman, P., Karthikeyan, S.V., Nikolov, M., Fischle, W., and Brik, A. (2013). Convergent chemical synthesis of histone H2B protein for the site-specific ubiquitination at Lys34. Angew Chem Int Ed Engl *52*, 8059-8063.

Sims, R.J., 3rd, Millhouse, S., Chen, C.F., Lewis, B.A., Erdjument-Bromage, H., Tempst, P., Manley, J.L., and Reinberg, D. (2007). Recognition of trimethylated histone H3 lysine 4 facilitates the recruitment of transcription postinitiation factors and pre-mRNA splicing. Mol Cell *28*, 665-676.

Soboleva, T.A., Jans, D.A., Johnson-Saliba, M., and Baker, R.T. (2005). Nuclear-cytoplasmic shuttling of the oncogenic mouse UNP/USP4 deubiquitylating enzyme. J Biol Chem *280*, 745-752.

Song, E.J., Werner, S.L., Neubauer, J., Stegmeier, F., Aspden, J., Rio, D., Harper, J.W., Elledge, S.J., Kirschner, M.W., and Rape, M. (2010). The Prp19 complex and the Usp4Sart3 deubiquitinating enzyme control reversible ubiquitination at the spliceosome. Genes Dev *24*, 1434-1447.

Sowa, M.E., Bennett, E.J., Gygi, S.P., and Harper, J.W. (2009). Defining the human deubiquitinating enzyme interaction landscape. Cell *138*, 389-403.

Spies, N., Nielsen, C.B., Padgett, R.A., and Burge, C.B. (2009). Biased chromatin signatures around polyadenylation sites and exons. Mol Cell *36*, 245-254.

Stanek, D., and Neugebauer, K.M. (2006). The Cajal body: a meeting place for spliceosomal snRNPs in the nuclear maze. Chromosoma *115*, 343-354.

Stanek, D., Rader, S.D., Klingauf, M., and Neugebauer, K.M. (2003). Targeting of U4/U6 small nuclear RNP assembly factor SART3/p110 to Cajal bodies. J Cell Biol *160*, 505-516.

Strahl, B.D., and Allis, C.D. (2000). The language of covalent histone modifications. Nature *403*, 41-45.

Sun, Z.W., and Allis, C.D. (2002). Ubiquitination of histone H2B regulates H3 methylation and gene silencing in yeast. Nature *418*, 104-108.

Tan, M., Luo, H., Lee, S., Jin, F., Yang, J.S., Montellier, E., Buchou, T., Cheng, Z., Rousseaux, S., Rajagopal, N.*, et al.* (2011). Identification of 67 histone marks and histone lysine crotonylation as a new type of histone modification. Cell *146*, 1016-1028.

Tilgner, H., Nikolaou, C., Althammer, S., Sammeth, M., Beato, M., Valcarcel, J., and Guigo, R. (2009). Nucleosome positioning as a determinant of exon recognition. Nature structural & molecular biology *16*, 996-1001.

Trujillo, K.M., and Osley, M.A. (2012). A role for H2B ubiquitylation in DNA replication. Mol Cell *48*, 734-746.

Turner, S.D., Ricci, A.R., Petropoulos, H., Genereaux, J., Skerjanc, I.S., and Brandl, C.J. (2002). The E2 ubiquitin conjugase Rad6 is required for the ArgR/Mcm1 repression of ARG1 transcription. Mol Cell Biol *22*, 4011-4019.

van der Knaap, J.A., Kumar, B.R., Moshkin, Y.M., Langenberg, K., Krijgsveld, J., Heck, A.J., Karch, F., and Verrijzer, C.P. (2005). GMP synthetase stimulates histone H2B deubiquitylation by the epigenetic silencer USP7. Mol Cell *17*, 695-707.

van der Veen, A.G., and Ploegh, H.L. (2012). Ubiquitin-like proteins. Annu Rev Biochem *81*, 323-357.

Ventii, K.H., and Wilkinson, K.D. (2008). Protein partners of deubiquitinating enzymes. The Biochemical journal *414*, 161-175.

Villeneuve, N.F., Tian, W., Wu, T., Sun, Z., Lau, A., Chapman, E., Fang, D., and Zhang, D.D. (2013). USP15 negatively regulates Nrf2 through deubiquitination of Keap1. Mol Cell *51*, 68-79.

Vitaliano-Prunier, A., Babour, A., Herissant, L., Apponi, L., Margaritis, T., Holstege, F.C., Corbett, A.H., Gwizdek, C., and Dargemont, C. (2012). H2B ubiquitylation controls the formation of export-competent mRNP. Mol Cell *45*, 132-139.

Wahl, M.C., Will, C.L., and Luhrmann, R. (2009). The spliceosome: design principles of a dynamic RNP machine. Cell *136*, 701-718.

Wang, H., Wang, L., Erdjument-Bromage, H., Vidal, M., Tempst, P., Jones, R.S., and Zhang, Y. (2004). Role of histone H2A ubiquitination in Polycomb silencing. Nature *431*, 873-878.

Weake, V.M., and Workman, J.L. (2008). Histone ubiquitination: triggering gene activity. Mol Cell *29*, 653-663.

Winkler, D.D., Muthurajan, U.M., Hieb, A.R., and Luger, K. (2011). Histone chaperone FACT coordinates nucleosome interaction through multiple synergistic binding events. J Biol Chem *286*, 41883-41892.

Wood, A., Krogan, N.J., Dover, J., Schneider, J., Heidt, J., Boateng, M.A., Dean, K., Golshani, A., Zhang, Y., Greenblatt, J.F*., et al.* (2003a). Bre1, an E3 ubiquitin ligase required for recruitment and substrate selection of Rad6 at a promoter. Mol Cell *11*, 267-274.

Wood, A., Schneider, J., Dover, J., Johnston, M., and Shilatifard, A. (2003b). The Paf1 complex is essential for histone monoubiquitination by the Rad6-Bre1 complex, which signals for histone methylation by COMPASS and Dot1p. J Biol Chem *278*, 34739-34742.

Wood, A., Schneider, J., Dover, J., Johnston, M., and Shilatifard, A. (2005). The Bur1/Bur2 complex is required for histone H2B monoubiquitination by Rad6/Bre1 and histone methylation by COMPASS. Mol Cell *20*, 589-599.

Wright, D.E., Wang, C.Y., and Kao, C.F. (2012). Histone ubiquitylation and chromatin dynamics. Frontiers in bioscience *17*, 1051-1078.

Wu, L., Zee, B.M., Wang, Y., Garcia, B.A., and Dou, Y. (2011). The RING finger protein MSL2 in the MOF complex is an E3 ubiquitin ligase for H2B K34 and is involved in crosstalk with H3 K4 and K79 methylation. Mol Cell *43*, 132-144.

Wu, R.S., Kohn, K.W., and Bonner, W.M. (1981). Metabolism of ubiquitinated histones. J Biol Chem *256*, 5916-5920.

Wunsch, A.M., Haas, A.L., and Lough, J. (1987). Synthesis and ubiquitination of histones during myogenesis. Dev Biol *119*, 85-93.

Wyce, A., Xiao, T., Whelan, K.A., Kosman, C., Walter, W., Eick, D., Hughes, T.R., Krogan, N.J., Strahl, B.D., and Berger, S.L. (2007). H2B ubiquitylation acts as a barrier to Ctk1 nucleosomal recruitment prior to removal by Ubp8 within a SAGA-related complex. Mol Cell *27*, 275-288.

Wyrick, J.J., Kyriss, M.N., and Davis, W.B. (2012). Ascending the nucleosome face: recognition and function of structured domains in the histone H2A-H2B dimer. Biochim Biophys Acta *1819*, 892-901.

Xiao, T., Kao, C.F., Krogan, N.J., Sun, Z.W., Greenblatt, J.F., Osley, M.A., and Strahl, B.D. (2005). Histone H2B ubiquitylation is associated with elongating RNA polymerase II. Mol Cell Biol *25*, 637-651.

Yao, T., Song, L., Jin, J., Cai, Y., Takahashi, H., Swanson, S.K., Washburn, M.P., Florens, L., Conaway, R.C., Cohen, R.E*., et al.* (2008). Distinct modes of regulation of the Uch37 deubiquitinating enzyme in the proteasome and in the Ino80 chromatin-remodeling complex. Mol Cell *31*, 909-917.

Yao, T., Song, L., Xu, W., DeMartino, G.N., Florens, L., Swanson, S.K., Washburn, M.P., Conaway, R.C., Conaway, J.W., and Cohen, R.E. (2006). Proteasome recruitment and activation of the Uch37 deubiquitinating enzyme by Adrm1. Nat Cell Biol *8*, 994-1002.

Ye, Y., and Rape, M. (2009). Building ubiquitin chains: E2 enzymes at work. Nature reviews. Molecular cell biology *10*, 755-764.

Yin, L., Krantz, B., Russell, N.S., Deshpande, S., and Wilkinson, K.D. (2000a). Nonhydrolyzable diubiquitin analogues are inhibitors of ubiquitin conjugation and deconjugation. Biochemistry *39*, 10001-10010.

Yin, L., Krantz, B., Russell, N.S., Deshpande, S., and Wilkinson, K.D. (2000b). Nonhydrolyzable diubiquitin analogues are inhibitors of ubiquitin conjugation and deconjugation. Biochemistry *39*, 10001-10010.

Zhang, X.Y., Varthi, M., Sykes, S.M., Phillips, C., Warzecha, C., Zhu, W., Wyce, A., Thorne, A.W., Berger, S.L., and McMahon, S.B. (2008). The putative cancer stem cell marker USP22 is a subunit of the human SAGA complex required for activated transcription and cell-cycle progression. Mol Cell *29*, 102-111.

Zhang, Z., Jones, A., Joo, H.Y., Zhou, D., Cao, Y., Chen, S., Erdjument-Bromage, H., Renfrow, M., He, H., Tempst, P.*, et al.* (2013). USP49 deubiquitinates histone H2B and regulates cotranscriptional pre-mRNA splicing. Genes Dev *27*, 1581-1595.

Zhao, W., Liu, Y., Timani, K.A., and He, J.J. (2014). Tip110 protein binds to unphosphorylated RNA polymerase II and promotes its phosphorylation and HIV-1 long terminal repeat transcription. J Biol Chem *289*, 190-202.

Zhao, Y., Lang, G., Ito, S., Bonnet, J., Metzger, E., Sawatsubashi, S., Suzuki, E., Le Guezennec, X., Stunnenberg, H.G., Krasnov, A.*, et al.* (2008). A TFTC/STAGA module mediates histone H2A and H2B deubiquitination, coactivates nuclear receptors, and counteracts heterochromatin silencing. Mol Cell *29*, 92-101.

Zhou, W., Zhu, P., Wang, J., Pascual, G., Ohgi, K.A., Lozach, J., Glass, C.K., and Rosenfeld, M.G. (2008). Histone H2A monoubiquitination represses transcription by inhibiting RNA polymerase II transcriptional elongation. Mol Cell *29*, 69-80.

Zhu, P., Zhou, W., Wang, J., Puc, J., Ohgi, K.A., Erdjument-Bromage, H., Tempst, P., Glass, C.K., and Rosenfeld, M.G. (2007). A histone H2A deubiquitinase complex coordinating histone acetylation and H1 dissociation in transcriptional regulation. Mol Cell *27*, 609-621.

Zhu, Q., Pao, G.M., Huynh, A.M., Suh, H., Tonnu, N., Nederlof, P.M., Gage, F.H., and Verma, I.M. (2011). BRCA1 tumour suppression occurs via heterochromatin-mediated silencing. Nature *477*, 179-184.

Zhu, Q., Wani, G., Arab, H.H., El-Mahdy, M.A., Ray, A., and Wani, A.A. (2009). Chromatin restoration following nucleotide excision repair involves the incorporation of ubiquitinated H2A at damaged genomic sites. DNA repair *8*, 262-273.

APPENDIX I: REGULATION OF H2B DEUBIQUITINATION IS UNRELATED TO SAGA^{DUB} EXPRESSION AND IS NOT CONTROLLED BY THE SPLICEOSOME

A1.1 The ubH2B increase observed in SART3-depleted cells is not caused by a reduction in SAGA^{DUB} transcript levels

Depletion of the U4/U6 spliceosome recycling factor, SART3, caused a dramatic increase in total ubH2B levels. Because splicing defects can affect transcription elongation rates, we proposed that the ubH2B increase observed in SART3-depleted cells could be a result of decreased transcript levels of a histone DUB. Our primary suspect was SAGA^{DUB} as this complex has been identified as a key regulator of Ub-histone levels during transcription (Lang et al., 2011). The human SAGA^{DUB} is comprised of 4 major proteins: Ataxin7, Ataxin7L3, Eny2, and Usp22. Depletion of Ataxin7L3 and Eny2 results in an increase in ubH2A and ubH2B levels (Figure A1.1A) (Lang et al., 2011). Notably, transfection of Usp22-targeted RNAi resulted in decreased Usp22 transcript levels, but a corresponding reduction in Usp22 protein levels was not observed. These results suggest the Usp22 protein is has a long half-life and the protein level is therefore unaffected after 72 hours of RNAi treatment (Figure A1.1B-C). Not surprisingly, transfection of Usp22 RNAi had no effect on global ubH2A or ubH2B levels (Figure A1.1C).

We observed that depletion of SART3 using different siRNAs (#1 and #2) at various concentrations resulted in varying degrees of SART3 depletion at both the RNA and protein levels where SART3 #2 (high) > SART3 #2 (low) > SART3 #1 (high) (Figure 3.12C and Figure A1.1D). Changes in ubH2B levels also corresponded to the degree of SART3 knockdown in that more efficient depletion of SART3 was accompanied by a greater increase in ubH2B levels (Figure 3.12C). Using these tools to generate varying degrees of

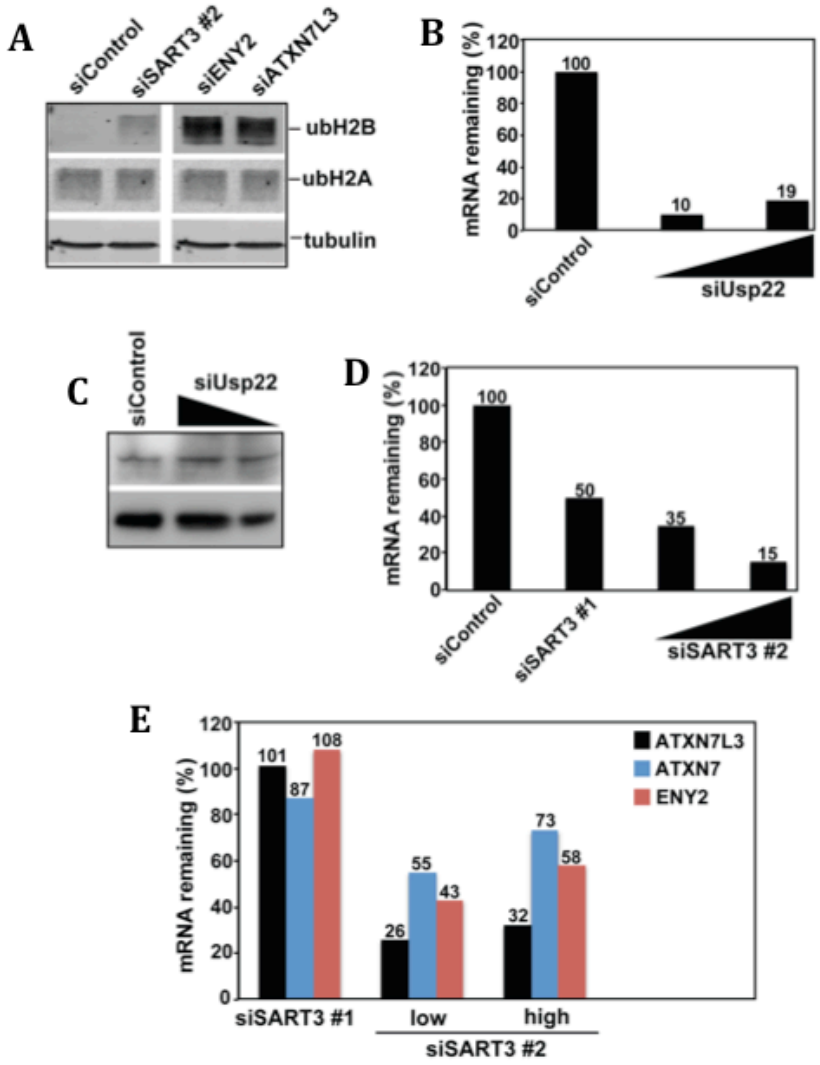

Figure A1.1. The ubH2B increase observed in SART3-depleted cells is not caused by a reduction in SAGA^{DUB} transcript levels. (A) Depletion of SAGA^{DUB} components increases ubH2B levels. SART3, Eny2, and Ataxin7L3 were depleted from HeLa cells by siRNA and proteins were visualized by immunoblotting as described in Figure 3.12A. Slices of immunoblots that came from the same gel are boxed together. **(B)** Transfection of Usp22 RNAi reduces Usp22 transcript levels. Usp22 was depleted from cells by siRNA as described in Figure 3.12B. 72 h post transfection, total RNA was extracted from these cells, reverse transcribed, and mRNA levels of Usp22 was determined by quantitative real-time PCR (qRT-PCR). **(C)** Depletion of Usp22 transcripts does not decrease Usp22 protein levels. Usp22 was depleted from HeLa cells as described in (B). Proteins were visualized using antibodies specific to Usp22 or H2B. **(D-E)** SAGA^{DUB} transcript levels are independent of SART3 levels. SART3 was depleted from HeLa cells using two different SART3-specific siRNA oligos. SiControl and siSART3 #1 were transfected at a concentration of 6.6 nM. SiSART3 #2 was transfected at either low (3.3 nM) or high (6.6 nM) concentrations. Transcript levels of SART3, ATXN7, ATXN7L3, and ENY2 were measured using qRT-PCR. Transcript levels were normalized to GAPDH and the percent mRNA remaining was calculated relative to the siControl.

SART3 knockdown, we used quantitative real-time PCR to observe changes in transcript levels of SAGA^{DUB} components. We proposed that if ubH2B levels are regulated by components of SAGA^{DUB} in SART3-depleted cells, then as SART3 levels decrease, we would observe a corresponding decrease in transcript levels of Ataxin7 (ATXN7), Ataxin7L3 (ATXN7L3), and/or Eny2 (ENY2). (Usp22 was excluded from the analysis as a reduction in Usp22 transcript levels has no effect on ubH2B levels). Quantitative real-time PCR revealed the observed decrease transcript levels of SAGA^{DUB} components did not correspond to the magnitude of SART3 depletion (Figure A1.1E). This is most evident through a direct comparison between the SART3 #2 low and high samples. These observations are in accordance with another observation that SART3 depletion only causes and an increase in ubH2B levels while perturbation of SAGA^{DUB} affects both ubH2A and ubH2B levels (Figure 3.12A).

A1.2 SART3 does not regulate ubH2B levels through perturbation of snRNP levels

Because SART3 is a component of the spliceosome recycling machinery, we suggested that depletion of other splicing components might also increase ubH2B levels. We depleted several proteins associated with various snRNPs involved in spliceosome assembly (Figure A1.2A). Due to lack of antibody availability, we assessed the efficiency of depletion using quantitative real-time PCR (Figure A1.2B). Notably, depletion of some snRNP-associated proteins resulted in an overall reduction in GAPDH transcript levels. As GAPDH transcript levels were used for normalization, depletion efficiency of some proteins may not be accurately represented due to changes in GAPDH transcription or transcript stability (Figure A1.2B, see PRPF3 and Usp39). Western blotting showed that depletion of

A

Protein	Associated snRNP
PRPF3	U4/U6
PRPF6	U5
PRPF31	U4
PRPF19	modifies U4
SF3A3	U2
Usp39	U4/U6.U5

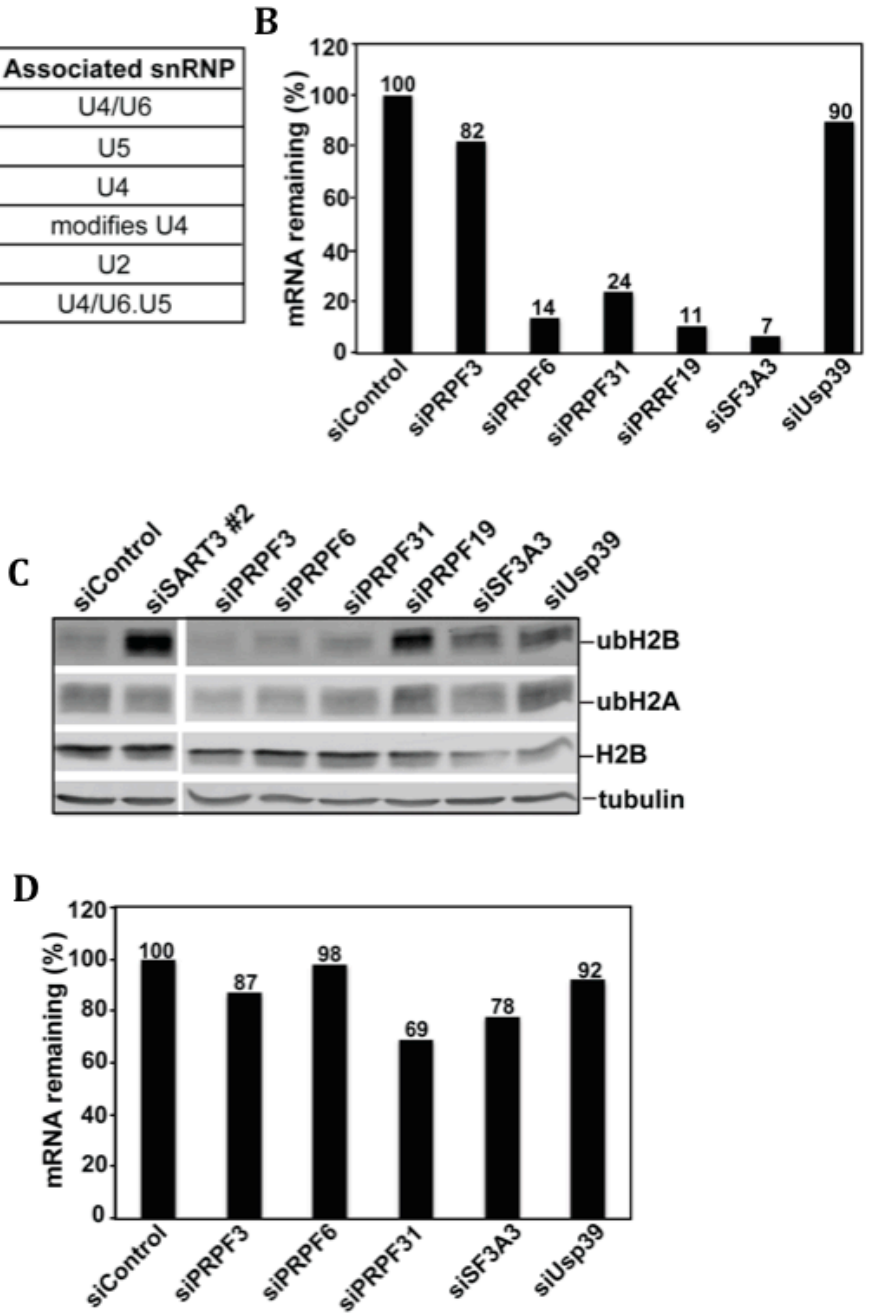

Figure A1.2. SART3 does not regulate ubH2B levels through perturbation of snRNP levels. (A) Table describing snRNP-associated protiens. **(B)** Knockdown efficiency of splicosome components. HeLa cells were depleted of snRNP-associated proteins using 3.3 nM siRNA. 72 hours post-transfection, RNA was extracted, reverse transcribed, and quantitated using real-time PCR. GAPDH transcript levels were used for normalization. **(C)** Depletion of some splicing factors affects ubH2B levels. Splicing factors were depleted as described in (B). Protein levels were monitored by immunoblotting as described in Figure 3.12A. **(D)** SART3 knockdown does not perturb transcript levels of many spliceosome components. Depletion of SART3 and quantitation of RNA was performed as described in (B).

PRPF19 and Usp39 increased ubH2B levels (Figure A1.2C). Unlike as was observed in SART3-depleted cells, this increase in ubH2B levels was also accompanied by an increase in ubH2A levels. Uniquely, SF3A3 depletion resulted in a mild increase in ubH2B levels, which was not complimented by a change in ubH2A levels. Because depletion of PRPF19, Usp39, and SF3A3 caused ubH2B levels to increase, we analyzed changes in transcript levels of these proteins in SART3 depleted cells. Notably, transcript levels of snRNP-associated proteins were only marginally affected by SART3 depletion (Figure A1.2D). These data indicate the mechanism of SART3-mediated regulation of ubH2B is predominantly independent of other spliceosome factors.

AI.3 SART3 depletion does not affect splicing of Usp49-regulated genes

Recent work showed depletion of a H2B histone DUB, Usp49, resulted in increased ubH2B levels and affected the splicing efficiency of a subset of genes (Zhang et al., 2013). We were curious to see if these Usp49-affected genes also displayed aberrant splicing patterns in SART3-depleted cells. We examined two genes RPS3 and RPS6, which displayed increased retention of the 4^{th} intron (5- and 7-fold, respectively) in Usp49-depleted cells. We found a mild increase in RPS3 intron levels and a slight decrease in RPS6 intron levels (2.53- vs. 0.82-fold, respectively) in SART3-depleted cells (Figure A1.3A). Additionally, we used primers spanning exon-exon junctions of exons 2 and 3 to monitor changes in the spliced products and found splicing efficiency of these genes was unaffected upon SART3 depletion (Figure A1.3B). Although our RNA-seq results revealed many differentially spliced genes in SART3-depleted cells, these data did not overlap with the splicing defects observed in Usp49-depleted cells. These data suggest the function of SART3 and Usp49 is exerted at a distinct, non-overlapping set of genes.

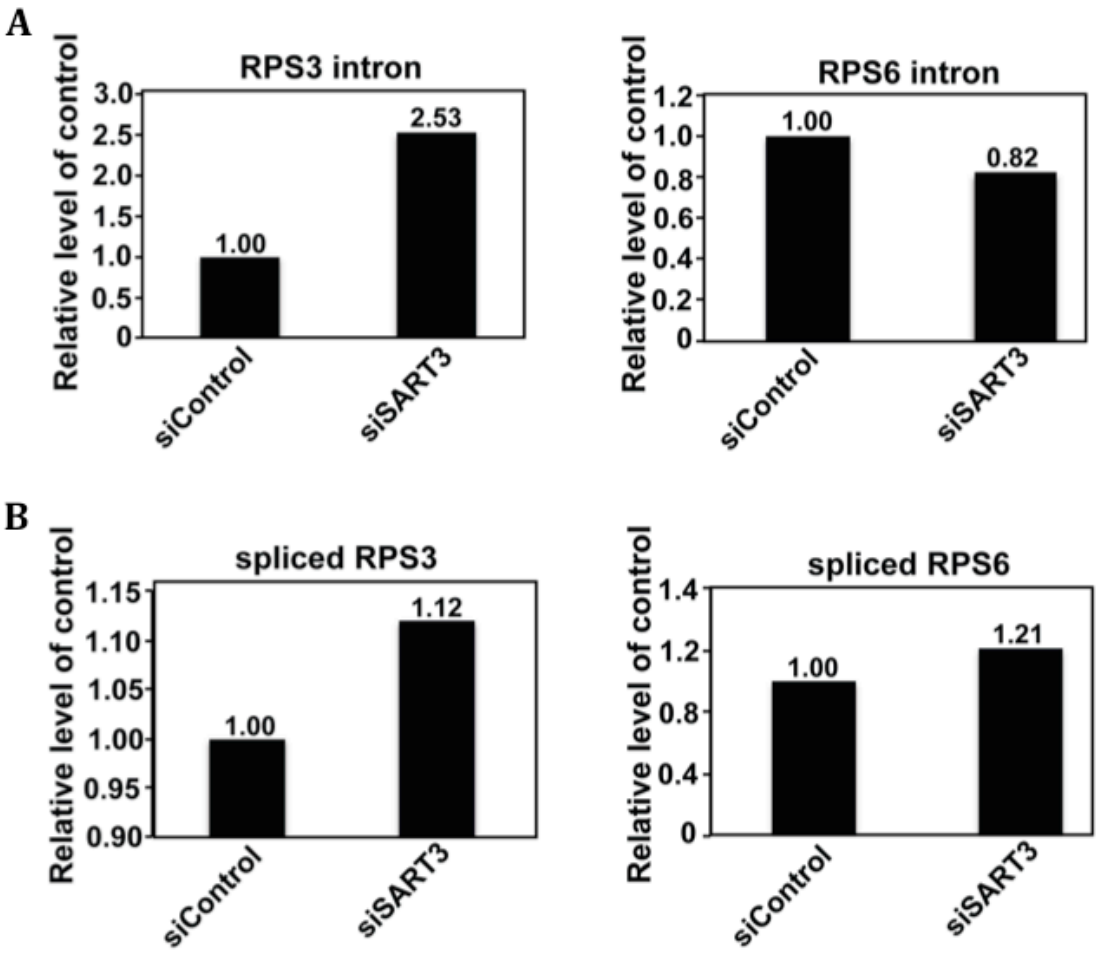

Figure A1.3. SART3 depletion does not affect splicing of Usp49-regulated genes. **(A)** SART3 was depleted from cells as described in Figure 3.12A. RPS3 and RPS6 transcript levels were monitored 72 hours post-knockdown as described in A1.1B. Primers amplifying a portion of intron 4 in RPS3 and RPS6 were used to measure intron inclusion in control and SART3-depleted cells. Transcript levels were normalized to GAPDH and compared to transcript levels in the siControl sample. **(B)** SART3 was depleted and RNA was harvested as described in (A). Primers spanning exons 2 and 3 in RPS3 and RPS6 were used to measure the quantity of spliced product using qRT-PCR. Normalization was performed as described in (A).

APPENDIX II: PRIMER SETS AND LENTIVIRUS PLASMIDS

Table A2.1. Primers used in qRT-PCR analysis to measure knockdown efficiency of Usp15, Usp4, Usp11, and SART3. Pertains to Chapter 3.

Gene	Forward	Reverse	Primer #
Usp15	CGACGCTGCTCAAAACCTC	TCCCATCTGGTATTTGTCCCAA	485, 486
Usp4	TGACAGCCGGTGGTTCAAG	GGTAGGGACCAATACATAGTCCA	487, 488
Usp11	TATAAGCAGTGGGAGGCATACG	ATGACCTTGCGTTCAATGGGT	967, 968
SART3	TGAGGTTAAGGCGGCTAGGA	CATGGCGTACTCATCCCCATC	848, 849

Table A2.2. Lentivirus packaging vectors and shSART3 plasmids. Pertains to Chapter 4.

Plasmid number	Description	TRC number	Identification number
-	non-targeting shRNA	-	-
-	GFP	-	-
pPAX	Gag-Pol	-	-
PMD2.G	VSV-G	-	-
1	shSART3	148744	5326
2	shSART3	148806	5327
3	shSART3	128080	5329
4	shSART3	147508	5330
5	shSART3	127760	5328
6	shSART3	146268	5331
7	shSART3	129569	5332
8	shSART3	149271	5333
9	shSART3	344340	5334
10	shSART3	344260	5335
11	shSART3	344338	5336
12	shSART3	344339	5337

Table A2.3. Primers used in qRT-PCR analysis to measure transcript levels of genes reported to have transcript changes in RNA-seq analysis. Pertains to Chapter 4.

Gene	Forward	Reverse	Primer #
Unspliced GAPDH	CTCTCCAGAACATCATCCCTG	TGGCAGGTTTTTCTAGACGG	1045, 1046
USP18	TTTTGGAGTGATCACGAATGAGC	CATGAGGGTAGTCCCAGGC	1245, 1247
CTR9	GTGCCCTTTCAGCCTATGGA	CTTAGCCTCCCCTAGGTTTCC	1248, 1249
F11R	TCCATCCAAGCCTACAGTTAACAT	AGCTCTCCTGTTGTGGGATT	1250, 1251
PDGFB	GTGAGAAAGATCGAGATTGTGCG	CTCGCTGCTCCTGGGAAC	1252, 1253
SPINT1	ACTGCGTGGACCTGCCAG	TGGAGATGCCGCGACAAGA	1254, 1255
LAMP3	ATGGCAGTCAAATGAGAGCAA	CTGTTTGAAAGGTGATATGACCATC	1260, 1261
MFAP5	AAGGTGCTGCTGTTTCTTGC	TAGGATCTTCTGTGAATGTTTCTGGA	1262, 1263
GRAMD1B	GCCAAAACGGAGAGCACTTAT	CTGCCACATGTTTGATCCTGT	1264, 1265
CDKN1A	AACTTCGACTTTGTCACCGAG	AGAGTCTCCAGGTCCACCT	1268, 1269
MEG3	TCTCTCCTCAGGGATGACATC	TGAGGTGTAGATGGGCAGC	1270, 1271

Table A2.4. Primers used in ChIP analysis to assay genomic localization of SART3 and RNAPII. Pertains to Chapter 4.

Gene	Forward	Reverse	Primer #
CTR9 (1)	AGAAGCCAGAGCTCCAGCG	GCTCTGGTCTTGACTGCCG	1384, 1385
CTR9 (2)	TTAAGACCTACCTTTTGTATTTTAGGTC	GGTAACTGATCGAAGTCAAGTTCAAT	1388, 1389
F11R (1)	AAAGGCGCAAGTCGAGAGG	ACAACAGGATCGCCAATATGAAGAG	1392, 1393
F11R (2)	CACTCCTGACAGGGCCCA	AATGCCAGGGAGCCTAAGGAG	1396, 1397
FAT3 (1)	AAGAAGGAGGTTTATAAACTGGAGGT	GACCTGTGCTTTTAAATCTCCTTCCT	1408, 1409
FAT3 (2)	GGAAGGTTCAGTATAGACGACGAG	AACACTCTTGGCACAAAATATTACACTT	1410, 1411
FAT3 (3)	CAGTAACACTTCTCTTTTTTGTCTCAGG	GAATGTCTGCGGCAGTGATGA	1412, 1413
Intergenic	TACACCACTCAAGGGAAACTGGAA	TGGAACTTCTGGAAGACACTGGAA	650, 651

Table A2.5. Primers used in qRT-PCR analysis to measure changes in transcript levels of $SAGA^{DUB}$ subunits, spliceosome components, and RPS3/RPS6 intronic and spliced products. Pertains to Appendix I.

Gene	Forward	Reverse	Primer #
ATXN7L3	CCAGGCCCTGATCAGCC	TGGCTTCTTCTTCTTGTTGGAA	1017, 1018
USP22	CCATTGATCTGATGTACGGAGG	TCCTTGGCGATTATTTCCATGTC	534, 535
ENY2	TGATTTGTTTTTTGCTTTTGCATA	ACACAACACAATCTAATTCAATCTTA	1001, 1002
ATXN7	CAAAGGTTGCCAAAGTGC	TCGTGGAGTCCAGAGTGC	1005, 1006
PRPF3	CACGACAAATCGAGGAGAGGA	GGCTGAATAGTGTTGCCAATAGG	902, 903
PRPF31	CTTTCCGGGGATTCAGTCAAG	CAGCTCGTTTTCGATCTCCAC	963, 964
USP39	CACTTACCTGCCGGGTATTGT	CCTGGAGGACGTTTGATGTTCT	965, 966
SF3A3	GTCATGGCTAAAGAGATGCTCAC	TCCTCCTTTCGTAATCCATCCTT	971, 972
PRPF6	CCGTTGGGGACCAGATGAAG	GGCGTTCCATACGATATTTCTCT	973, 974
PRPF19	CGAGAACTACATTGCGGAGAAT	GCTGGTACAGAGCGTGTGAC	1138, 1139
RPS3 intron	TGTTTGCACACATTGAAGCA	CTCCAGGCCCTTTCACATTA	1146, 1147
RPS3 spliced	TCTCTGCGTTACAAACTCCT	ATCAGGCCATCCACAAACTT	1178, 1179
RPS6 intron	CTGAAAAGGCCTATGCTCCA	TGACAATTCCTGCCAATTCA	1148, 1148
RPS6 spliced	GCAGAATCCGCAAACTTTTC	TTTTCTTGGTACGCTGCTTC	1179, 1180